Final Report

FHWA/IN/JTRP-2004/3

Evaluation of Seismic Hazard Assessments for Indiana

by

Jennifer Haase
Robert Nowack
Department of Earth and Atmospheric Sciences
School of Science

Chi Hyun Park
Alison Hunyar
School of Civil Engineering

John Hill
Indiana Geological Survey

Michael Hamburger
Indiana University

Joint Transportation Research Program
Project No. C-36-30C
File No. 9-4-3
SPR-2812

Prepared in Cooperation with the
Indiana Department of Transportation and the
U.S. Department of Transportation
Federal Highway Administration

Purdue University
West Lafayette, Indiana 47907
September 2004

TECHNICAL REPORT STANDARD TITLE PAGE

1. Report No.	2. Government Accession No.	3. Recipient's Catalog No.
FHWA/IN/JTRP-2004/3		

4. Title and Subtitle	5. Report Date
Evaluation of Seismic Hazard Assessments for Indiana	September 2004
	6. Performing Organization Code

7. Author(s)	8. Performing Organization Report No.
Jennifer Haase, Robert Nowack, Chi Hyun Park, Alison Hunyar, John Hill, Michael Hamburger	FHWA/IN/JTRP-2004/3

9. Performing Organization Name and Address	10. Work Unit No.
Joint Transportation Research Program 1284 Civil Engineering Building Purdue University West Lafayette, IN 47907-1284	
	11. Contract or Grant No. SPR-2812

12. Sponsoring Agency Name and Address	13. Type of Report and Period Covered
Indiana Department of Transportation State Office Building 100 North Senate Avenue Indianapolis, IN 46204	Final Report
	14. Sponsoring Agency Code

15. Supplementary Notes

Prepared in cooperation with the Indiana Department of Transportation and Federal Highway Administration.

16. Abstract

Current USGS probabilistic seismic hazard estimates (Frankel et al., 2002) show a higher seismic hazard in southwestern Indiana than for the rest of the state. This is expected based on past work documenting large pre-historic events in the Wabash Valley, and also based on isoseismal levels of shaking from the New Madrid 1811-1812 earthquakes. When assessing the hazard on a county by county basis, the local soil conditions produce amplification of shaking in regions with soft or unconsolidated sediments relative to firm-rock sites. We have reproduced the probabilistic seismic hazard calculation following the USGS methodology for the state of Indiana and provided details for the shaking level on each county of the state. Here we compare the 1996 and 2002 versions of the seismic hazard maps [*Frankel et al.*, 1996; *Frankel et al.*, 2002]. We also compare the results with an assumed maximum magnitude for the New Madrid earthquake of 7.3. This produces significantly lower acceleration levels. The USGS probabilistic maps were constructed assuming firm-rock sites. Versions of the maps were produced assuming other NEHRP classification levels, however no information was provided specific to the state of Indiana that suggests which site classification is appropriate for a given location. More recent studies have attempted to provide more detailed soil amplification classifications for the central U.S. These are described by [*Bauer et al.*, 2001] and [*Street et al.*, 2001]. A new methodology has been developed to incorporate soil profile site effects into the probabilistic calculation [*Cramer*, 2003; *Cramer et al.*, 2003]. We demonstrate the usefulness of this approach by applying it to a low resolution near-surface velocity model based on a limited amount of soil profile data in Indiana, and we report on the relative amplification and deamplification expected given the available data. The results show particular regions of amplification on the order of 2 or greater for both the 1 Hz and the 5 Hz spectral acceleration with 2% probability of being exceeded in 50 years, between the standard NEHRP B/C site and the probabilistic site effect calculation. For the 1 Hz maps, this occurs in the central and central northern part of the state including the Indianapolis metropolitan area, where the surficial units of glacial tills are particularly thick because of the sediments that both fill the bedrock Teays Valley and that overlie it in thickness up to 1,370 meters. Lower amplitudes are noted for much of the south central part of the state because bedrock crops out or is present near the surface. These results are useful because they give a first order estimate that illustrates the potential effect of geology. They are demonstration maps that lack the detailed data required for practical use, but serve as a proof-of-concept for the probabilistic site effect methodology. Even with these approximate maps it is clear that there is a significant variation in the number of counties that would be impacted by the engineering design criteria, depending on the level of approximation in the methodology chosen. We describe the datasets that we have collected and used to establish the input geology-based velocity model, including comparisons with independent datasets that allow us to estimate the true uncertainty of the measurements. Future versions of PSHA maps with site effects are planned that will use a database with higher resolution information on shear wave velocity structure. These future maps will provide information at the level necessary for planning and budgeting, though site specific studies will still be needed for engineering.

17. Key Words	18. Distribution Statement
seismic hazard, seismic design, bridges, earthquake, risk, acceleration.	No restrictions. This document is available to the public through the National Technical Information Service, Springfield, VA 22161

19. Security Classif. (of this report)	20. Security Classif. (of this page)	21. No. of Pages	22. Price
Unclassified	Unclassified	146	

TABLE OF CONTENTS

LIST OF TABLES

LIST OF FIGURES

1 Seismic Hazard and County by County Analysis

1.1 Introduction

The Recommended Load-and-Resistance-Factor Design (LRFD) Guidelines for the Seismic Design of Highway Bridges (ATC/MCEER, 2003) is currently under consideration by the American Association of State Highway and Transportation Officials (AASHTO), of which the Indiana Department of Transportation (INDOT) is a member. The proposed bridge design guidelines make reference to the United States Geological Survey published probabilistic earthquake hazard maps for the United States, which are based on current knowledge of past earthquake activity and geological constraints on earthquake potential (Frankel et al. 1996, 2002). In order to gain more understanding of the seismic hazard specific to Indiana as expressed in the specifications, this project was requested with the objectives of reviewing available seismic hazard assessments, analyzing the seismic hazard on a county by county basis, analyzing the recent seismicity and its implications for seismic hazard in the state, and making recommendations for seismic hazard monitoring. The study also includes an intercomparison of methodologies used for determining the shear wave velocity in surface unconsolidated sediments, which significantly affects the ground motion shaking levels in the probabilistic seismic hazard assessments.

1.2 Review of Seismic Hazard Assessments Applicable to Indiana

Research on the past earthquakes within the New Madrid seismic zone of eastern Missouri has had a great impact on seismic hazard assessment for the central US, including the state of Indiana. The large magnitude of earthquakes on this fault system in 1811-1812 is evidence that the seismic hazard is high despite the low background seismicity and long return periods for seismic events in the region. This situation has posed problems for the engineering community, whose regulations have been developed in the context of southern California earthquakes which display a simpler correlation between the occurrence of large earthquakes and background seismicity. This chapter reviews what is known about the basic data that are used to make probabilistic estimates of seismic hazard, and reviews the available estimates concerning Indiana.

The two most significant data relevant to seismic hazard assessment in Indiana are 1) the occurrence of 3 major earthquakes in New Madrid in 1811-1812 and 2) the presence of paleoliquefaction features in older sediments in both the New Madrid area and the Wabash Valley area, demonstrating the past occurrence of significant shaking events. The uncertainties in the dates, sizes, and effects of these events translate into significant uncertainties in the hazard assessment. For the central U.S. hazard, one of the controlling factors is the maximum moment magnitude (M_w) for New Madrid and the surrounding regions. For the stable continental areas, a M_w of 6.5 was used for the maximum magnitude and for the New Madrid region a maximum magnitude of 8.0 with a recurrence time of 1000 years was used for the analysis. However, more recent

estimates of the magnitudes of the 1811-1812 earthquakes by Hough et al. (1999) have inferred lower magnitudes for these large historic events in contrast to magnitude 8 level estimates given by Johnston (1996) and Johnston and Schweig (1996). The range of uncertainty in the magnitude of these events translates into a large range of uncertainty for the probabilistic seismic hazard estimates (PSHA). The current 2002 maps are constructed using a weighted average of the likely current estimates of the magnitude of these events.

The effects of this uncertainty for most of Indiana are not great, with the exception of Posey County. From our review of the seismic hazard estimates, modifications in New Madrid event maximum magnitude, for example between the 1996 and 2002 USGS maps created only a small difference in the PSHA for peak ground acceleration in Indiana, because of counterbalancing changes that were made in the attenuation relationships.

In comparisons, we find that the new 2002 USGS seismic hazard maps (Figure 1-1, Figure 1-2, Figure 1-3) call for a higher level of ground shaking in Posey county (the county with the highest hazard) compared to the earlier seismic hazard maps published in 1996. This implies that a greater number of counties would have a hazard level greater than the 0.15 g acceleration specified in the building guidelines compared to the previous publication. In our own runs of the PSHA calculations, we found that reducing the maximum magnitude of the New Madrid event to a value as low as 7.3, the minimum credible magnitude, had small effects at distance ranges appropriate for Indiana. Our calculations indicated a smaller region above the 0.15 g criteria (Figure 1-5, Figure 1-4, and Figure 1-6). This work does not imply that the hazard is less than that estimated by the USGS, but only that if future research on the New Madrid event indicates that M 7.3, which is currently equally favored by the research community, turns out to be supported by further evidence, then a significantly lower number of Indiana counties would be at a high hazard level.

We have reviewed the differences between the Probabilistic Seismic Hazard maps published by the USGS in 1996 and 2002. The impact that this change has for Indiana is an overall decrease in the expected accelerations at all frequencies due to the significant change in input parameters for the magnitude of the New Madrid earthquake. The magnitude was 8.0 for the 1996 simulations but for the 2002 simulations, it is specified as a weighted combination of the estimates for a magnitude 7.3 to 8.0. We have implemented the programs for calculating these probabilistic accelerations here at Purdue. We have validated that we can reproduce the USGS results and proceed in the next section to examine the effects of near surface geologic materials in Indiana on these probabilistic seismic hazard estimates. Lateral variations in surface structure in the later sections will be shown to have larger effects within the state of Indiana than variations of the maximum credible magnitude.

1.3 Probabilistic Seismic Hazard Assessment with Site Effects

The U.S. Geological Survey has published probabilistic earthquake hazard maps for the United States quantifying this hazard [*Frankel et al.*, 1996; *Frankel et al.*, 2002]. These have been incorporated into the Recommended Load-and-Resistance-Factor Design

(LRFD) Guidelines for the Seismic Design of Highway Bridges (ATC/MCEER, 2003), which is currently under review by AASHTO and the Indiana Department of Transportation (INDOT). These maps assume standard B/C type site conditions, which imply S-wave velocities of 760 m/sec in the top 30 meters. For planning and long-term budgeting of road and bridge projects, INDOT is interested in a similar probabilistic seismic hazard map that takes into account the near surface geological materials typical for the state. In particular the information is needed for budgeting retrofitting of bridges on interstate and state highways. An estimate of the number of counties to be affected by the new Bridge Specifications is desired.

Previous estimates of probabilistic seismic hazard, including the USGS maps which implicitly assume B/C site conditions and others [*Toro and Silva*, 2001] make a simple assumption that the acceleration levels in the probabilistic seismic hazard maps can be multiplied by the relevant amplification factor to incorporate site effects. Similarly, the proposed LRFD guidelines (ATC/MCEER, 2003) also publish generic multiplicative factors for different site classifications. However, this does not take into account the uncertainties in the knowledge of the amplification factor, which has been shown in some cases to make a difference of 0.1g or greater [*Cramer*, 2003] in the final PSHA estimate. For a completely probabilistic treatment of the ground motions, several methods have been proposed [*Bechtel-Jacobs*, 2002; *Cramer*, 2003; *Lee*, 2000; *Toro and Silva*, 2001] to incorporate the uncertainties in the soil profile by modifying the attenuation curve appropriately within the probabilistic seismic hazard calculation directly.

In this report, we describe the input data sets used in the methodology for estimating the geology-based shear-wave velocity model necessary for estimating the site effect and its uncertainty, we describe the methodology followed for the probabilistic calculation, and the methodology used for calculating the site response. Finally we compare the results of several methods with the original USGS 2002 maps to comment on the consequences of the expected overall increase in acceleration levels.

1.4 Data and input velocity model

An estimate of the shear wave velocity profile and its uncertainties is required to implement a probabilistic calculation that incorporates site information. This is not directly available at the 0.05 degree resolution of the national seismic hazard maps. Though some direct measurements are available, it is necessary to extrapolate the available information to the entire region of interest in a logical manner based on geological data. In a study of the Memphis area [*Gomberg et al.*, 2003], the authors were able to uniquely classify 5 lithologic units, reaching depths of approximately 30 m. This was possible because of the dense subsurface sampling (1200 geophysical well logs and 76 new velocity profiles) within a 45 by 25 km area. The depositional environment in and around Memphis is somewhat simpler, without the overlapping and crosscutting sequences of tills and outwash commonly present in the river valleys of Indiana, so that layers are relatively continuous over the area. Because fewer data are available in Indiana over a greater area, we necessarily use a simplified method to achieve a comparable type of velocity model. We use the data described below to infer a gridded model of shear wave velocity for a single layer of unconsolidated sediment over bedrock on a 0.125 degree grid.

1.4.1 Geologic data

The geology of Indiana consists of gently eastward dipping sequences of shales, carbonates, and sandstones of Paleozoic age formed from material deposited when shallow seas covered most of the North American continent. These bedrock units are covered partly by unconsolidated deposits left from several intervals of glaciation in the Pleistocene. Glacial tills from both northeastern and northern sources overlie glacial outwash, loess, and some sand and mud deposits from shallow pro-glacial lakes. Bedrock is exposed at or near the surface throughout much of south-central Indiana, south of the Wisconsinian and pre-Wisconsinan margins. Significant thicknesses of alluvium occur within the Wabash, White and Ohio River valleys. The 1:500,000 scale bedrock geology map (Figure 1-8) and quaternary geologic map (Figure 1-7) of Indiana are available electronically in Geographical Information System (GIS) format [*Gray*, 1989] [see http://igs.indiana.edu/]. On the surficial map, there are 34 units distinguished by lithology and depositional environment. We group these into 6 general types of materials: alluvium, aeolian sand, loess, outwash, lacustrine deposits, and glacial tills to create a simplified surficial geologic map that is better suited to our purposes (Figure 1-9).

Each of these units is assigned a shear wave velocity based on the available data. Borehole shear wave velocity measurements are available in the Evansville and Vincennes region [*Eggert et al.*, 1994]. These are primarily in the glacial outwash and alluvial sequences that are found in the Ohio River valley [*Eggert et al.*, 1997]. The maximum depth of the boreholes is 40 meters, with many reaching bedrock, and shear wave velocities range up to 600 m/sec in the unconsolidated sediments. These data were used to create a site classification map based on geology and the average shear wave velocity in the upper 30 meters [*Bauer*, 1997] using the National Earthquake Hazards Reduction Program (NEHRP) site classifications [*FEMA-222A*, 1994]. To better characterize other unconsolidated units in Indiana, additional borehole shear-wave velocity measurements were made by the Indiana Geological Survey in the summer of 2003. For each material type, the available data were averaged to derive a mean velocity and standard deviation (Table 1-1). The individual values used in the derivation are shown in Table 1-4. Units containing primarily sand have higher velocities than finer grained materials, as expected [*Hamilton*, 1979], and the highest velocities are in the glacial tills.

We create a grid using the center points of the USGS topographic map quadrangles with 0.125 degree spacing. Each grid point is assigned the average shear wave velocity from Table 1-1 for the geologic material within which the grid point falls. Shear wave velocities for grid points where bedrock is mapped at the surface are taken from values compiled for similar Illinois bedrock units [*Bauer et al.*, 2001] (Table 1-2).

Seismic refraction data are used to constrain the depth of unconsolidated sediments and derive the underlying bedrock shear-wave velocities. Over 13,000 refraction measurements of compressional wave velocity were made between the years of 1954 and 1973 [*Rudman et al.*, 1973; *Whaley et al.*, 2002]. Seismic velocities for bedrock were determined for each profile, as well as velocities for 3 or less layers within the unconsolidated sediments, and the sediment layer depths. Shear wave velocity cannot be reliably related to compressional wave velocity in the unconsolidated sediments, however

the bedrock shear wave velocities can reasonably be inferred from the compressional velocity by dividing by the theoretical Vp/Vs ratio of 1.73 for a Poisson solid. We assume the P-wave layer interface depths can be used to approximate the shear-wave velocity layer interface depths for the unconsolidated sediments.

The refraction measurements were first screened to remove data of lower quality. This reduced the dataset to 11873 profiles (Figure 1-10). Then the bedrock velocities within each 0.125 by 0.125 degree quadrangle were averaged to derive a mean velocity and standard deviation. The individual profiles have as many as 3 distinct layers over bedrock. There is not sufficient ground truth data to determine velocities for all of the individual layers, but we estimate average velocity in one near surface layer if it exists (Figure 1-11), one layer that represents the majority of the unconsolidated sediment thickness (Figure 1-12), and in the bedrock layer (Figure 1-13). Though it is not possible to make a direct correlation of P-wave velocity and S-wave velocity in the unconsolidated sediments, it is important to note the strong correlation of P-wave velocity with surface geology and sediment thickness, which supports our arguments for a S-wave velocity model where velocity is assigned from surface geology. Typically, most quadrangles contained at least 4 measurements. For quadrangles with less than 2 measurements, the average velocity from the nearest quadrangle with data was assigned. The average bedrock velocity is closely correlated with bedrock type (and provided some of the original evidence for constructing the bedrock geologic map). The values for each quadrangle were divided by 1.73 to get an average shear wave velocity and standard deviation.

The average thickness of the unconsolidated sediments is derived from the seismic refraction data within each quadrangle. Depths were determined for one near surface layer (if it exists) and the intermediate layer of substantial unconsolidated sediments. The depths of the individual interfaces were retained so that in the randomization process later on, some velocity contrast would be allowed. The depths to bedrock and the depths to any intermediate layer were averaged for each quadrangle and the standard deviation was calculated (Figure 1-14, Figure 1-15, Figure 1-16). For quadrangles where there were no profiles available, the thickness from the nearest quadrangle with data was used. An alternate interpreted map of the thickness of unconsolidated sediments is available at 1:500,000 scale for Indiana [*Gray*, 1983]. The map is based principally on seismic refraction data and well records on file at the Indiana Dept. of Natural Resources, Division of Water and Division of Geological Survey. For this map, the thickness is contoured at 50 ft (15.4 m) intervals. In general the thickness that we have derived correlates well with this interpreted map (Figure 1-16), and is within the 50 ft contour interval of the interpreted map. From the thickness and velocity information from the unconsolidated thickness layer, we can calculate the expected resonant period of the sediments (Figure 1-20).

In summary, the final velocity model (Figure 1-17) has the characteristics in Table 1-3. Parameters for shear modulus reduction curve and for the damping ratio have been assigned to each unit based on the texture and composition [*Rockaway*, 1997] (Figure 1-18, Figure 1-19). The methodology that we have adopted for determining a shear-wave velocity model is certainly limited in resolution given the true geologic complexity of the state. In the future we hope to make more direct measurements of seismic velocity in the

units to reduce the uncertainty for each classification and also to allow a more complicated representation of the unconsolidated sediments with depth. However, as long as the uncertainty for each of the parameters is estimated correctly, the uncertainties in the final seismic hazard estimates are correctly represented.

1.5 Probabilistic Hazard Methodology

The methodology used to create a probabilistic hazard map that includes site effects is based on the USGS probabilistic seismic hazard calculation for hard rock sites. The USGS maps show the hazard in terms of the levels of horizontal ground shaking that have a specified chance of being exceeded in a given time period. These maps incorporate a linear (as a function of input ground motion level) site response, assuming a firm rock site where there the surface soil profile is a NEHRP B/C site with S-wave velocity of 760 m/sec.

The methodology is shown schematically in Figure 1-21. For a given site, the probability, P, of exceeding a specific ground motion, A_0 [*Reiter*, 1990] is the sum of the probability of exceeding that ground motion level for all possible source earthquakes

Eq 1 $$P(A_r > A_0) = \sum_i \alpha_i \int_M \int_R f_i(M) g_i(R) P(A_r > A_0 \mid M, R)\, dR\, dM$$

where A_r is the ground motion parameter (i.e., peak ground acceleration or spectral acceleration) observed at a rock site, α_i is the annual rate of occurrence of the ith earthquake source, $f_i(M)$ is the probability density distribution of earthquake magnitude M of the ith source, and $g_i(R)$ is the probability density distribution of distance R from the ith source. $P(A_r>A_0|M,R)$ is the probability of exceeding ground motion A_0 given an earthquake of magnitude M at distance R, and is given by an attenuation relation (i.e. [*Frankel et al.*, 1996], [*Toro et al.*, 1997]) with a lognormal distribution.

This probability is variable if site effects are incorporated into the calculations. The probability of ground motion at a soil site, A_s, exceeding a specific ground motion A_0 [*Cramer*, 2003] is given by

Eq 2 $$P(A_s > A_0) = 1 - \int_{A_s=-\infty}^{A_0} \int_{A_r} P(A_s \mid A_r) P(A_0 = A_r \mid M, R)\, dA_r\, dA_s$$

where $P(A_s|A_r)$ is the probability of soil ground motion A_s given an input ground motion A_r to the base of the soil column.

The ground motion at the surface of a stack of soil layers given an input ground motion at the base of the soil layers is calculated using the program SHAKE91 [*Idriss and Sun*, 1992]. This program uses a frequency domain approach to calculate the transfer function of motions at consecutive layer interfaces. It assumes vertically propagating shear waves that can be approximated as a sum of sine waves. The transfer function depends on the complex shear modulus (shear wave velocity, specific gravity, and soil damping ratio) of the layers and the thickness of the layers. It takes into account nonlinear and inelastic behavior of the soil (changes in the shear modulus of the soil depending on the amplitude of the strain) using an iterative equivalent linear approach. This requires estimates of the modulus reduction curve for the soil type which specify how shear modulus decreases as

strain increases, which have been studied by various authors for many soil types. Typically, the transfer function for a stack of low shear wave velocity soil layers produces an amplification of ground motion. Including nonlinear behavior has the effect that for very large ground motions, the amplification due to the soil layers is reduced, or can even be de-amplified. The soil damping ratio (not to be confused with structural damping used to produce a response spectrum) describes the viscous attenuation of the amplitude of the seismic waves, and has also been characterized for many soil types.

In summary, if the shear wave velocity, specific gravity, soil damping ratio, and modulus reduction curves are known exactly for each layer of soil above bedrock, the response of the soil layers can be computed very precisely with SHAKE91. For seismic hazard mapping, as opposed to site specific studies, one is working at a scale where the geologic structure is approximated from a limited amount of borehole data with limited precision, and these parameters are not known exactly. For this reason, we have characterized the uncertainties in these parameters, as described in the data section above. These uncertainties are used to calculate empirically the probability distribution function required in Eq 2.

By randomizing the velocity profiles following the characteristics of its error distribution a large number of these profiles can be used as input to the site response calculation to determine the error statistics of the site response. A distribution of possible site amplification factors is calculated at each site (or in this case at each 0.2 degree grid point of the state of Indiana). In addition to the site parameters described above, the site response also depends on the amplitude and frequency content of the ground motion at the base of the soil column.

The steps are summarized below.

- create a set of input ground motions (6 motions used in Memphis)
- specify a set of 10 ground motion levels where the response will be calculated (this will allow one to take into account the magnitude of the earthquake through consideration of bedrock amplitude)
- select an input ground motion randomly from the set of 6 motions.
- scale the motion so that amplitude at the frequency of interest (1 Hz or 5 Hz) is at the specified level
- retrieve the shear wave velocity profile at the site and the uncertainties
- create a realization of the shear wave velocity profile sampled from a distribution of velocities and layer depths with the specified uncertainties
- retrieve the specific gravity, modulus reduction curve, and soil damping curve depending on the site geology
- randomize the modulus reduction and soil damping curves assuming a 0.35 sigma lognormal distribution
- calculate the site response using SHAKE91

- Repeat this calculation for each of the 10 ground motion levels, creating a suite of 100 estimates of the site response for each ground motion level using the randomly sampled soil properties and input ground motions.
- Calculate the distribution of site amplification factors from these 100 estimates for each ground motion level for each frequency of interest (PGA, 0.2s and 1.0s)

We then compute the probabilistic seismic hazard maps following the same methodology as used in the USGS national seismic hazard maps [*Frankel et al.*, 1996; *Frankel et al.*, 2002] with site specific attenuation relations. For each site (0.2 degree grid point) the following steps are performed.

- For each potential source region, calculate the probability of occurrence of an earthquake of a given magnitude based on the current seismicity rate or based on models of characteristic earthquake occurrence on known active faults.
- Calculate the distance from the source region to the grid point
- Select the probable input rock ground motion level from the hard rock site attenuation curves
- Select the site amplification distribution for the appropriate input ground motion level.
- Modify the bedrock attenuation relation distribution by the site amplification distribution as in Eq 2 to get the probability of exceeding a given ground motion
- Repeat the calculation for all potential source regions and earthquake magnitudes
- Sum the contributions for all source regions and earthquake magnitudes (Eq 1).
- Repeat the calculation for all sites (grid points)

1.6 Results

The results from the first phase of the calculation are the amplification factors for each point of the grid for input ground motions from 0.05 to 1.00 g. The site response amplification as a function of frequency is different depending on the input ground motion level. This is because the shear modulus reduction curves reduce the amplification at higher strains. An example of the site response for an individual grid point, in this case a site within the Indianapolis urban area, is shown in Figure 1-22. In this example the amplification at 5 Hz is a factor of 3 for input ground motions of .05 g, but for input ground motions of .5g, the amplification at 5 Hz is only a factor of 1.4. These site responses and the probability of their occurrence given an input rock motion at the base of the column are tabulated for use in the hazard calculation. An example for the Evansville area is shown in Figure 1-23. A contour map of the amplification at 1 Hz for input motions of 0.05 g is shown in Figure 1-24, and illustrates the amplification of thicker sediment sequences. The amplification is illustrated for 1 Hz and 5 Hz and PGA at ground motion levels of 0.05g, 0.2g, and 0.5g in Figure 1-24 through Figure 1-32. The

amplification maps already give a preliminary indication of the effect that these site geology will have on the final calculation.

The results of the second phase of the calculation are the ground motions for a given probability level. The calculation is run separately for each probability level. The outputs are smoothed so that the roughness of the map is consistent with the sampling of the input velocity model which is very low resolution in this preliminary version. For reference, the USGS PSHA maps, which assume NEHRP B/C site classifications, maps are shown in Figure 1-33 and Figure 1-34 for 1 Hz and 5 Hz. The map of 1 Hz spectral acceleration including the probabilistically determined site response is shown in Figure 1-35. Comparison with the USGS PSHA map (Figure 1-33) shows that there is high amplification of ground motions in several areas of the state, and that the ground motion does not decrease simply with distance from the southwest. There is a general trend of decreasing accelerations with the distance from the primary source regions factoring into the seismic hazard, the Wabash Valley and New Madrid, in the USGS PSHA maps. This trend has been partially obscured by significant smaller scale variations in acceleration. There is an extensive region of higher accelerations on the order of 0.2g running northwest-southeast across the center of the state. This region corresponds with the location of the subsurface Teays Valley, a valley in the relic topography of the bedrock formed by the impoundment of the drainage system by Early Pleistocene glaciation. The valley is filled with thick sequences of Plio-Pleistocene glacial till. There is another smaller region of relatively higher accelerations in the north of the state.

The map of 5 Hz spectral acceleration is shown in Figure 1-36. The pattern of accelerations is very different from both the 1 Hz maps and the USGS PSHA maps outside the southwestern corner of the state. The regions of high acceleration tend to lie in between the regions with high 1 Hz spectral acceleration. There is much less significant amplification in the PGA maps. In all maps there is de-amplification in the bedrock regions in the south-central portion of the state relative to the USGS PSHA maps. This can be expected since the high S-wave velocities in the surface bedrock are significantly higher than those corresponding to a NEHRP B/C site.

To check the results we have constructed PSHA maps that use an approximate simplified method for incorporating site effects. This simplified method multiplies the PSHA for a hard rock site by the amplification factor (illustrated in Figure 1-24 through Figure 1-32) appropriate for the site's ground motion level. This is approximately the method [*Toro and Silva*, 2001] used before the development of the probabilistic methodology [*Cramer*, 2003]. The site B/C response must be removed from the USGS PSHA maps before multiplication, which we approximate by division by the factors given in [*Frankel et al.*, 1996]. While this method does not accurately model the probabilities, it confirms the amplification patterns evident in the completely probabilistic calculation. All acceleration levels in these approximate maps (Figure 1-37 and Figure 1-38) are slightly higher in the completely probabilistic approach.

We compare the maps to a simple calculation of the expected resonant period of the surface unconsolidated sediment layer as a cross check on the validity of our results. The site response amplification is extracted for each grid point in the 1 Hz spectral acceleration PSHA map, and plotted as a function of the resonant period, where the

resonant period was calculated as T = 4Z2/Vs2 (Figure 1-20). This empirical amplification as a function of frequency derived from the 1 Hz and 5 Hz maps is shown in Figure 1-39 and Figure 1-40. The curves demonstrate that the higher amplitudes do indeed occur where the surface geology is expected to produce a resonance. The curves illustrate the decrease in amplification for increasing ground motion level. The curves are resolvably different for different soil shear-wave velocity types.

A primary objective of future research with this methodology is to provide input to INDOT for estimating the number of Indiana counties that will be affected by the new Recommended LRFD Guidelines for the Seismic Design of Highway Bridges [*ATC/MCEER*, 2003]. Acceleration levels for 1 Hz and 5 Hz that determine the seismic hazard level in that document are given in Table 1-5. The amplification factors for NEHRP site classifications in that document are given in Table 1-6 and Table 1-7. The USGS PSHA maps and the preliminary PSHA maps that incorporate site effects are presented on a quadrangle scale, with the contour interval corresponding to the criteria set for the seismic hazard levels defined in the proposed LRFD guidelines and thus illustrate the impact of the criteria on the spatial distribution of hazard for both 1 Hz and 5 Hz (Figure 1-33 through Figure 1-38). We chose to quantify the seismic level in each quadrangle because that is the nominal resolution of the input geology based velocity model. Thematic maps that show the maximum seismic hazard level for each county for both 1 Hz and 5 Hz are shown in Figure 1-41 through Figure 1-49. These are useful preliminary estimates of the number of counties affected. However, it is clear that the surface area classified at each seismic hazard level in the county map representation may not be as accurate as the quadrangle scale map for planning purposes.

We create the following summary maps and tables by applying the proposed LRFD guidelines criteria to the results, which takes the maximum of the seismic hazard level at 1 Hz or 5 Hz:

- USGS 2002 PSHA with default (B/C) site classification county map (Figure 1-43, Table 1-8)
- USGS 2002 PSHA with D site classification county map (Figure 1-44, Table 1-9)
- Probabilisitic site effect county map (Figure 1-47, Table 1-10)

Of particular note are the following conclusions:

With most of the counties in Indiana having NEHRP Class D or Class E NEHRP classification [*Bauer et al.*, 2001], there is a great impact in applying the amplification factors in the recommended LRFD guidelines even if the only information known is that provided in the USGS 2002 maps. This can be seen by comparing the seismic hazard levels from the USGS 2002 map (Figure 1-43) with the USGS 2002 map with Class D site effects (Figure 1-44). In particular, there is an increase in the number of counties at seismic hazard level IV from 5 to 11, and all counties at the lowest seismic hazard level I move to seismic hazard level II.

Estimating site amplifications with a probabilistic method should give the most accurate results. There are differences between the number of counties affected using the simplified site effects method (Figure 1-48, Figure 1-49) and the probabilistic method

(Figure 1-45,Figure 1-46), even though the input geology based velocity model is the same.

Using the probabilistic method, even with an approximate geology based shear wave velocity model, actually *reduces* the number of counties at seismic hazard level IV compared to both the 2002 USGS maps with and without Class D site effects. This can be seen by comparing the probabilistic site effect map (Figure 1-47) with the two versions of the USGS 2002 maps (Figure 1-43 and Figure 1-44). Most importantly, the counties at seismic hazard level III are not the same between the class D site effect method and the probabilistic site effect map.

Based on these preliminary maps with probabilistic site effects and the criteria defined in the Recommended LRFD Guidelines for the Seismic Design of Highway Bridges, there are 4 Indiana counties at seismic hazard level IV, 24 counties at seismic hazard level III, and sixty four counties at seismic hazard level II and none at seismic hazard level I. In comparison, the USGS 2002 maps without considering site effects (using the B/C site classification) have 5 counties at seismic hazard level IV, 10 counties at seismic hazard level III, 62 counties at seismic hazard level II, and 15 counties at seismic hazard level I. These comparisons are summarized in Table 1-11 and Table 1-12. Future versions of PSHA maps with site effects should be planned that will create and use a database with higher resolution information on shear wave velocity structure, and which address some of the approximations that were necessary given the scope of the current project.

1.7 Discussion

Our calculations of probabilistic seismic hazard with probabilistic incorporation of site effects are intended to demonstrate the methodology on a test input geology-based velocity model for Indiana. The calculations are useful in that they provide a preliminary understanding of the way the geology of Indiana may affect expected acceleration levels in the state. However, it is clear that the model is oversimplified and lacks the precision and resolution necessary to produce PSHA maps with the required level of accuracy. As a starting point it achieves its objectives, however we note below the most significant of the improvements that are necessary to implement.

1) Depth dependence of surficial velocities. We have assumed that the velocities assigned at the surface continue to bedrock depths when it is more reasonable to assume that velocities increase with effective stress. In this sense the maps probably represent the upper limit on the amplification. Future versions of the maps would be improved by incorporating the true depth dependence of seismic velocity or at least a theoretical increase in velocity with depth.

2) Characterization of surficial velocity by lithology. The lithologic classification that we have chosen was limited because of the limited number of shear-wave profile measurements available. In this case we used approximately 40. The number of observations should be increased by collecting more data or including other types of compiled data such as shear and cone penetration test data. It is necessary to either sample the shear wave velocity sufficiently densely across the

state, or make more measurements to provide better characterization of each lithology. This latter would also permit a more detailed classification (more units) that would help give a better spatial representation of the shear wave velocity model. The nature of tills, for example, which cover so much of Indiana, is that their material properties are highly variable. Future versions of the maps then would be improved in spatial resolution.

3) Uncertainties of near layer thicknesses. The extensive P-wave data set can also be used to derive uncertainties in layer thickness from the standard deviation of the observed data, rather than assuming 20% of the layer thickness for the uncertainty. This may have a significant effect on the probability levels associated with the amplification functions.

4) Map resolution. For simplicity we sampled the surficial geologic maps at the quadrangle center points to determine the properties of the site used in the site response calculation. Therefore, smaller scale features such as river valleys, which are expected to provide significantly higher amplification, are not sampled properly. The uncertainties associated with each site velocity could be improved to take into account the probability of sampling each type of lithology found in the quadrangle, for example. This would provide a better spatial smoothness to the output maps.

1.8 Conclusions

We have reproduced the probabilistic seismic hazard calculation following the USGS methodology for the state of Indiana and provided details for the shaking level on each county of the state. The original seismic hazard maps [*Frankel et al.*, 1996; *Frankel et al.*, 2002] were constructed assuming firm-rock sites with B/C site classifications. We have assessed the hazard on a county by county basis, taking into account that the local soil conditions produce amplification of shaking in regions with soft or unconsolidated sediments relative to firm-rock sites. We have used a low resolution geology-based shear wave velocity model with characteristics specific to the state of Indiana as input to a completely probabilistic incorporation of site effects into the probabilistic seismic hazard calculation. Thus we produce maps with amplification and de-amplification relative to the 2002 USGS PSHA maps, with relatively low resolution, given the low resolution information of the input velocity model. For the 1 Hz ground motion with 2% probability of being exceeded in 50 years, the maximum difference between the standard NEHRP B/C site and the probabilistic site effect calculation is over a factor of two. This occurs in the central and central northern part of the state, where the surficial units of glacial tills are particularly thick. For the 5 Hz ground motion with 2% probability of being exceeded in 50 years, the maximum difference between the standard NEHRP B/C site and the probabilistic site effect calculation is over a factor of 2.5 in the north-eastern part of the state due to sediments of intermediate thickness with slow velocities. The 5 Hz ground motion was de-amplified somewhat in the extreme southwest part of the state because of the nonlinear response of the soils at high ground motions. 50% lower amplitudes are also noted for a good portion of the south-central part of the state because of the surficial bedrock units that are present. These preliminary results are useful, since they give a first order estimate that illustrates the potential effect of geology and in particular the spatial

patterns of amplificaton. They are demonstration maps that do not yet have the resolution required for practical use, but serve as a proof-of-concept for the probabilistic site effect methodology.

Based on these preliminary maps with probabilistic site effects and the criteria defined in the Recommended LRFD Guidelines for the Seismic Design of Highway Bridges, there are 4 Indiana counties at seismic hazard level IV, 24 counties at seismic hazard level III, and sixty four counties at seismic hazard level II and none at seismic hazard level I. In comparison, the USGS 2002 maps with simple consideration of D classification site effects (most of Indiana has D or E site classifications) has 11 counties at seismic hazard level IV, 24 counties at seismic hazard level III, 57 counties at seismic hazard level II, and 0 counties at seismic hazard level I. In this case, a more precise methodology actually *reduces* the number of counties at the highest seismic hazard level. Future versions of PSHA maps with site effects should be planned that will use a database with higher resolution information on shear wave velocity structure, and which address some of the approximations that were necessary given the scope of the current project. These future maps will provide information at the level necessary for planning and budgeting, though site specific studies will still be needed for engineering.

Table 1-1 Column shear wave velocity averaged by unit type from borehole velocity measurements. Map symbol and description refer to the mapped units from [*Gray*, 1989]. Values assigned for specific gravity were taken from [*Rockaway*, 1997].

unit type	avg Vs m/sec	stdev Vs m/sec	N obs	specific gravity	shear modulus reduction curve	soil damping ratio
alluvial	256	41	12	1.92	average gravel (Seed et al. 1986)	average gravel (Seed et al. 1986)
eolian sand or sand	249	59	7	1.76	EPRI generic sand	EPRI generic sand
lacustrine	202	31	4	1.92	clay (Sun et al, 1988)	clay (Vucetic and Dobry, 1991)
loess	208	40	11	1.84	clay (Sun et al., 1988)	EPRI generic sand
outwash	230	18	7	1.92	average gravel (Seed et al. 1986)	average gravel (Seed et al. 1986)
till	350	34	9	1.92	average gravel (Seed et al. 1986)	average gravel (Seed et al. 1986)
rock	--	--		2.4	EPRI generic rock	EPRI generic rock

Table 1-2 Indiana surface bedrock units [*Gray*, 1989] and assigned surficial shear wave velocity values for similar Illinois bedrock units [*Bauer et al.*, 2001].

Map symbol and description		Illinois unit	Vs
1	Middle Pennsylvanian sandstone, shale, limestone and coal	Pennsylvanian sandstone	2000 m/sec
2	Late Mississippian Early Pennsylvanian sandstone, shale, and limestone	Pennsylvanian sandstone	2000 m/sec
3	Middle Mississippian limestone	Mississippian limestone	2900 m/sec
3K	Middle Mississippian karst	Mississippian limestone	2900 m/sec
3T	Middle Mississippian terra rossa	Mississippian limestone	2900 m/sec
4	Early to middle Mississippian siltstone/shale	Mississippian shale	2000 m/sec
5	Middle Devonian to Early Mississippian black shale	Mississippian shale	2000 m/sec
6	Silurian and Devonian limestone/dolomite	Silurian/ Devonian limestone and dolomite	2900 m/sec
7	Late Ordivician Shale and limestone	Ordovician limestone/dolomite	2900 m/sec

Table 1-3 Summary of methodology for derivation of seismic velocity model.

Each grid point is assigned the following.		
V1	Layer 1 S-wave velocity, if layer exists.	Average velocity of all S-wave measurements made in the surficial material type found at grid point (from [*Bauer et al.*, 2001] and this report) or velocity from Table 1-2.
σ_{V1}	Layer 1 S-wave velocity uncertainty, if layer exists.	Standard deviation of all S-wave measurements made in the surficial material type found at grid point (from [*Bauer et al.*, 2001] and this report) or 20% of V1 for surface bedrock.
Z1	Depth to base of Layer 1, if layer exists	Average over quadrangle of P-wave refraction profile depth of layer 1.
σ_{Z1}	Uncertainty in depth to base of Layer 1, if layer exists	20% of layer depth.
$G/Gmax_1$	Layer 1 shear modulus reduction curve	Curve assigned from [*Rockaway*, 1997] according to the material type at grid point.
R_1	Layer 1 soil damping ratio	Soil damping curve assigned from [*Rockaway*, 1997] according to the material type at grid point.
$\gamma 1$	Layer 1 specific gravity	Value assigned from [*Rockaway*, 1997] according to the material type at grid point.
V2	Layer 2 S-wave velocity	Same as V1
σ_{V2}	Layer 2 S-wave velocity uncertainty	Same as $\sigma_{V1.}$
$G/Gmax_2$	Layer 2 shear modulus reduction curve	Same as $G/Gmax_1$
R_2	Layer 2 soil damping ratio	Same as R1
$\gamma 2$	Layer 2 specific gravity	Value assigned from [*Rockaway*, 1997] according to the material type at grid point.
Z2	Depth to base of Layer 2, if layer exists	Average over quadrangle of P-wave refraction profile depth of layer 2.
σ_{Z2}	Uncertainty in depth to base of Layer 2, if layer exists	20% of the layer 2 depth
V3	Layer 3 S-wave velocity	Average P-wave bedrock velocity from all refraction profiles within quadrangle divided by Vp/Vs of 1.73
σ_{V3}	Layer 3 S-wave velocity uncertainty	Standard deviation of P-wave bedrock velocity from all refraction profiles within quadrangle divided by Vp/Vs of 1.73
$G/Gmax_3$	Layer 3 shear modulus reduction curve	Curve for rock assigned from [*Rockaway*, 1997]
R_3	Layer 3 soil damping ratio	Curve for rock assigned from [*Rockaway*, 1997]
$\gamma 3$	Layer 3 specific gravity	2.4 for all bedrock types ([*Rockaway*, 1997])

Table 1-4 Data used to determine column shear wave velocity averaged by unit type from borehole velocity measurements. Map symbol and description refer to the mapped units from [*Gray*, 1989]. Measurements with source (SRC) indicated by IGS2 are measurements made by the Indiana Geological Survey and published in [*Bauer*, 1997]. IGS1 measurements are new unpublished measurements made by the Indiana Geological Survey.

ID	UTM_X	UTM_Y	MAP SYMBOL AND DESCRIPTION		SRC	LOCATION	Vs ft/sec	Vs m/sec	unit type
17	552660	4384953	a	Alluvium	IGS2	Morgan	1037	316	Alluvial
18	547303	4365333	a	Alluvium	IGS2	Morgan	1096	334	Alluvial
19	547298	4365325	a	Alluvium	IGS2	Morgan	961	293	Alluvial
--	--	--	--	--	IGS1	Jasper	704	215	Alluvial
--	--	--	--	--	IGS1	Huntingburg	790	241	Alluvial
--	--	--	--	--	IGS1	Newburgh	701	214	Alluvial
--	--	--	--	--	IGS1	Wheatland	762	232	Alluvial
--	--	--	--	--	IGS1	Oaktown	825	251	Alluvial
--	--	--	--	--	IGS1	Carlisle	743	208	Alluvial
--	--	--	--	--	IGS1	S. Evansville	840	256	Alluvial
--	--	--	--	--	IGS1	Vincennes	939	286	Alluvial
--	--	--	--	--	IGS1	Vincennes	728	222	Alluvial
								256	Average velocity
								41	standard deviation
4	461868	4302620	s	Dune sand	IGS2	Knox	863	263	Eolian Sand
--	--	--	--	--	IGS1	Newburgh	695	212	Eolian Sand
--	--	--	--	--	IGS1	Newburgh	882	299	Eolian Sand
--	--	--	--	--	IGS1	N. Evansville	599	183	Eolian Sand
--	--	--	--	--	IGS1	S. Evansville	729	222	Eolian Sand
--	--	--	--	--	IGS1	S. Evansville	696	212	Eolian Sand
--	--	--	--	--	IGS1	S. Evansville	1156	353	Eolian Sand
								249	Average velocity
								59	standard deviation
--	--	--	--	--	IGS1	Jasper	629	192	Lacustrine
--	--	--	--	--	IGS1	Huntingburg	809	247	Lacustrine
--	--	--	--	--	IGS1	N. Evansville	569	174	Lacustrine
--	--	--	--	--	IGS1	S. Evansville	639	195	Lacustrine
								202	Average velocity
								31	standard deviation
3	461346	4281670	lo	Loess	IGS2	Knox	781	238	Loess
5	465431	4312230	lo	Loess	IGS2	Sullivan	515	157	Loess
6	465360	4327487	lo	Loess	IGS2	Sullivan	522	159	Loess
7	467220	4344919	lo	Loess	IGS2	Sullivan	656	200	Loess
8	467207	4351260	lo	Loess	IGS2	Vigo	705	215	Loess
--	--	--	--	--	IGS1	Newburgh	857	261	Loess

--	--	--	--	--	IGS1	Newburgh	907	264	Loess
--	--	--	--	--	IGS1	N. Evansville	800	244	Loess
--	--	--	--	--	IGS1	Wheatland	566	172	Loess
--	--	--	--	--	IGS1	Oaktown	683	208	Loess
--	--	--	--	--	IGS1	Carlisle	561	171	Loess
								208	Average velocity
								40	standard deviation
1	442297	4246753	o	Undifferentiated outwash	IGS2	Gibson	653	199	outwash
2	454123	4263628	o	Undifferentiated outwash	IGS2	Knox	719	219	outwash
9	448647	4203517	o	Undifferentiated outwash	IGS2	Vanderburgh	781	238	outwash
10	448648	4203518	o	Undifferentiated outwash	IGS2	Vanderburgh	755	230	outwash
11	448649	4203519	o	Undifferentiated outwash	IGS2	Vanderburgh	738	225	outwash
20	507753	4599142	of	Outwash-fan	IGS2	La Porte	791	241	outwash
21	575188	4619110	o	Undifferentiated outwash	IGS2	St. Joseph	840	256	outwash
								230	Average velocity
								18	standard deviation
12	640577	4460209	tc	Silty clay-loam to clay-loam till	IGS2	Delaware	965	294	till
14	538818	4462182	tb	Loam till	IGS2	Clinton	1253	382	till
16	601182	4513667	tc	Silty clay-loam to clay-loam till	IGS2	Wabash	1017	310	till
22	505088	4476490	tb	Loam till	IGS2	Tippecanoe	1066	325	till
23	505093	4476452	tb	Loam till	IGS2	Tippecanoe	1142	348	till
24	505128	4476467	tb	Loam till	IGS2	Tippecanoe	1293	394	till
25	505112	4476475	tb	Loam till	IGS2	Tippecanoe	1247	380	till
26	681116	4472522	tc	Silty clay-loam to clay-loam till	IGS2	Jay	1181	360	till
27	671063	4479721	tc	Silty clay-loam to clay-loam till	IGS2	Jay	1165	355	till
								350	Average velocity
								34	standard deviation
				Other Units					
28	471642	4600741	ls	Lake sand	IGS2	Lake	2021	616	lake sand
15	586500	4305100	4	Siltstone and shale	IGS2	Jackson	899	274	siltstone and shale
13	541241	4336168	3T	Terra rossa	IGS2	Monroe	2927	892	terra rossa

Table 1-5 Seismic hazard levels defined in table 3.10.3-1 of the proposed bridge design guidelines. S1 and Ss are the 1 sec and 0.2 sec period spectral acceleration responses, respectively. Fa and Fv are site coefficients described in Article 3.10.2.2.3 [*ATC/MCEER*, 2003].

Seismic Hazard Level	Value of FvS1 (S1=1 Hz spectral accel.)	Value of FaSs (Ss = 5 Hz spectral accel.)
I	FvS1 <= 0.15	FaSs <= 0.15
II	0.15 < FvS1 <= 0.25	0.15 < FaSs <= 0.35
III	0.25 < FvS1 <= 0.40	0.35 < FaSs <= 0.60
IV	0.40 < FvS1	0.60 < FaSs

Table 1-6 Value of Fa as a function of site class and mapped short-period spectral acceleration (From Table 3.4.2.3-1 of the Recommended LRFD Guidelines for the Seismic Design of Highway Bridges (ATC/MCEER, 2003)

Site Class	Mapped Spectral Response Acceleration at Short Periods				
	Ss≤0.25g	Ss=0.50g	Ss=0.75g	Ss=1.00g	Ss≥1.25g
A	0.8	0.8	0.8	0.8	0.8
B	1.0	1.0	1.0	1.0	1.0
C	1.2	1.2	1.1	1.0	1.0
D	1.6	1.4	1.2	1.1	1.0
E	2.5	1.7	1.2	0.9	0.9
F	a	a	a	a	a

Table 1-7 Value of Fv as a function of site class and mapped 1 second period spectral acceleration (From Table 3.4.2.3-2 of the Recommended LRFD Guidelines for the Seismic Design of Highway Bridges (ATC/MCEER, 2003)

Site Class	Mapped Spectral Response Acceleration at 1 second Periods				
	Ss≤0.1g	Ss=0.2g	Ss=0.3g	Ss=0.4g	Ss≥0.5g
A	0.8	0.8	0.8	0.8	0.8
B	1.0	1.0	1.0	1.0	1.0
C	1.7	1.6	1.5	1.4	1.3
D	2.4	2.0	1.8	1.6	1.5
E	3.5	3.2	2.8	2.4	2.4
F	a	a	a	a	a

Table 1-8 Seismic hazard level for USGS 2002 maps with no site effects (default B/C classification) using criteria described in Table 1-5 (ATC/MCEER, 2003).

No.	NAME	1Hz	5Hz	Maximum of 1Hz and 5Hz
1	ADAMS	1	2	2
2	ALLEN	1	2	2
3	BARTHOLOMEW	1	2	2
4	BENTON	1	2	2
5	BLACKFORD	1	2	2
6	BOONE	1	2	2
7	BROWN	1	2	2
8	CARROLL	1	2	2
9	CASS	1	2	2
10	CLARK	1	2	2
11	CLAY	1	3	3
12	CLINTON	1	2	2
13	CRAWFORD	1	2	2
14	DAVIESS	1	3	3
15	DEARBORN	1	2	2
16	DECATUR	1	2	2
17	DEKALB	1	1	1
18	DELAWARE	1	2	2
19	DUBOIS	1	3	3
20	ELKHART	1	1	1
21	FAYETTE	1	2	2
22	FLOYD	1	2	2
23	FOUNTAIN	1	2	2
24	FRANKLIN	1	2	2
25	FULTON	1	1	1
26	GIBSON	2	4	4
27	GRANT	1	2	2
28	GREENE	1	3	3
29	HAMILTON	1	2	2
30	HANCOCK	1	2	2
31	HARRISON	1	2	2
32	HENDRICKS	1	2	2
33	HENRY	1	2	2
34	HOWARD	1	2	2
35	HUNTINGTON	1	2	2
36	JACKSON	1	2	2
37	JASPER	1	2	2
38	JAY	1	2	2
39	JEFFERSON	1	2	2
40	JENNINGS	1	2	2
41	JOHNSON	1	2	2
42	KNOX	2	4	4
43	KOSCIUSKO	1	1	1
44	LAGRANGE	1	1	1
45	LAKE	1	2	2
46	LAPORTE	1	1	1
47	LAWRENCE	1	2	2
48	MADISON	1	2	2
49	MARION	1	2	2

50	MARSHALL	1	1	1
51	MARTIN	1	3	3
52	MIAMI	1	1	1
53	MONROE	1	2	2
54	MONTGOMERY	1	2	2
55	MORGAN	1	2	2
56	NEWTON	1	2	2
57	NOBLE	1	1	1
58	OHIO	1	2	2
59	ORANGE	1	2	2
60	OWEN	1	2	2
61	PARKE	1	2	2
62	PERRY	1	3	3
63	PIKE	2	3	3
64	PORTER	1	2	2
65	POSEY	2	4	4
66	PULASKI	1	1	1
67	PUTNAM	1	2	2
68	RANDOLPH	1	2	2
69	RIPLEY	1	2	2
70	RUSH	1	2	2
71	SCOTT	1	2	2
72	SHELBY	1	2	2
73	SPENCER	2	3	3
74	ST JOSEPH	1	1	1
75	STARKE	1	1	1
76	STEUBEN	1	1	1
77	SULLIVAN	1	3	3
78	SWITZERLAND	1	2	2
79	TIPPECANOE	1	2	2
80	TIPTON	1	2	2
81	UNION	1	2	2
82	VANDERBURGH	2	4	4
83	VERMILLION	1	2	2
84	VIGO	1	3	3
85	WABASH	1	1	1
86	WARREN	1	2	2
87	WARRICK	2	4	4
88	WASHINGTON	1	2	2
89	WAYNE	1	2	2
90	WELLS	1	2	2
91	WHITE	1	2	2
92	WHITLEY	1	1	1

Table 1-9 Seismic hazard level for USGS 2002 maps with Class D site effects using criteria described in Table 1-5, Table 1-6, and Table 1-7 (ATC/MCEER, 2003).

No.	NAME	F_v	F_a	F_vS_1	F_aS_s	Maximum of F_vS_1 and F_aS_s
1	ADAMS	2.4	1.6	2	2	2
2	ALLEN	2.4	1.6	1	2	2
3	BARTHOLOMEW	2.4	1.6	2	3	3
4	BENTON	2.4	1.6	2	2	2
5	BLACKFORD	2.4	1.6	2	2	2
6	BOONE	2.4	1.6	2	2	2
7	BROWN	2.4	1.6	2	3	3
8	CARROLL	2.4	1.6	2	2	2
9	CASS	2.4	1.6	2	2	2
10	CLARK	2.4	1.6	2	3	3
11	CLAY	2.3	1.5	3	3	3
12	CLINTON	2.4	1.6	2	2	2
13	CRAWFORD	2.3	1.5	3	3	3
14	DAVIESS	2.2	1.4	3	4	4
15	DEARBORN	2.4	1.6	2	2	2
16	DECATUR	2.4	1.6	2	2	2
17	DEKALB	2.4	1.6	1	2	2
18	DELAWARE	2.4	1.6	2	2	2
19	DUBOIS	2.2	1.4	3	4	4
20	ELKHART	2.4	1.6	1	2	2
21	FAYETTE	2.4	1.6	2	2	2
22	FLOYD	2.4	1.6	3	3	3
23	FOUNTAIN	2.4	1.6	2	3	3
24	FRANKLIN	2.4	1.6	2	2	2
25	FULTON	2.4	1.6	2	2	2
26	GIBSON	2.0	1.2	3	4	4
27	GRANT	2.4	1.6	2	2	2
28	GREENE	2.3	1.5	3	4	4
29	HAMILTON	2.4	1.6	2	2	2
30	HANCOCK	2.4	1.6	2	2	2
31	HARRISON	2.3	1.5	3	3	3
32	HENDRICKS	2.4	1.6	2	3	3
33	HENRY	2.4	1.6	2	2	2
34	HOWARD	2.4	1.6	2	2	2
35	HUNTINGTON	2.4	1.6	2	2	2
36	JACKSON	2.4	1.6	2	3	3
37	JASPER	2.4	1.6	2	2	2
38	JAY	2.4	1.6	2	2	2
39	JEFFERSON	2.4	1.6	2	2	2
40	JENNINGS	2.4	1.6	2	2	2
41	JOHNSON	2.4	1.6	2	2	2
42	KNOX	2.1	1.3	3	4	4
43	KOSCIUSKO	2.4	1.6	1	2	2
44	LAGRANGE	2.4	1.6	1	2	2
45	LAKE	2.4	1.6	2	2	2
46	LAPORTE	2.4	1.6	1	2	2
47	LAWRENCE	2.3	1.5	3	3	3

48	MADISON	2.4	1.6	2	2	2
49	MARION	2.4	1.6	2	2	2
50	MARSHALL	2.4	1.6	1	2	2
51	MARTIN	2.3	1.5	3	3	3
52	MIAMI	2.4	1.6	2	2	2
53	MONROE	2.4	1.6	3	3	3
54	MONTGOMERY	2.4	1.6	2	3	3
55	MORGAN	2.4	1.6	2	3	3
56	NEWTON	2.4	1.6	2	2	2
57	NOBLE	2.4	1.6	1	2	2
58	OHIO	2.4	1.6	2	2	2
59	ORANGE	2.3	1.5	3	3	3
60	OWEN	2.3	1.5	3	3	3
61	PARKE	2.4	1.6	2	3	3
62	PERRY	2.2	1.5	3	3	3
63	PIKE	2.1	1.3	3	4	4
64	PORTER	2.4	1.6	2	2	2
65	POSEY	1.9	1.2	4	4	4
66	PULASKI	2.4	1.6	2	2	2
67	PUTNAM	2.4	1.6	2	3	3
68	RANDOLPH	2.4	1.6	2	2	2
69	RIPLEY	2.4	1.6	2	2	2
70	RUSH	2.4	1.6	2	2	2
71	SCOTT	2.4	1.6	2	3	3
72	SHELBY	2.4	1.6	2	2	2
73	SPENCER	2.1	1.4	3	4	4
74	ST JOSEPH	2.4	1.6	1	2	2
75	STARKE	2.4	1.6	2	2	2
76	STEUBEN	2.4	1.6	1	2	2
77	SULLIVAN	2.2	1.4	3	4	4
78	SWITZERLAND	2.4	1.6	2	2	2
79	TIPPECANOE	2.4	1.6	2	2	2
80	TIPTON	2.4	1.6	2	2	2
81	UNION	2.4	1.6	2	2	2
82	VANDERBURGH	2.0	1.2	4	4	4
83	VERMILLION	2.4	1.6	2	3	3
84	VIGO	2.3	1.5	3	3	3
85	WABASH	2.4	1.6	2	2	2
86	WARREN	2.4	1.6	2	2	2
87	WARRICK	2.1	1.3	3	4	4
88	WASHINGTON	2.4	1.6	3	3	3
89	WAYNE	2.4	1.6	2	2	2
90	WELLS	2.4	1.6	2	2	2
91	WHITE	2.4	1.6	2	2	2
92	WHITLEY	2.4	1.6	1	2	2

Table 1-10 Seismic hazard level for probabilitistic site effects hazard analysis using the criteria described in Table 1-5 (ATC/MCEER, 2003).

No.	NAME	1Hz	5Hz	maximum of 1Hz and 5 Hz
1	ADAMS	1	3	3
2	ALLEN	1	3	3
3	BARTHOLOMEW	1	3	3
4	BENTON	2	2	2
5	BLACKFORD	1	2	2
6	BOONE	2	2	2
7	BROWN	1	2	2
8	CARROLL	2	2	2
9	CASS	2	2	2
10	CLARK	1	2	2
11	CLAY	1	3	3
12	CLINTON	2	2	2
13	CRAWFORD	1	2	2
14	DAVIESS	2	3	3
15	DEARBORN	1	2	2
16	DECATUR	1	2	2
17	DEKALB	2	2	2
18	DELAWARE	2	2	2
19	DUBOIS	1	2	2
20	ELKHART	2	1	2
21	FAYETTE	1	2	2
22	FLOYD	1	2	2
23	FOUNTAIN	2	2	2
24	FRANKLIN	1	2	2
25	FULTON	2	2	2
26	GIBSON	2	4	4
27	GRANT	1	2	2
28	GREENE	1	3	3
29	HAMILTON	2	2	2
30	HANCOCK	2	2	2
31	HARRISON	1	2	2
32	HENDRICKS	2	3	3
33	HENRY	2	2	2
34	HOWARD	1	3	3
35	HUNTINGTON	1	2	2
36	JACKSON	1	3	3
37	JASPER	1	3	3
38	JAY	1	2	2
39	JEFFERSON	1	3	3
40	JENNINGS	1	2	2
41	JOHNSON	2	2	2
42	KNOX	2	3	3
43	KOSCIUSKO	2	2	2
44	LAGRANGE	2	1	2
45	LAKE	1	2	2
46	LAPORTE	1	2	2
47	LAWRENCE	1	2	2

48	MADISON	1	2	2
49	MARION	2	2	2
50	MARSHALL	2	2	2
51	MARTIN	1	2	2
52	MIAMI	2	2	2
53	MONROE	1	2	2
54	MONTGOMERY	2	2	2
55	MORGAN	1	3	3
56	NEWTON	1	2	2
57	NOBLE	2	2	2
58	OHIO	1	2	2
59	ORANGE	1	2	2
60	OWEN	1	3	3
61	PARKE	2	2	2
62	PERRY	1	2	2
63	PIKE	2	3	3
64	PORTER	2	2	2
65	POSEY	4	4	4
66	PULASKI	2	2	2
67	PUTNAM	1	3	3
68	RANDOLPH	2	2	2
69	RIPLEY	1	3	3
70	RUSH	1	3	3
71	SCOTT	1	3	3
72	SHELBY	2	3	3
73	SPENCER	2	3	3
74	ST JOSEPH	2	1	2
75	STARKE	2	2	2
76	STEUBEN	2	2	2
77	SULLIVAN	1	3	3
78	SWITZERLAND	1	2	2
79	TIPPECANOE	2	2	2
80	TIPTON	1	2	2
81	UNION	1	2	2
82	VANDERBURGH	3	4	4
83	VERMILLION	2	2	2
84	VIGO	1	3	3
85	WABASH	2	2	2
86	WARREN	2	2	2
87	WARRICK	2	4	4
88	WASHINGTON	1	2	2
89	WAYNE	2	2	2
90	WELLS	1	3	3
91	WHITE	2	2	2
92	WHITLEY	2	2	2

Table 1-11 Comparison of seismic hazard level estimated from USGS 2002, USGS2002 with Class D site effects, and for probabilitistic site effect hazard analysis.

No.	NAME	USGS2002	LRFD, D Site	Probabilistic site effects analysis
1	ADAMS	2	2	3
2	ALLEN	2	2	3
3	BARTHOLOMEW	2	3	3
4	BENTON	2	2	2
5	BLACKFORD	2	2	2
6	BOONE	2	2	2
7	BROWN	2	3	2
8	CARROLL	2	2	2
9	CASS	2	2	2
10	CLARK	2	3	2
11	CLAY	3	3	3
12	CLINTON	2	2	2
13	CRAWFORD	2	3	2
14	DAVIESS	3	4	3
15	DEARBORN	2	2	2
16	DECATUR	2	2	2
17	DEKALB	1	2	2
18	DELAWARE	2	2	2
19	DUBOIS	3	4	2
20	ELKHART	1	2	2
21	FAYETTE	2	2	2
22	FLOYD	2	3	2
23	FOUNTAIN	2	3	2
24	FRANKLIN	2	2	2
25	FULTON	1	2	2
26	GIBSON	4	4	4
27	GRANT	2	2	2
28	GREENE	3	4	3
29	HAMILTON	2	2	2
30	HANCOCK	2	2	2
31	HARRISON	2	3	2
32	HENDRICKS	2	3	3
33	HENRY	2	2	2
34	HOWARD	2	2	3
35	HUNTINGTON	2	2	2
36	JACKSON	2	3	3
37	JASPER	2	2	3
38	JAY	2	2	2
39	JEFFERSON	2	2	3
40	JENNINGS	2	2	2
41	JOHNSON	2	2	2
42	KNOX	4	4	3
43	KOSCIUSKO	1	2	2
44	LAGRANGE	1	2	2
45	LAKE	2	2	2
46	LAPORTE	1	2	2

47	LAWRENCE	2	3	2
48	MADISON	2	2	2
49	MARION	2	2	2
50	MARSHALL	1	2	2
51	MARTIN	3	3	2
52	MIAMI	1	2	2
53	MONROE	2	3	2
54	MONTGOMERY	2	3	2
55	MORGAN	2	3	3
56	NEWTON	2	2	2
57	NOBLE	1	2	2
58	OHIO	2	2	2
59	ORANGE	2	3	2
60	OWEN	2	3	3
61	PARKE	2	3	2
62	PERRY	3	3	2
63	PIKE	3	4	3
64	PORTER	2	2	2
65	POSEY	4	4	4
66	PULASKI	1	2	2
67	PUTNAM	2	3	3
68	RANDOLPH	2	2	2
69	RIPLEY	2	2	3
70	RUSH	2	2	3
71	SCOTT	2	3	3
72	SHELBY	2	2	3
73	SPENCER	3	4	3
74	ST JOSEPH	1	2	2
75	STARKE	1	2	2
76	STEUBEN	1	2	2
77	SULLIVAN	3	4	3
78	SWITZERLAND	2	2	2
79	TIPPECANOE	2	2	2
80	TIPTON	2	2	2
81	UNION	2	2	2
82	VANDERBURGH	4	4	4
83	VERMILLION	2	3	2
84	VIGO	3	3	3
85	WABASH	1	2	2
86	WARREN	2	2	2
87	WARRICK	4	4	4
88	WASHINGTON	2	3	2
89	WAYNE	2	2	2
90	WELLS	2	2	3
91	WHITE	2	2	2
92	WHITLEY	1	2	2

Table 1-12 Number of counties estimated at each seismic hazard level.

Maximum of 5 Hz and 1 Hz seismic hazard level	Number of counties for 2002 USGS map with default B/C site effects	Number of counties for 2002 USGS with class D site effects	Number of counties for map including probabilistic site effects
I	15	0	0
II	62	57	64
III	20	24	24
IV	5	11	4

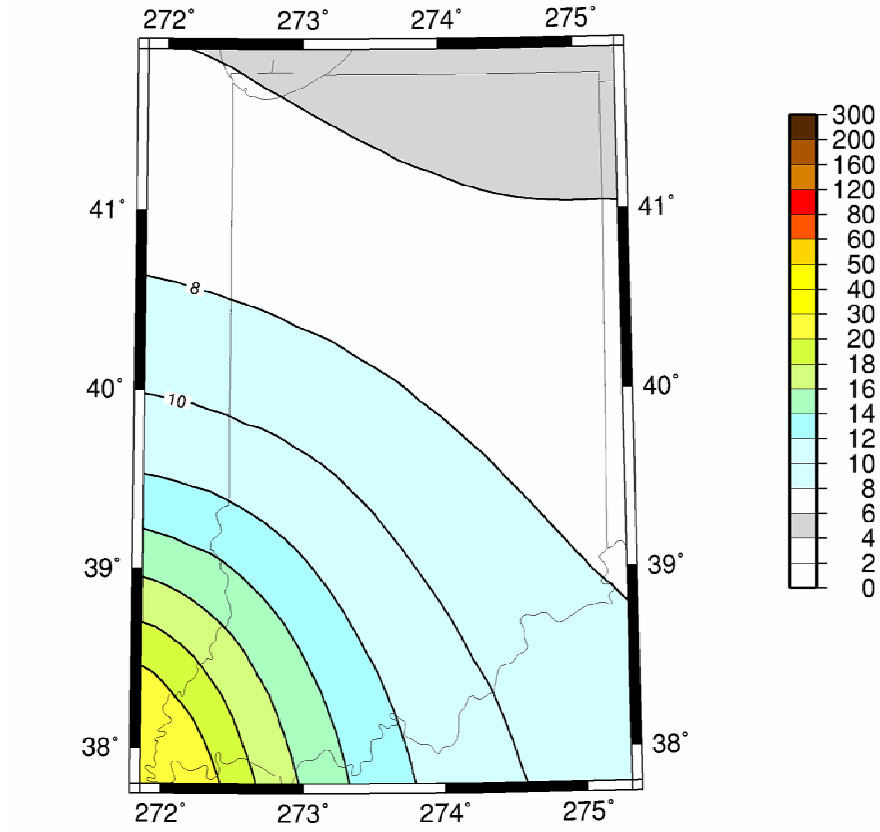

Figure 1-1 2002 USGS map of the probabilistic seismic hazard with 2% probability of exceedence in 50 years at *1* Hz spectral acceleration, which includes by default the site response for a NEHRP B/C site classification.

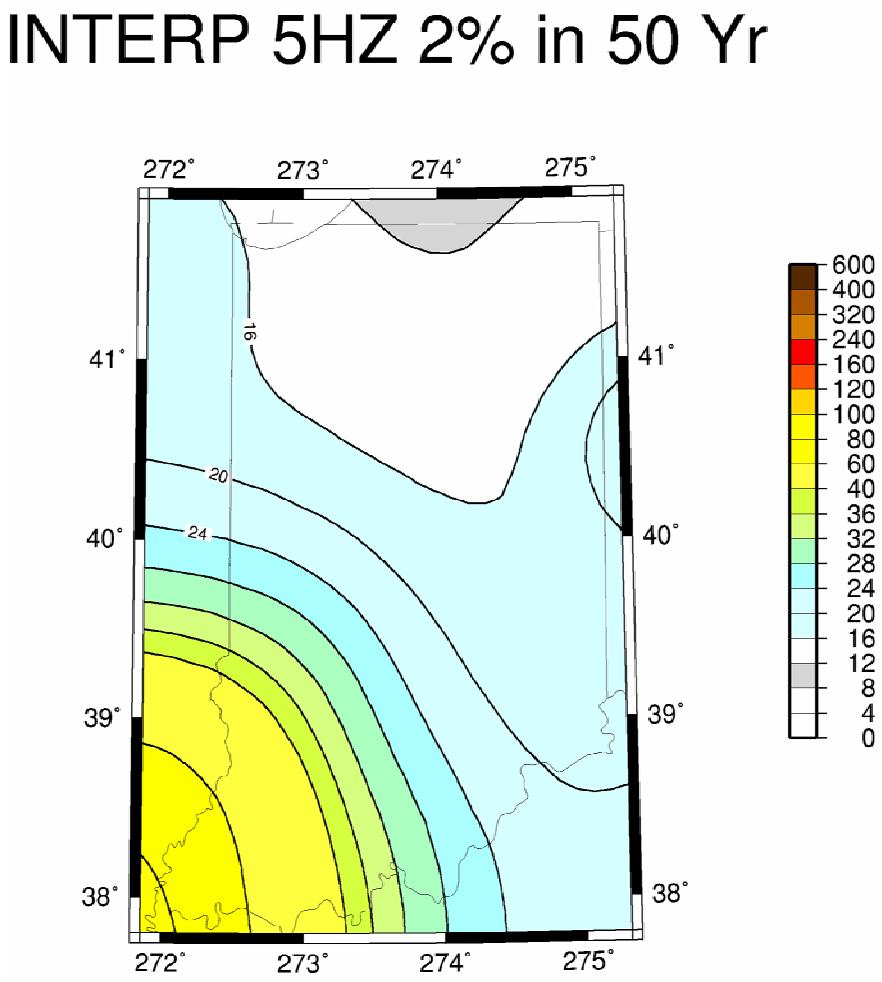

Figure 1-2 2002 USGS map of the probabilistic seismic hazard with 2% probability of exceedence in 50 years at *5 Hz spectral acceleration,* which includes by default the site response for a NEHRP B/C site classification.

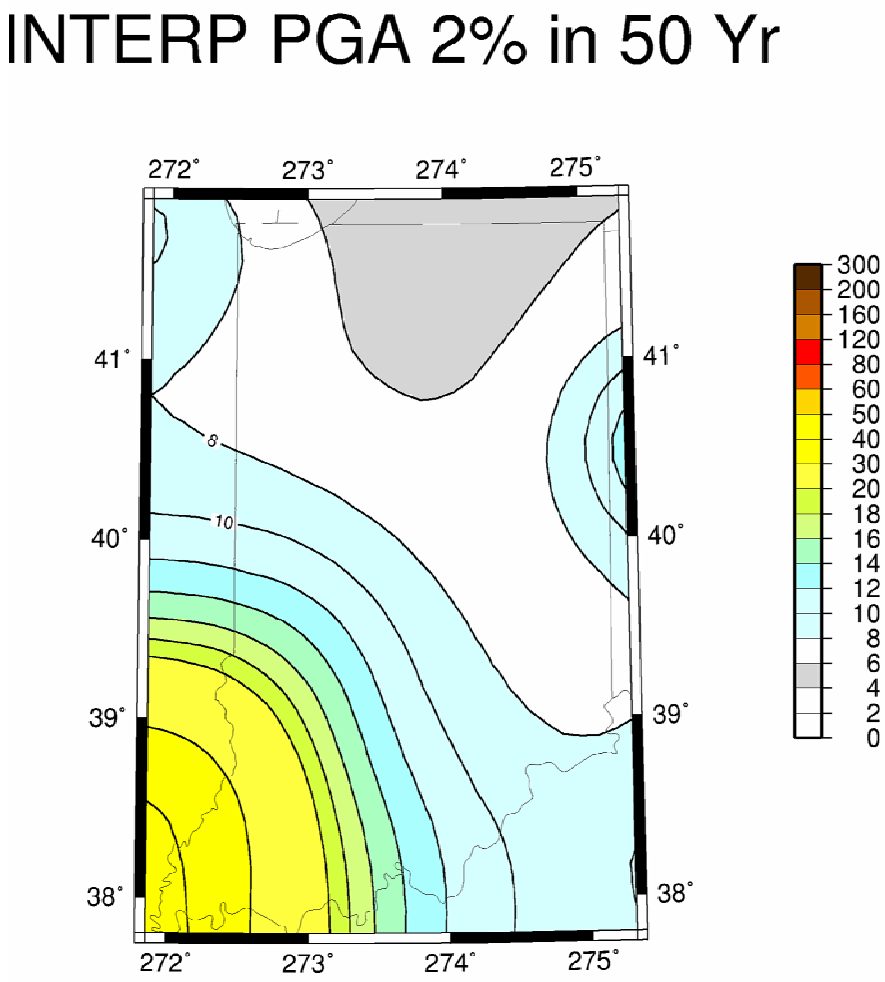

Figure 1-3 2002 USGS map of the probabilistic seismic hazard with 2% probability of exceedence in 50 years for *peak ground acceleration (PGA),* which includes by default the site response for a NEHRP B/C site classification.

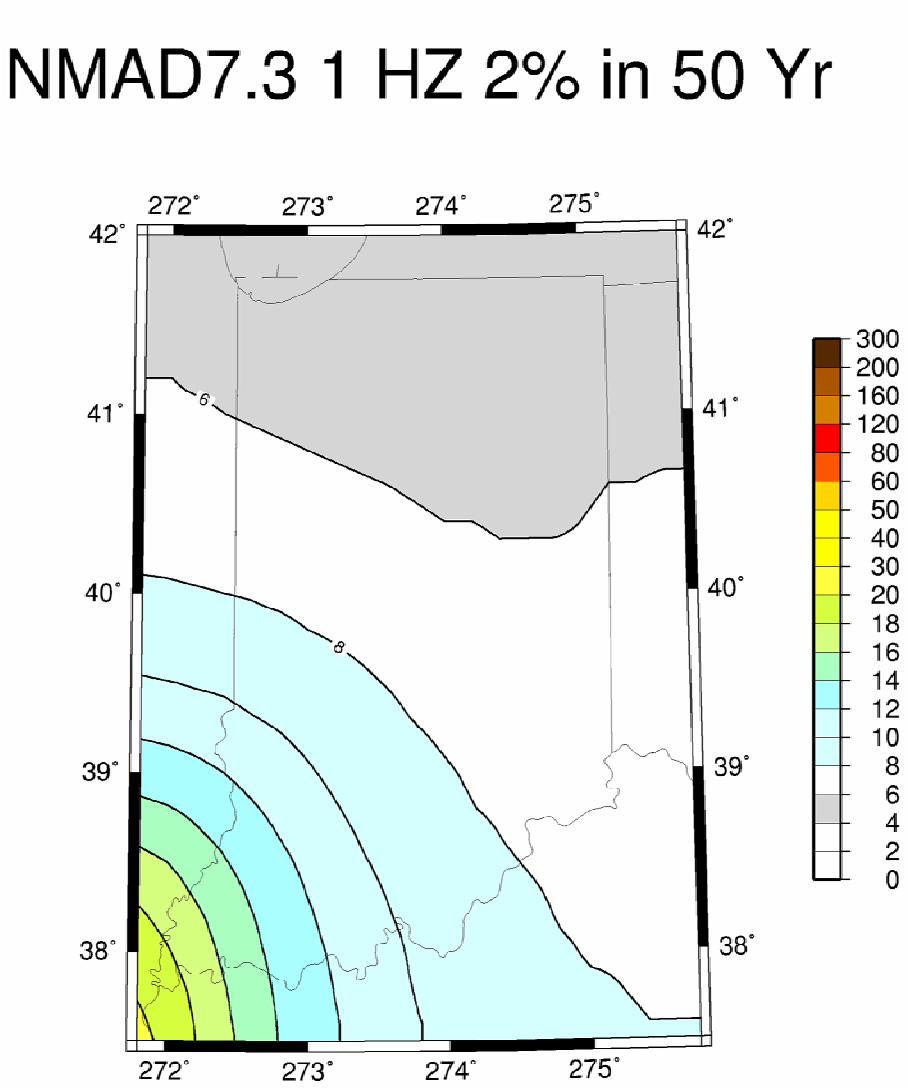

Figure 1-4 Simulation of the USGS map of the probabilistic seismic hazard with 2% probability of exceedence in 50 years at *1* Hz spectral acceleration, where the maximum magnitude of the New Madrid type earthquake has been set to 7.3.

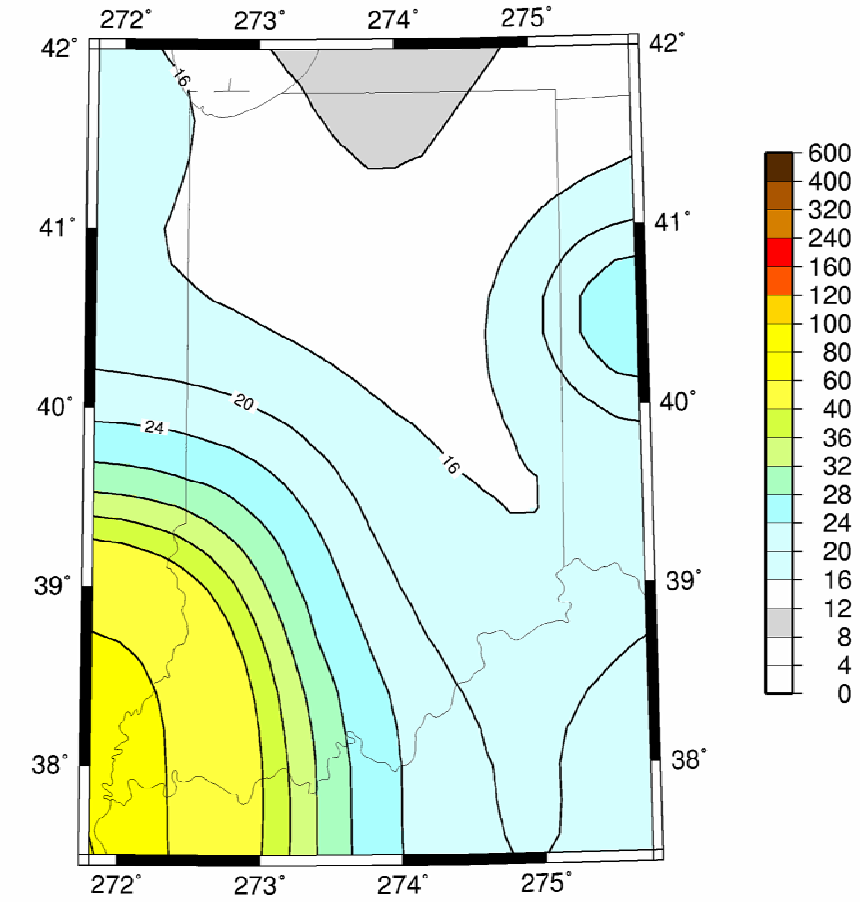

Figure 1-5 Simulation of the USGS map of the probabilistic seismic hazard with 2% probability of exceedence in 50 years at *5 Hz spectral acceleration,* where the maximum magnitude of the New Madrid type earthquake has been set to 7.3.

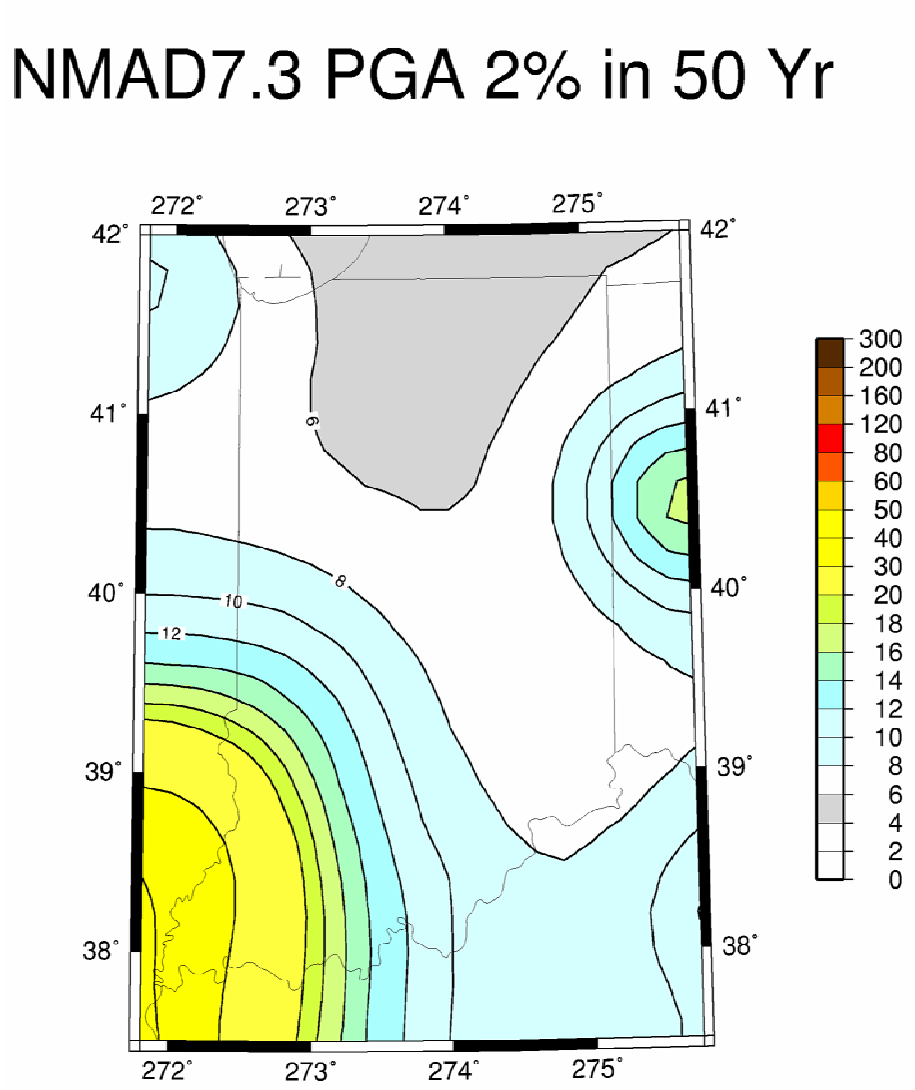

Figure 1-6 Simulation of the USGS map of the probabilistic seismic hazard with 2% probability of exceedence in 50 years for *peak ground acceleration (PGA),* where the maximum magnitude of the New Madrid type earthquake has been set to 7.3.

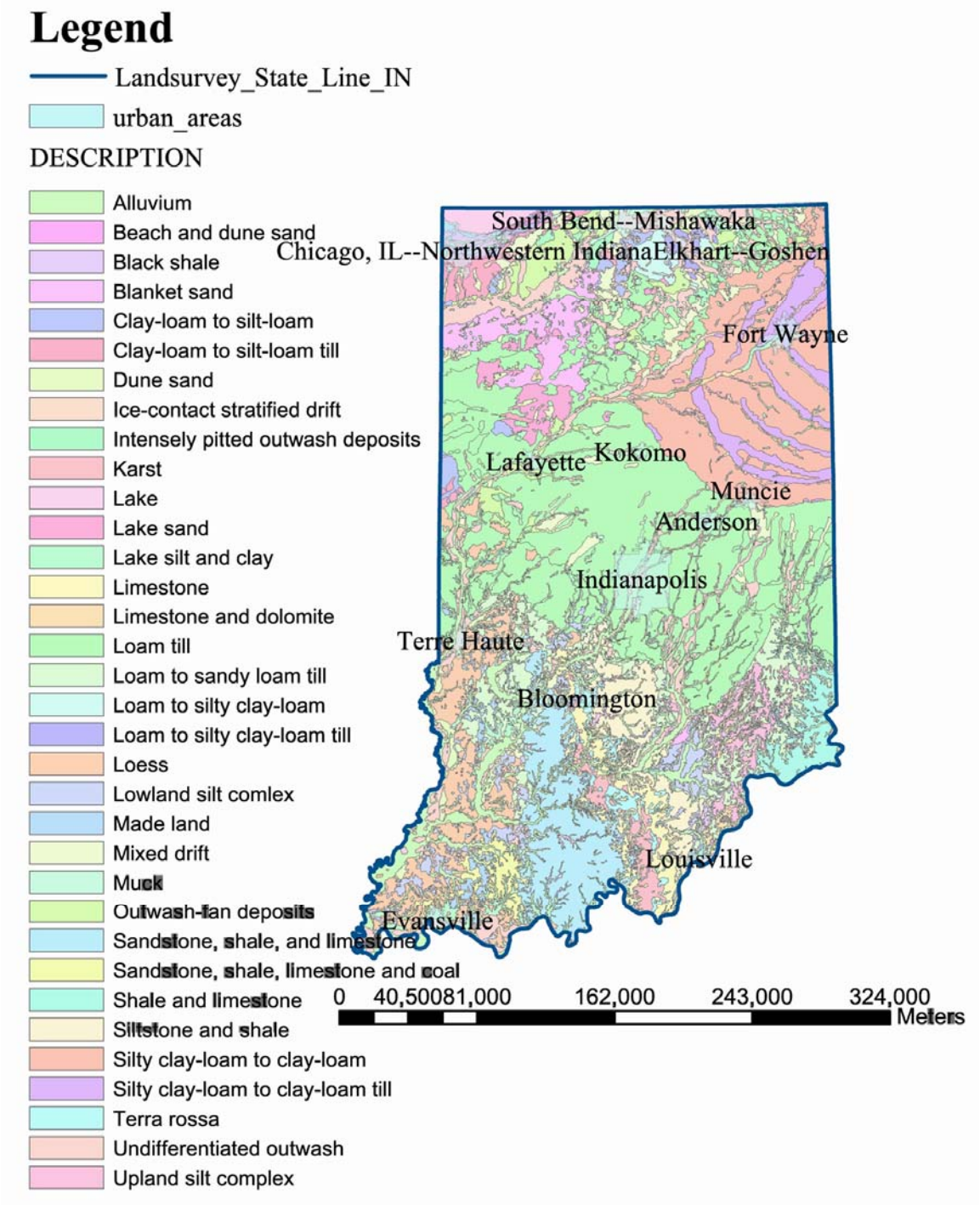

Figure 1-7 Surficial geology map of Indiana [*Gray*, 1989].

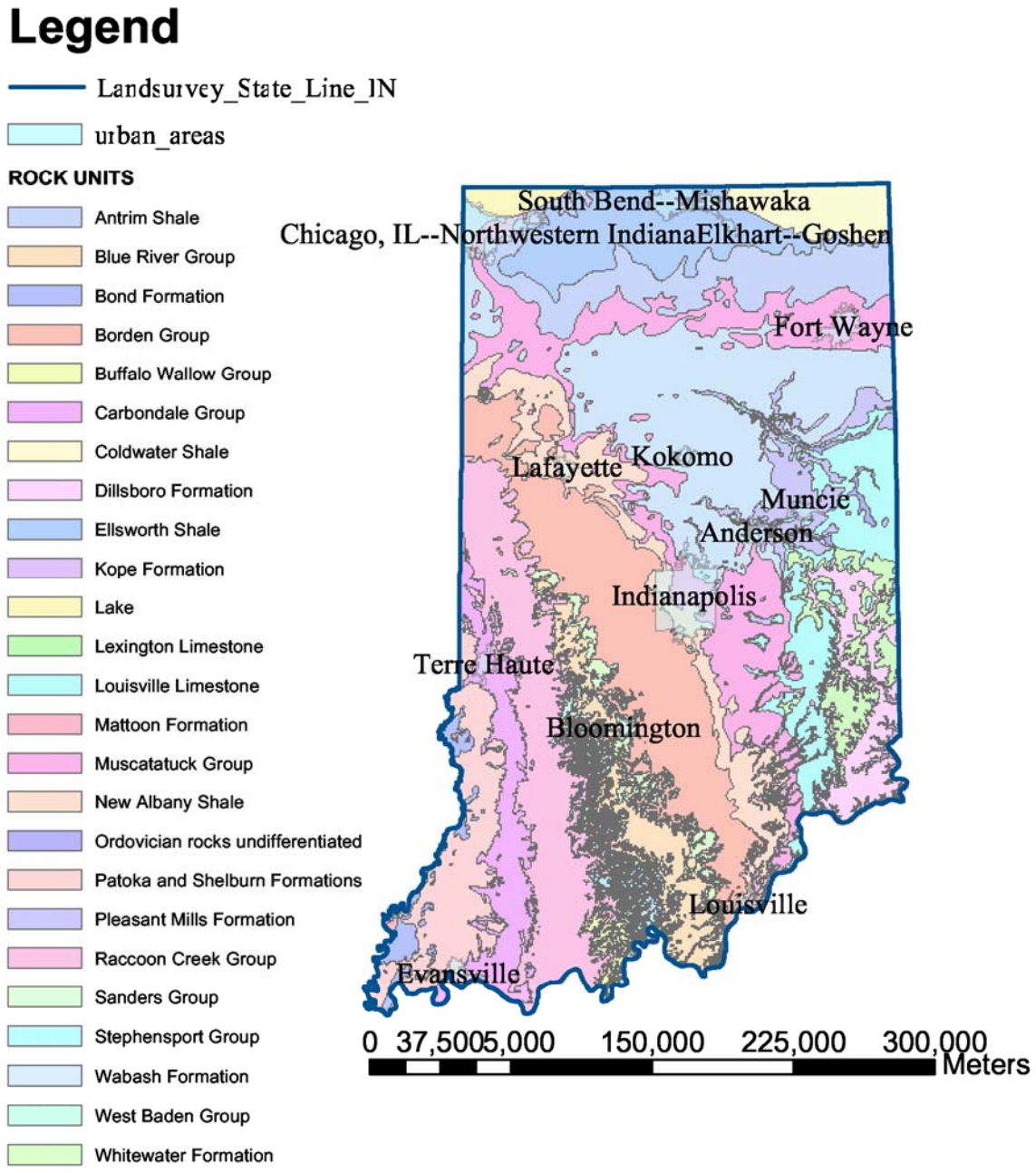

Figure 1-8 Bedrock geology map of Indiana [*Gray*, 1989].

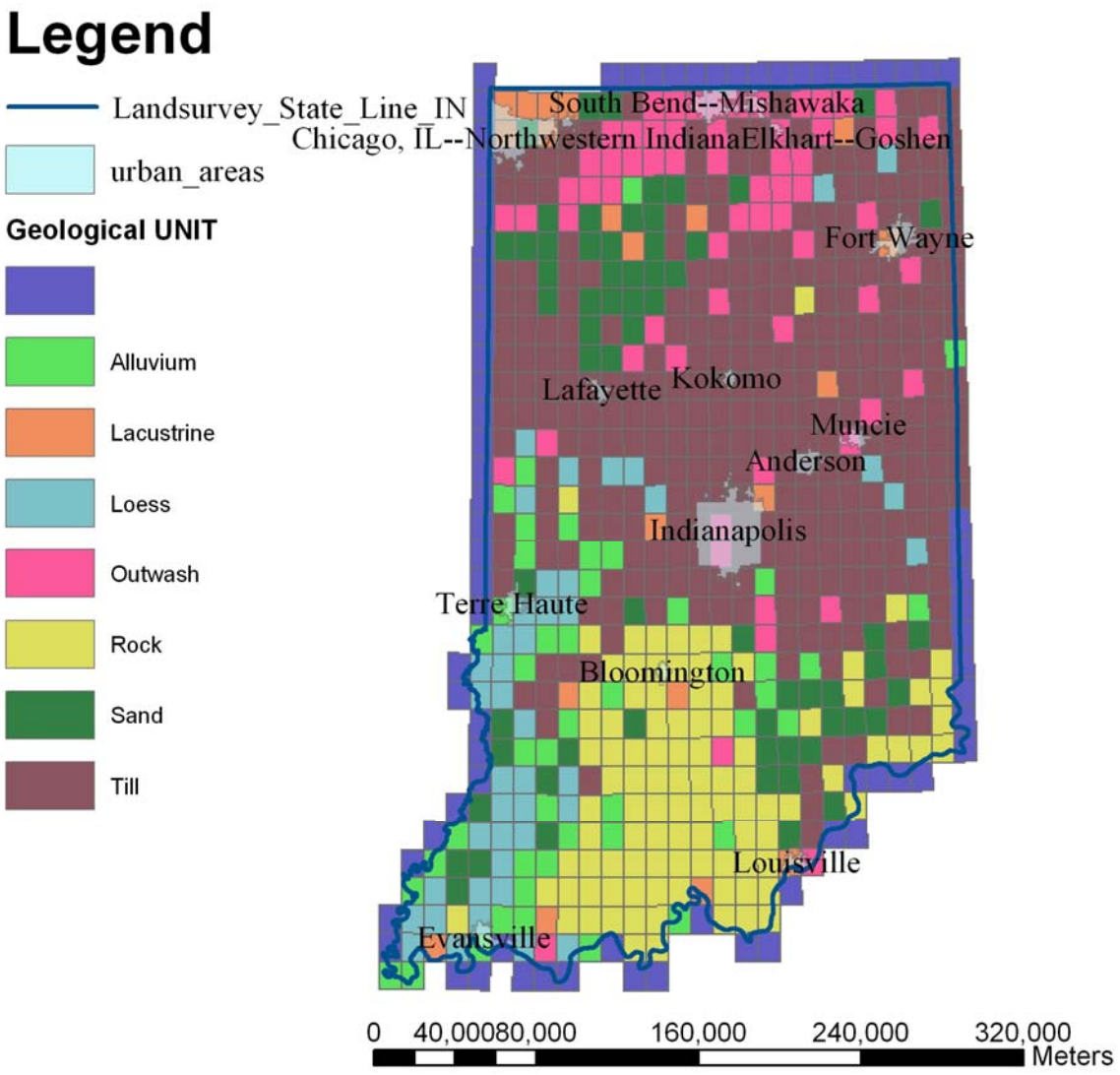

Figure 1-9 Surficial material type map, simplified from the surfical geology map. The original surficial geologic units have been grouped by material type given in Table 1-1.

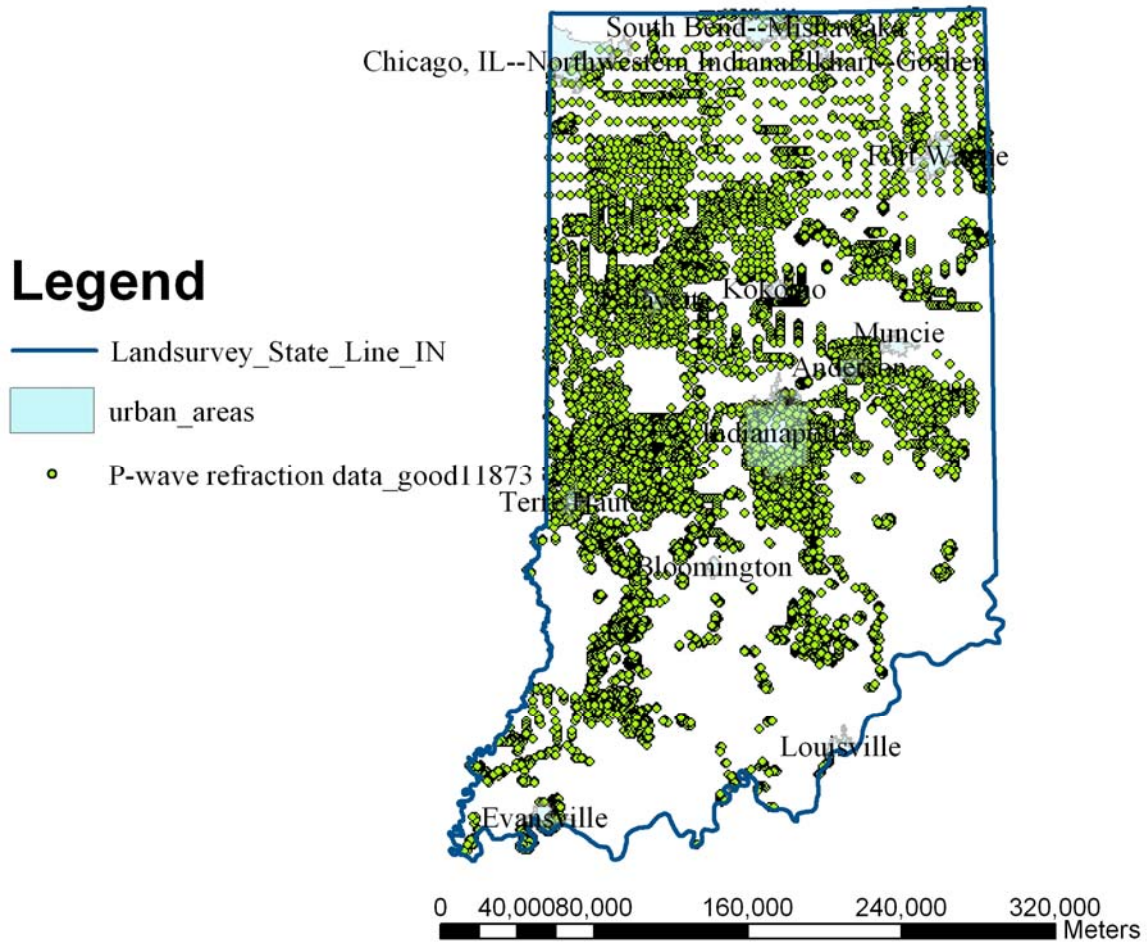

Figure 1-10 Map of locations of 11873 P-wave refraction profiles, and 28 borehole S-wave velocity profiles.

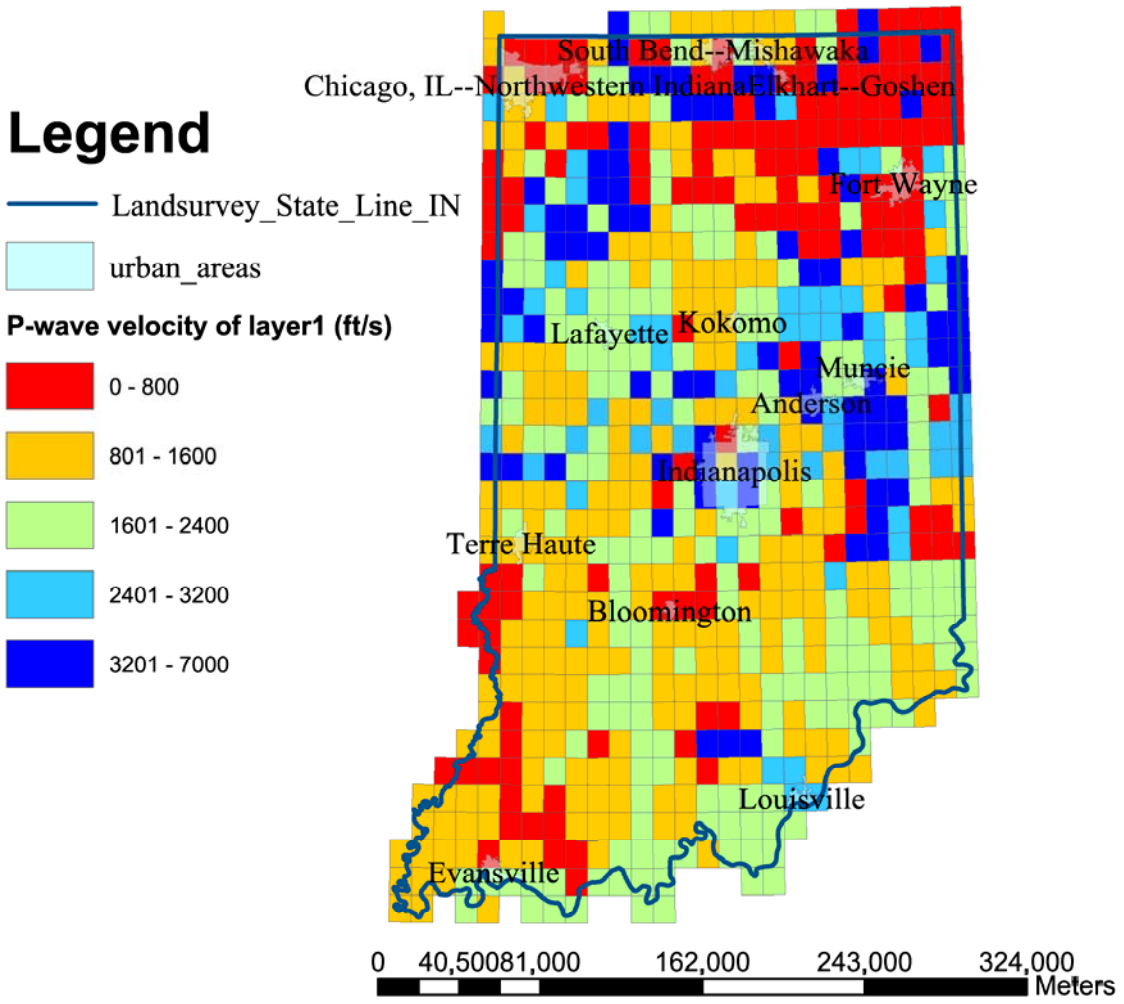

Figure 1-11 Average P-wave velocity in the near surface layer (Layer 1) for each 0.125 degree quadrangle. There is little correspondence with the surficial geology map.

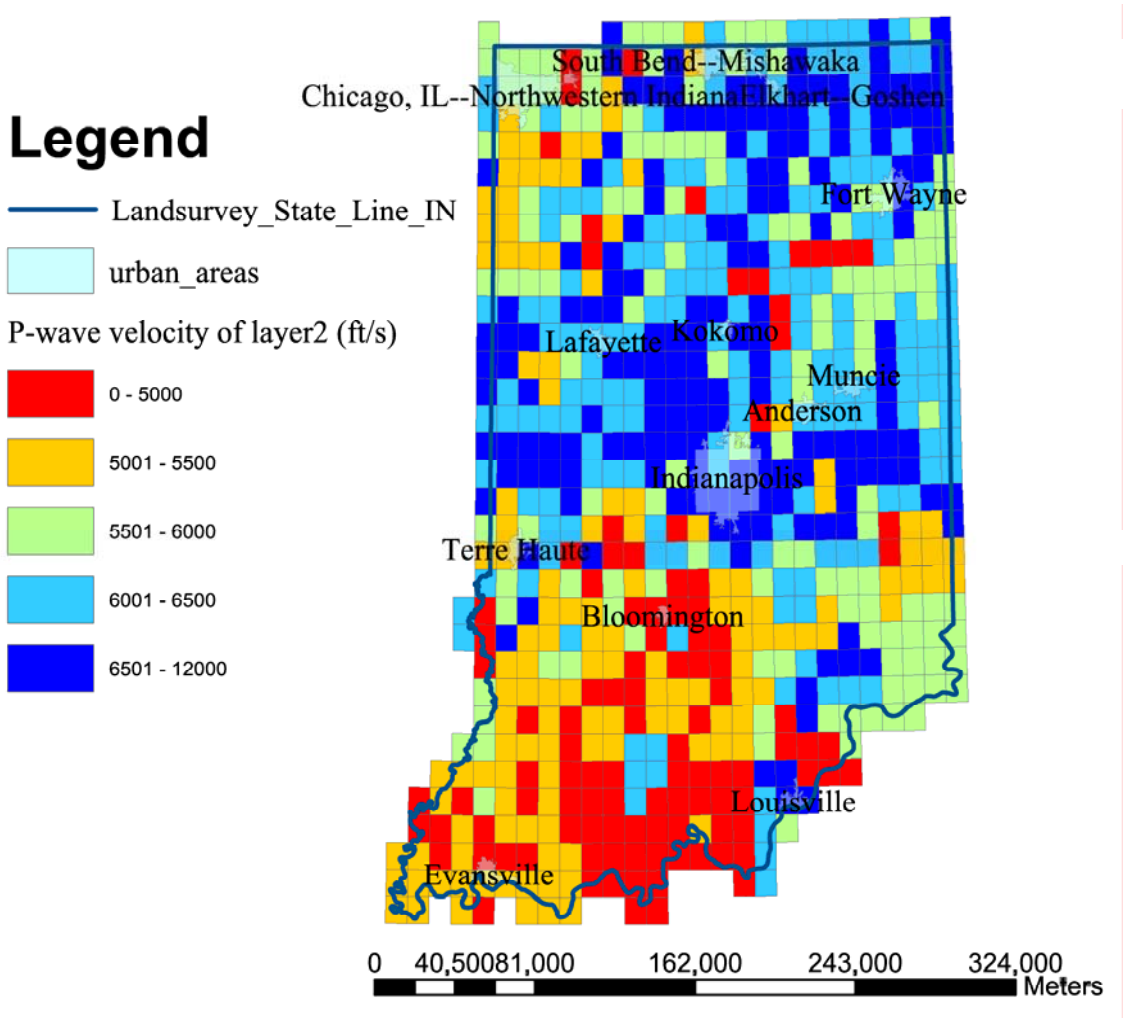

Figure 1-12 Average P-wave velocity in the intermediate layer (Layer 2) for each 0.125 degree quadrangle. There is a correlation of P-wave velocity with surficial geology.

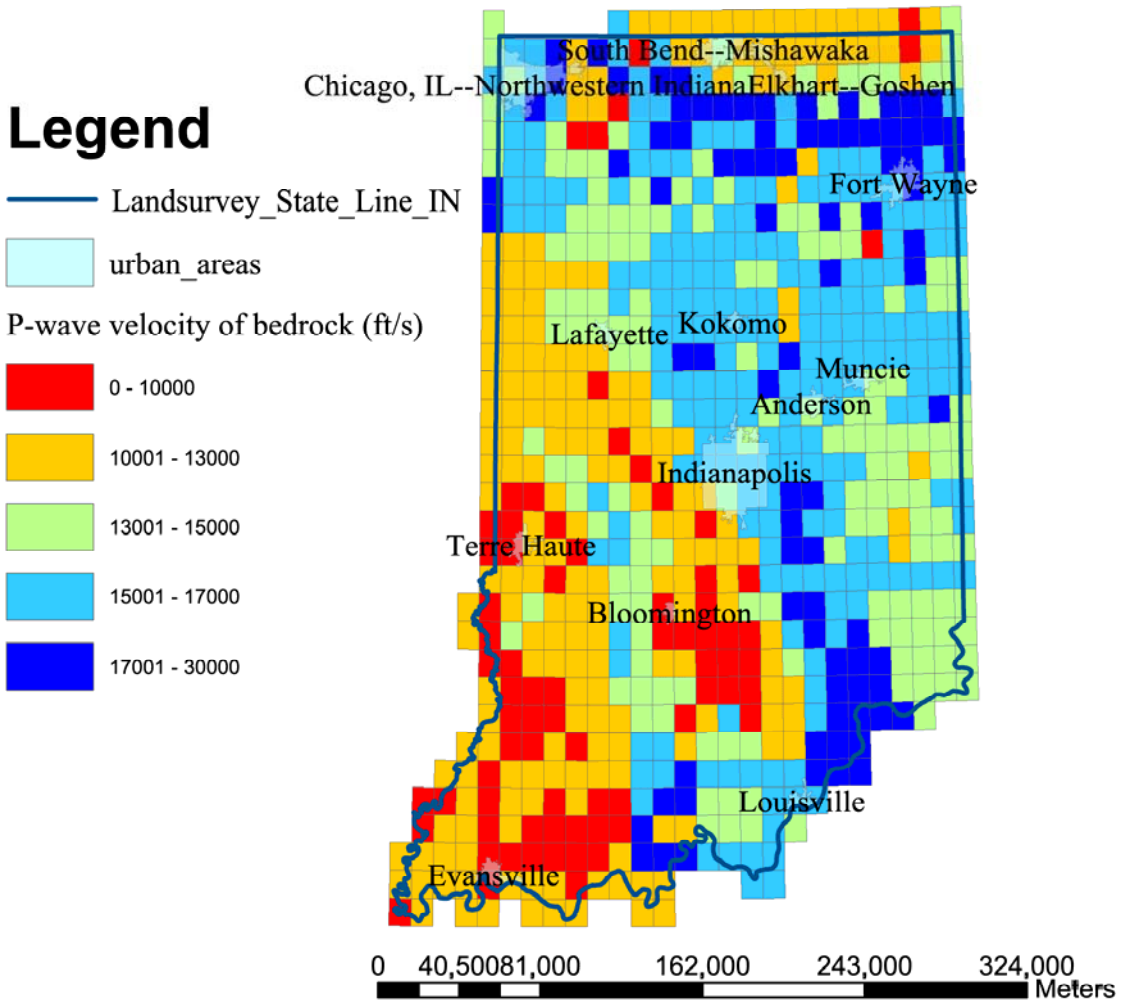

Figure 1-13 Averge bedrock P-wave velocity for each 0.125 degree quadrangle. Size of the symbol is proportional to velocity. Colors indicate bedrock geology [*Gray et al.*, 1987]. Note the strong correlation between seismic velocity and bedrock type.

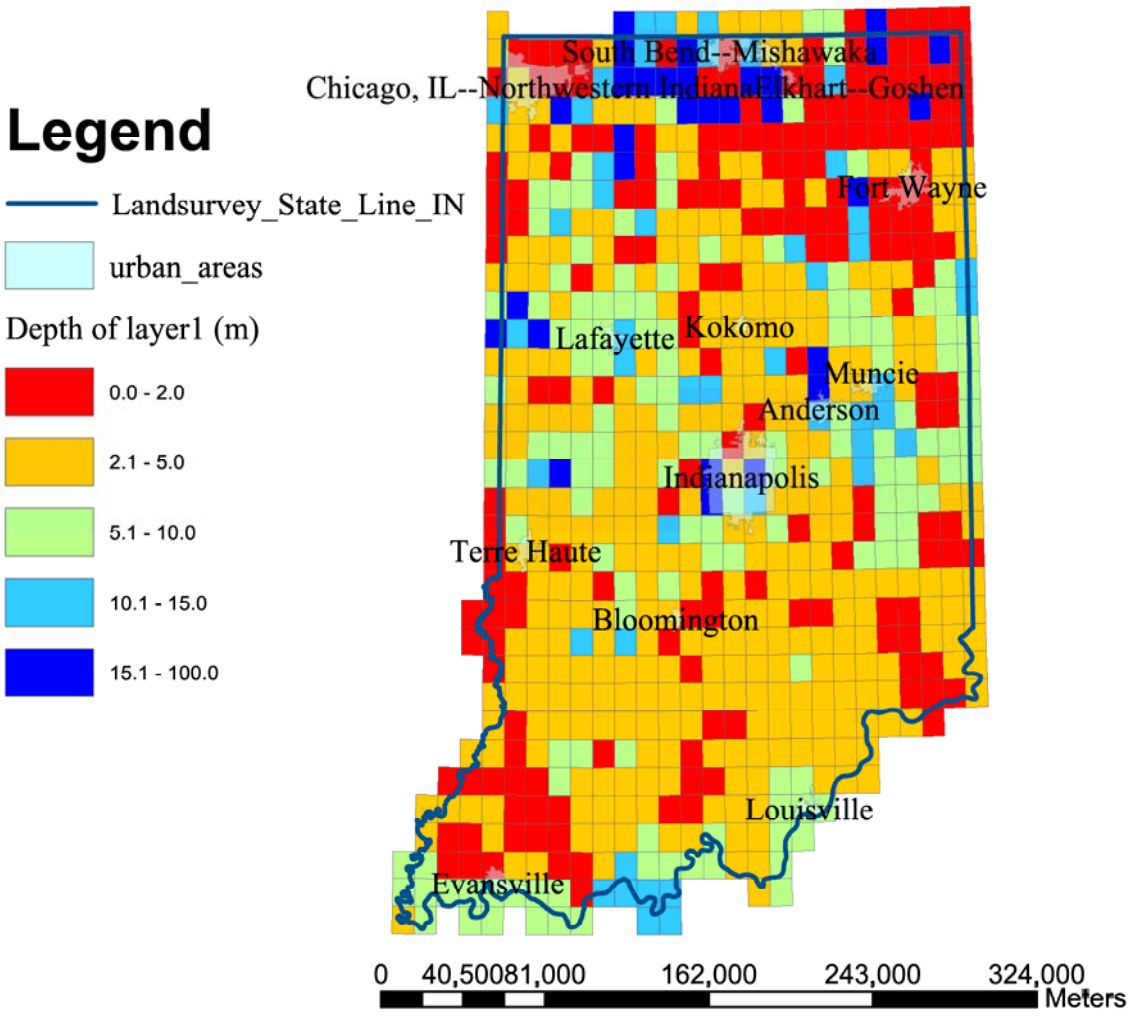

Figure 1-14 Average depth to the base of the near surface layer (Layer 1) for each 0.125 degree quadrangle where three layer profiles have been determined in the P-wave refraction dataset.

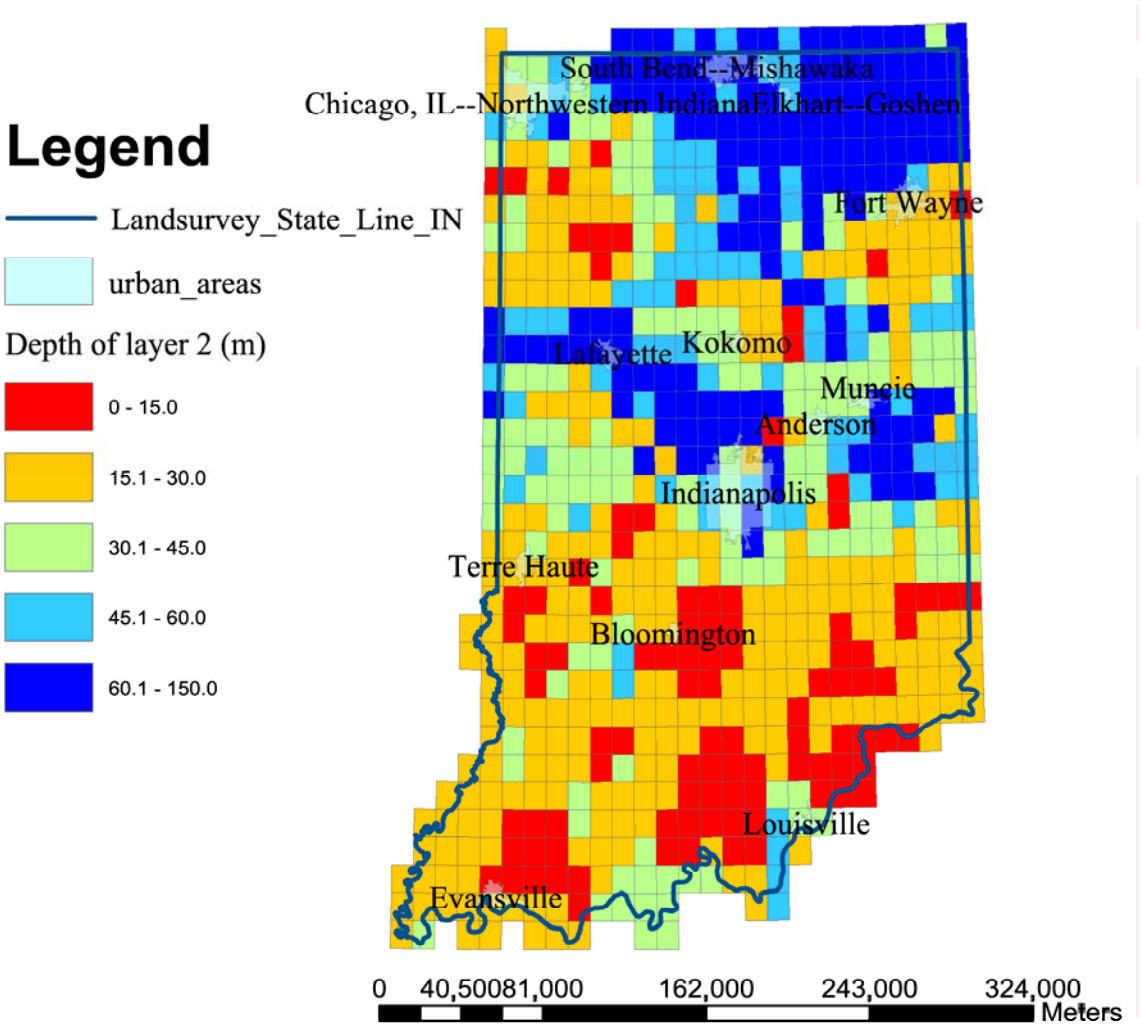

Figure 1-15 Average depth to the base of the unconsolidated sediments (base of both Layer 1 and Layer 2) for each 0.125 degree quadrangle determined from the P-wave refraction profiles. Note the correlation between depth and average P-wave velocity, indicating velocity is a strong function of effective stress.

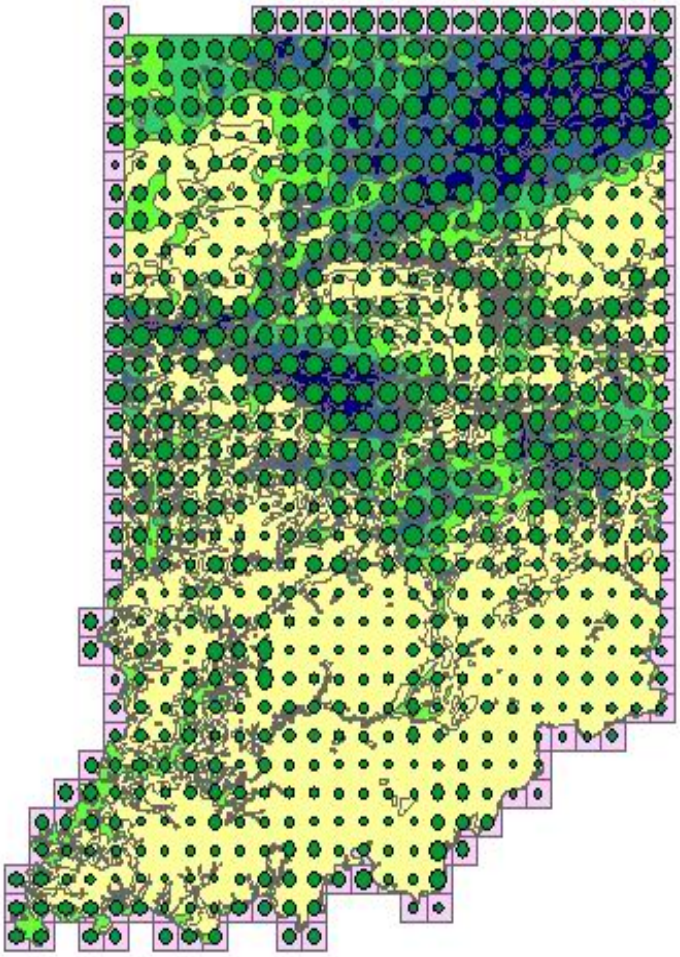

Figure 1-16 Seismic refraction data depths averaged over .125 degree cells with green circle size proportional to depth of layer B. The depth is correlated with the unconsolidated sediment depth derived both from water well logs, which is plotted in the background.

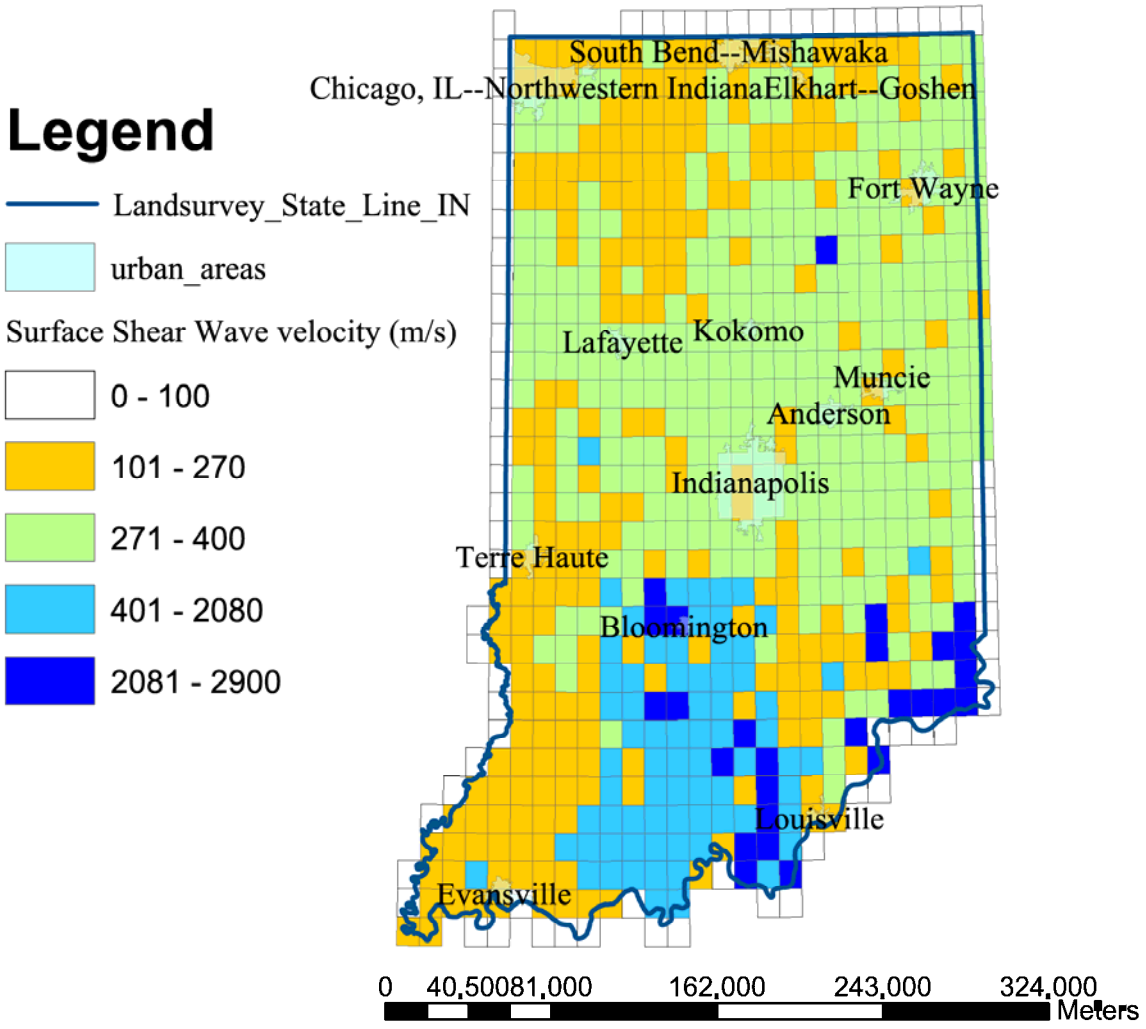

Figure 1-17 Surface shear wave velocity map, with velocity assigned to the unit type as shown in Table 1-1.

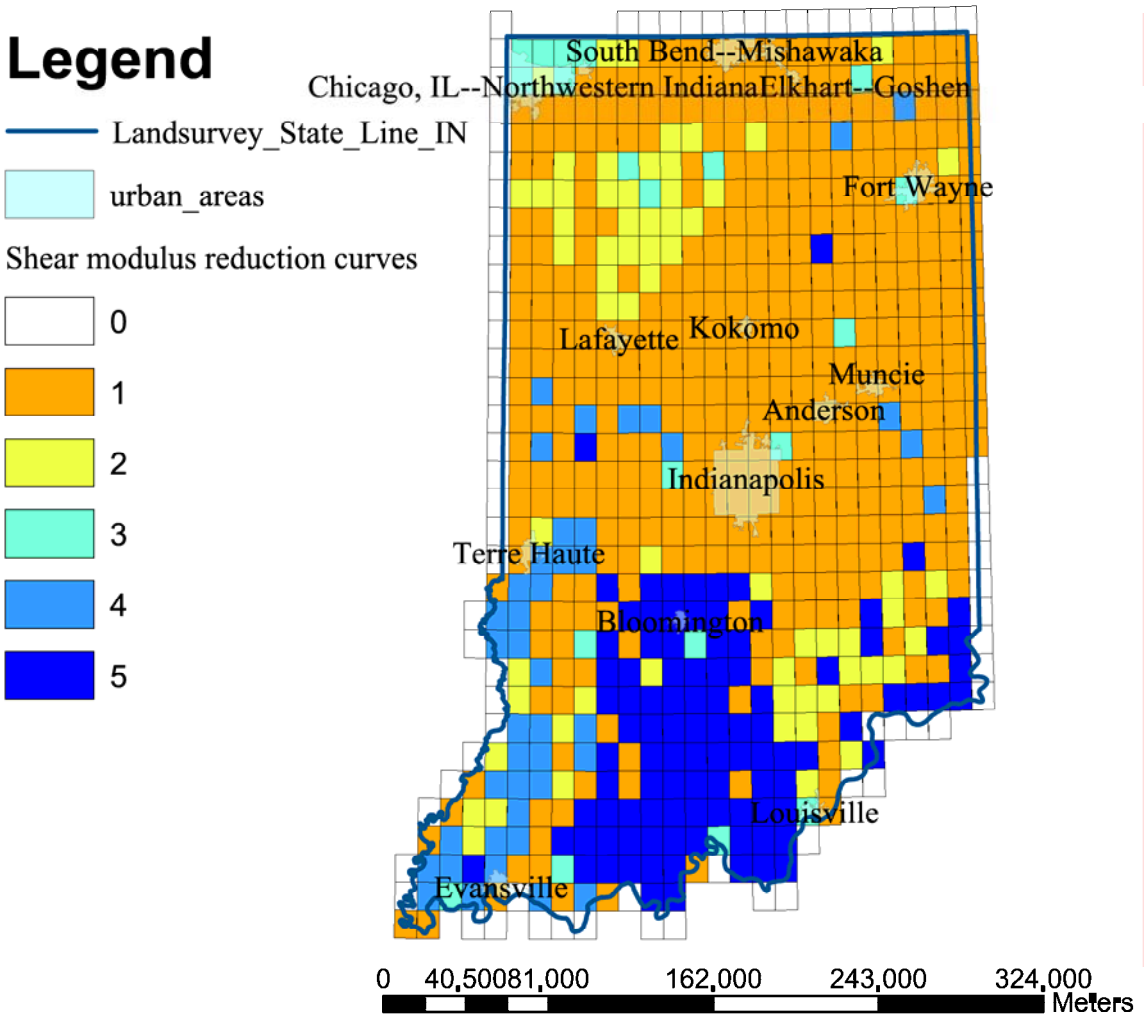

Figure 1-18 Map showing regions assigned the specific shear modulus reduction curves given in Table 1-1.

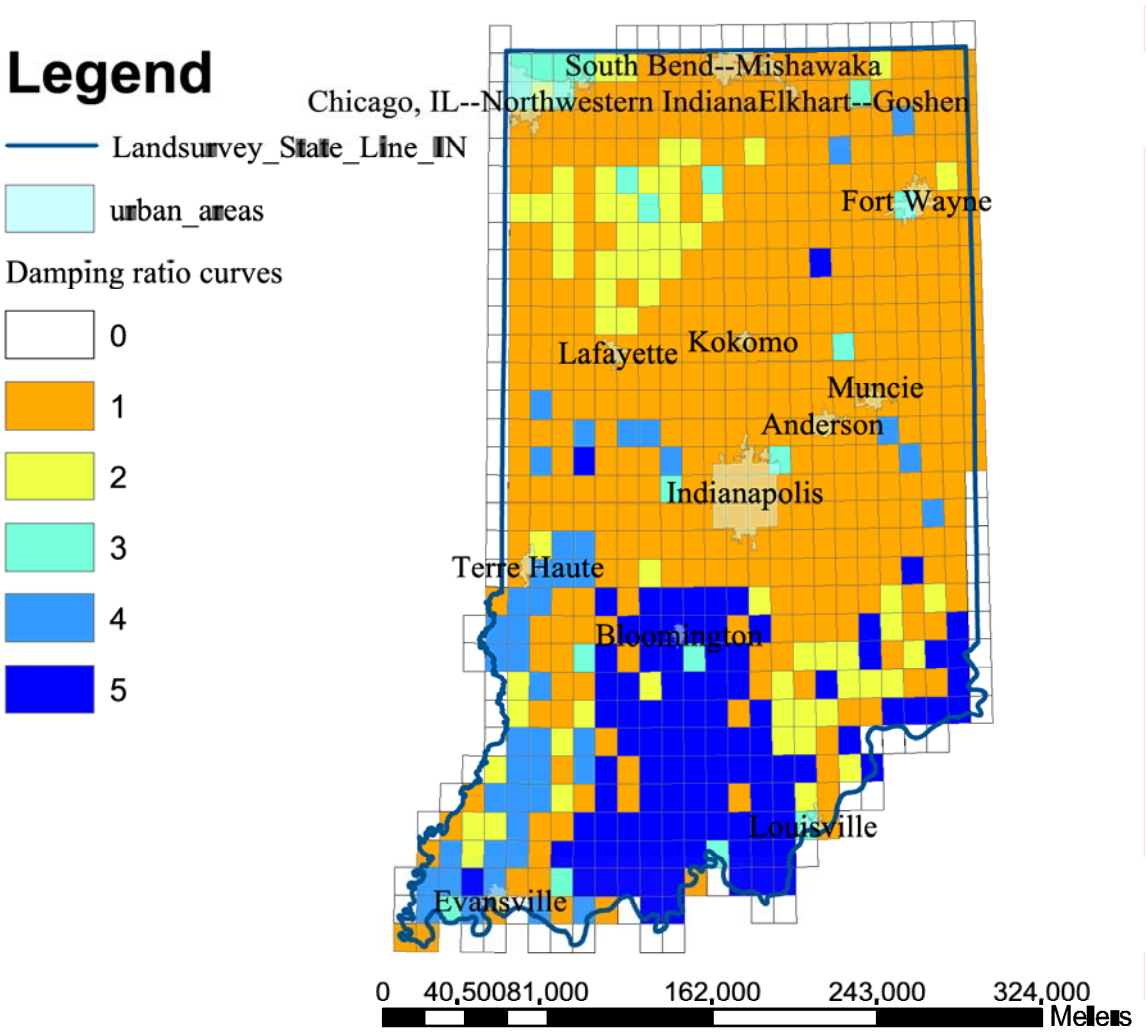

Figure 1-19 Map showing regions assigned the specific soil damping ratio curves given in Table 1-1

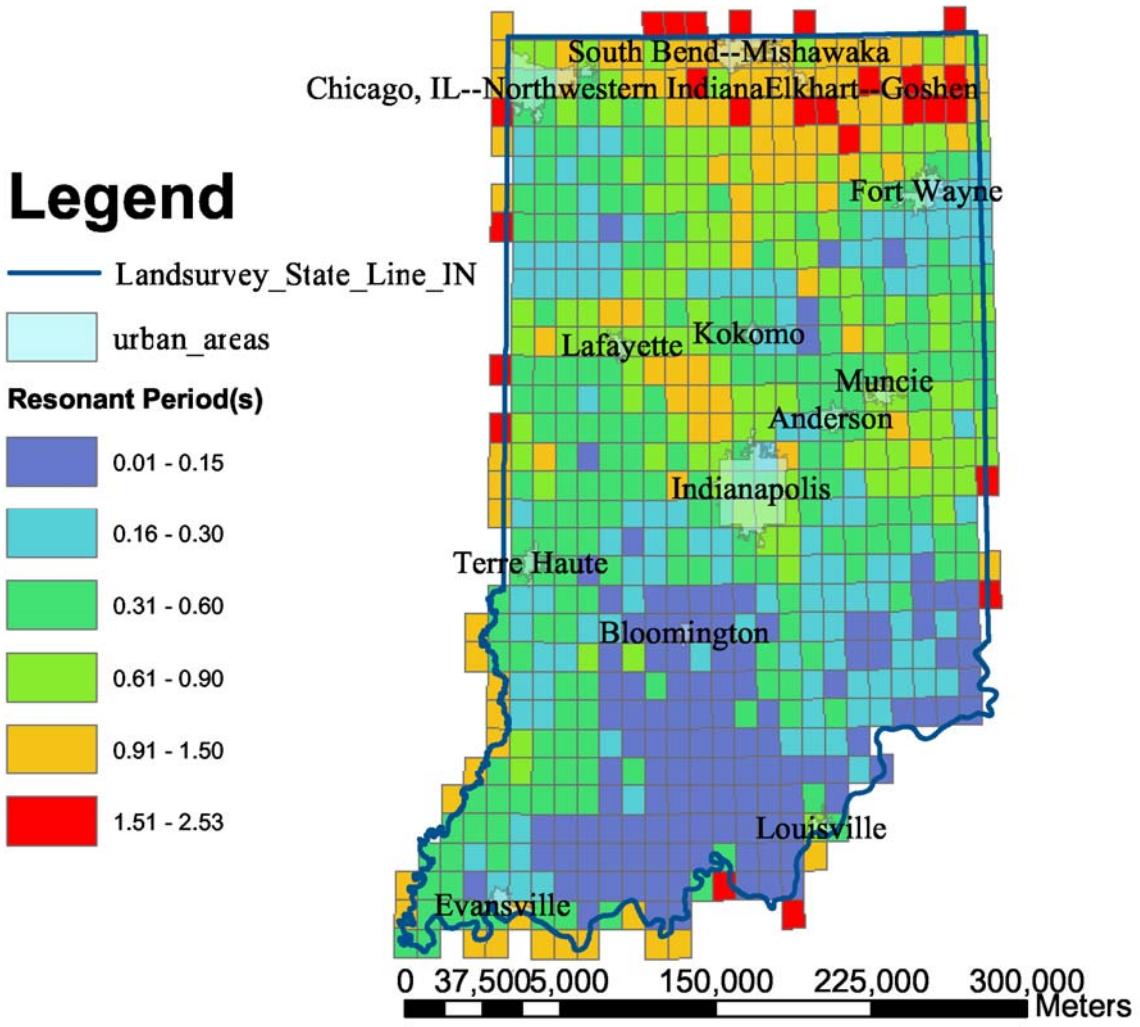

Figure 1-20 Map showing resonant period of unconsolidated sediment layer, given the shear wave velocity and thickness, calculated as T (period) = 4Z2/Vs2.

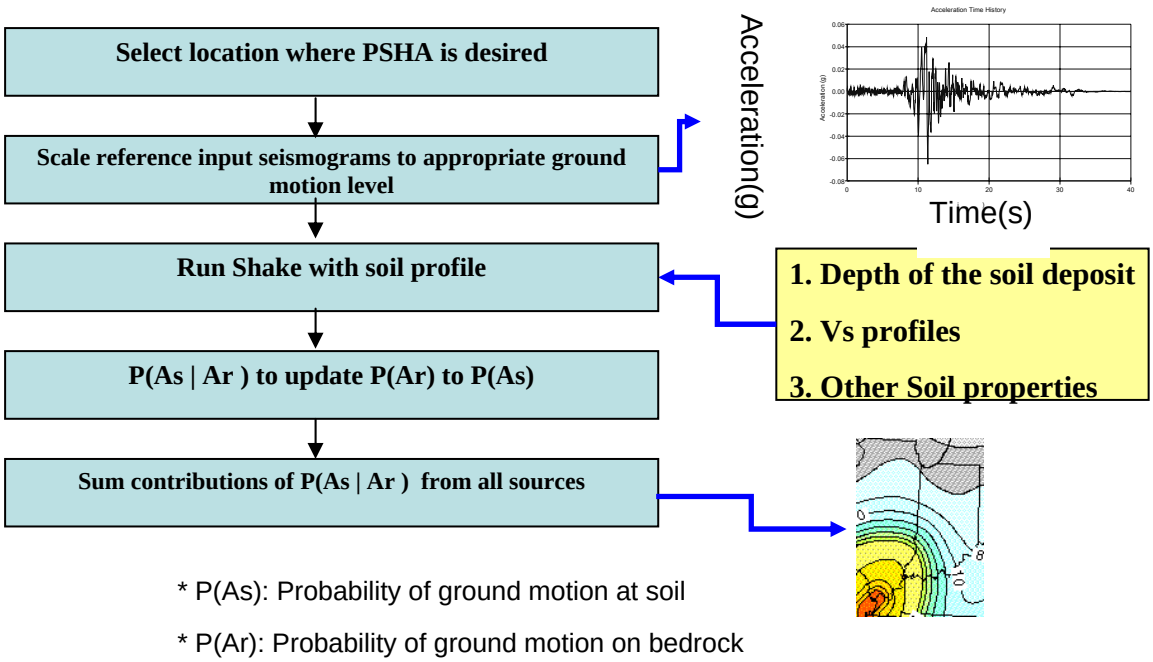

Figure 1-21 Outline of procedure to quantify site effects in a probabilistic methodology.

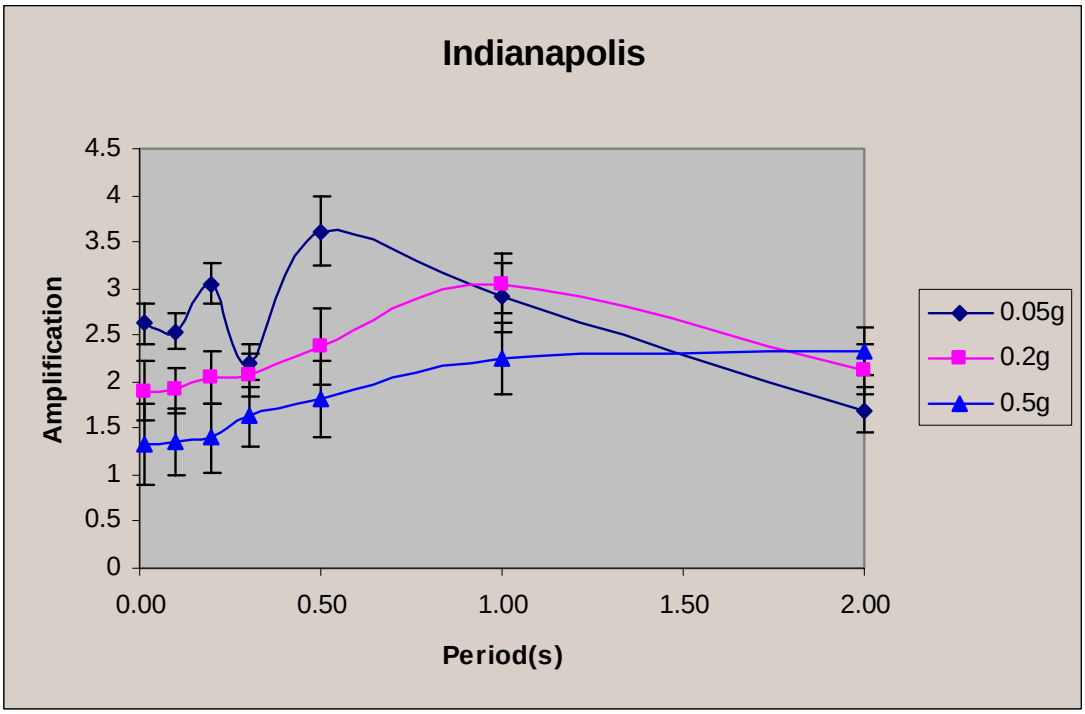

Figure 1-22 Site response amplification as a function of frequency for an example location near Indianapolis with one standard deviation uncertainties. These are calculated from 100 random realizations of the velocity profile with an input ground motion level of .05g, 0.2g and 0.5g. The site response will vary depending on the ground motion level because of the dynamic changes in the shear modulus at high strains.

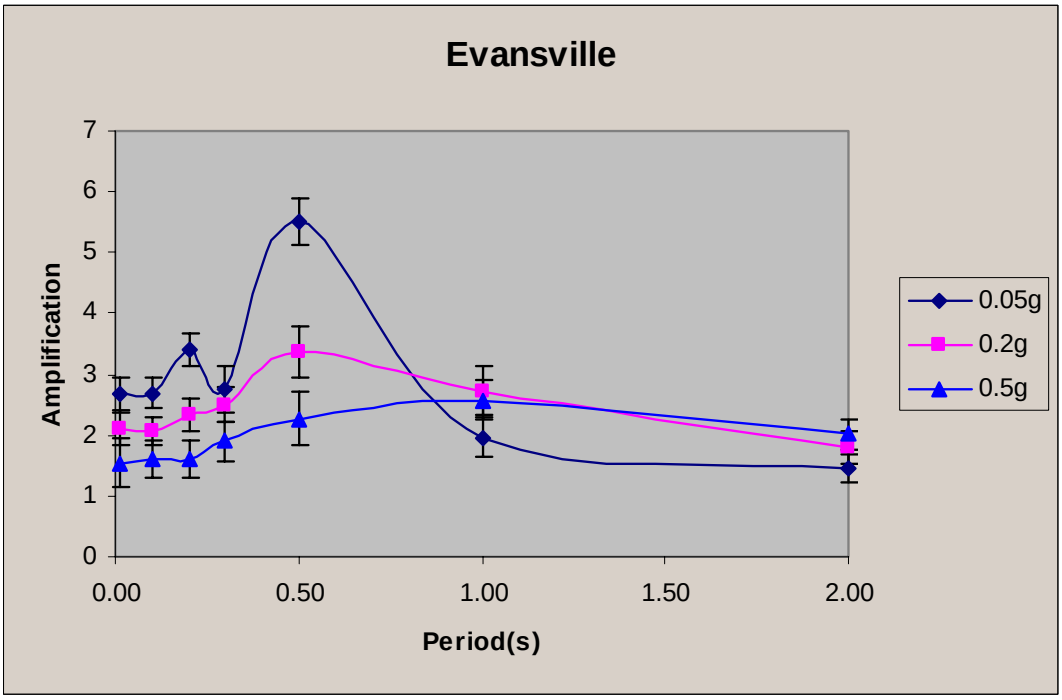

Figure 1-23 Amplification site response for an example location near Evansville in alluvial/outwash type soils for ground motion levels from 0.05 to 0.5 g.

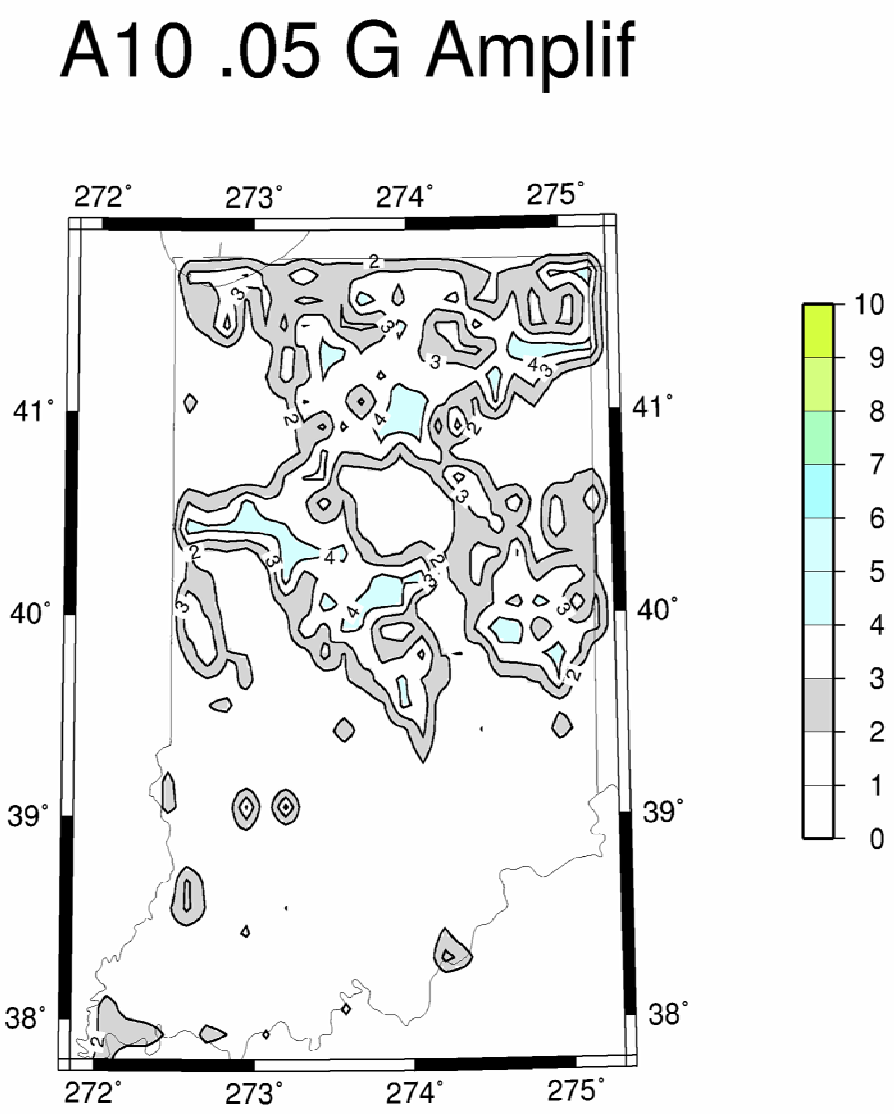

Figure 1-24 Map of amplification site response at *1 Hz for input ground motion levels of 0.05 g.*

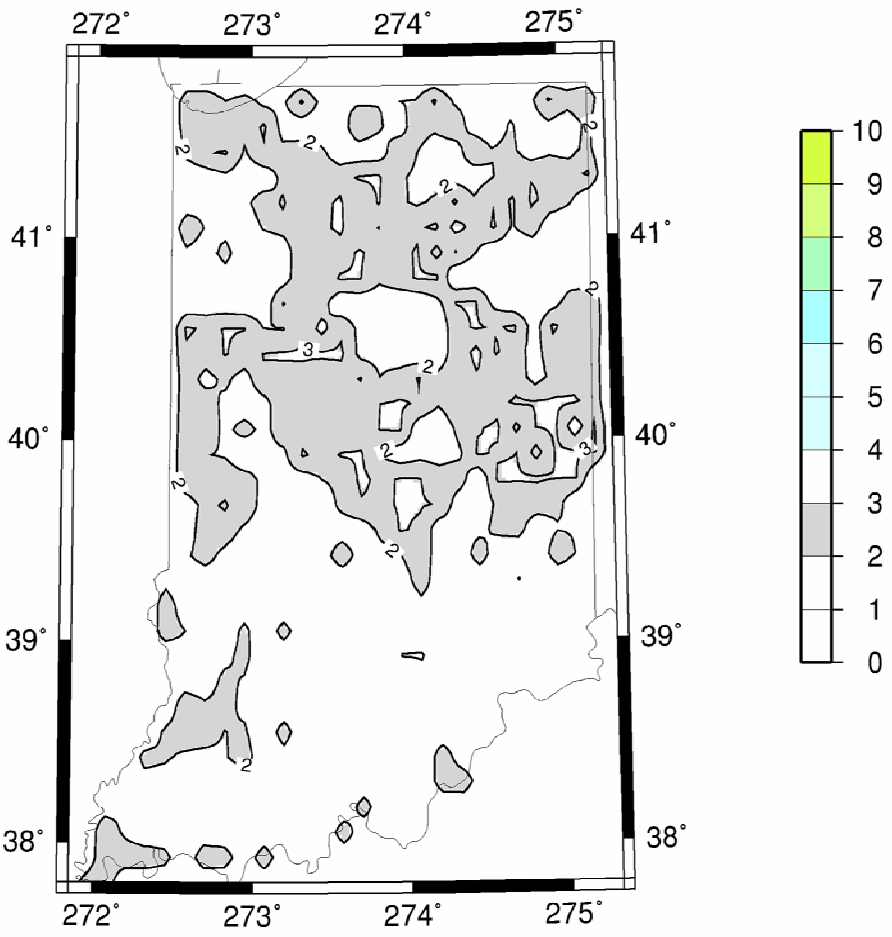

Figure 1-25 Map of amplification site response at *1 Hz for input ground motion levels of 0.2 g.*

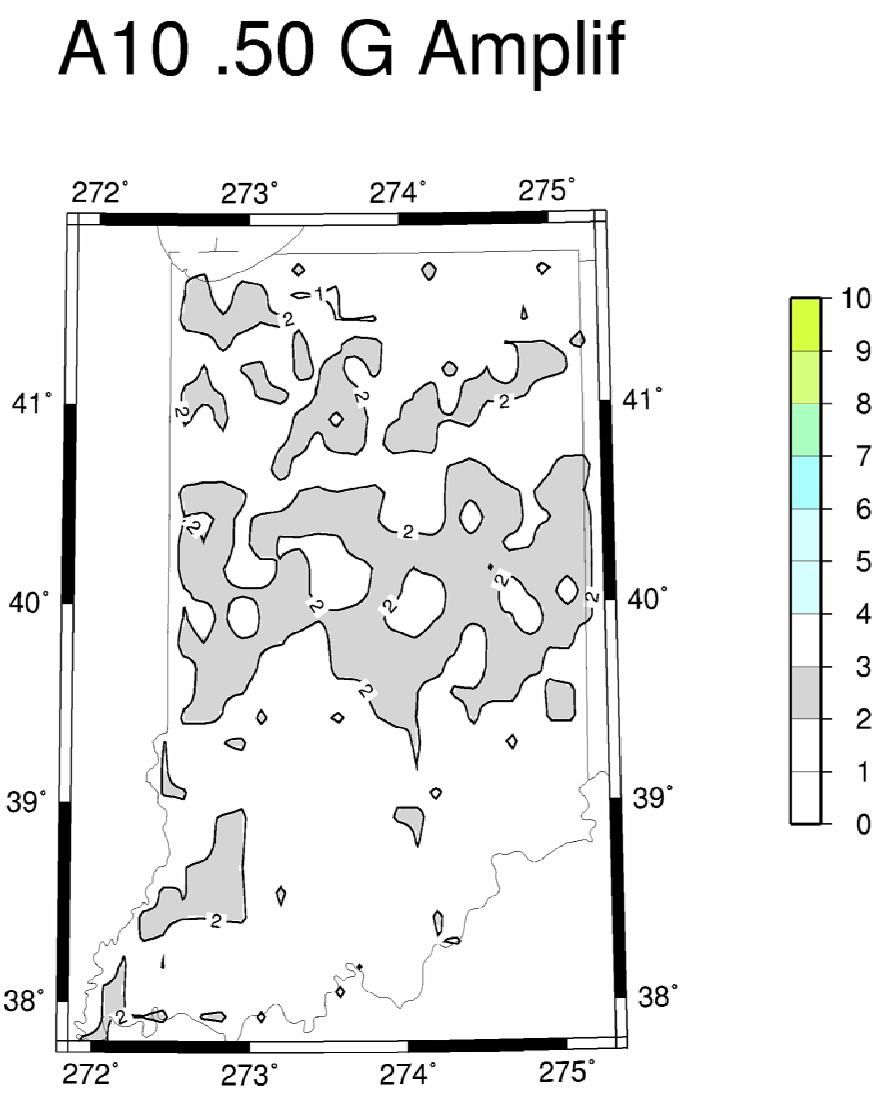

Figure 1-26 Map of amplification site response at *1 Hz for input ground motion levels of 0.5 g.*

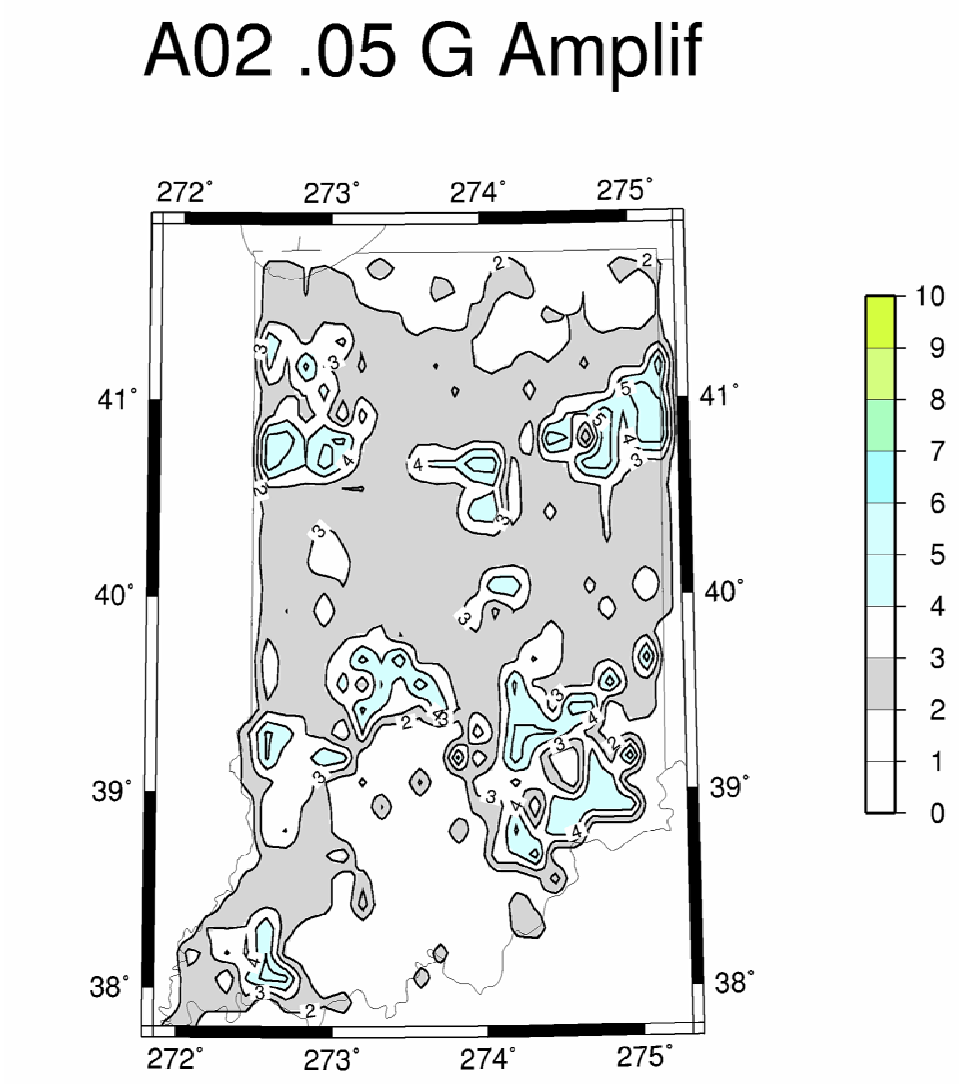

Figure 1-27 Map of amplification site response at 5 *Hz for input ground motion levels of 0.05 g.*

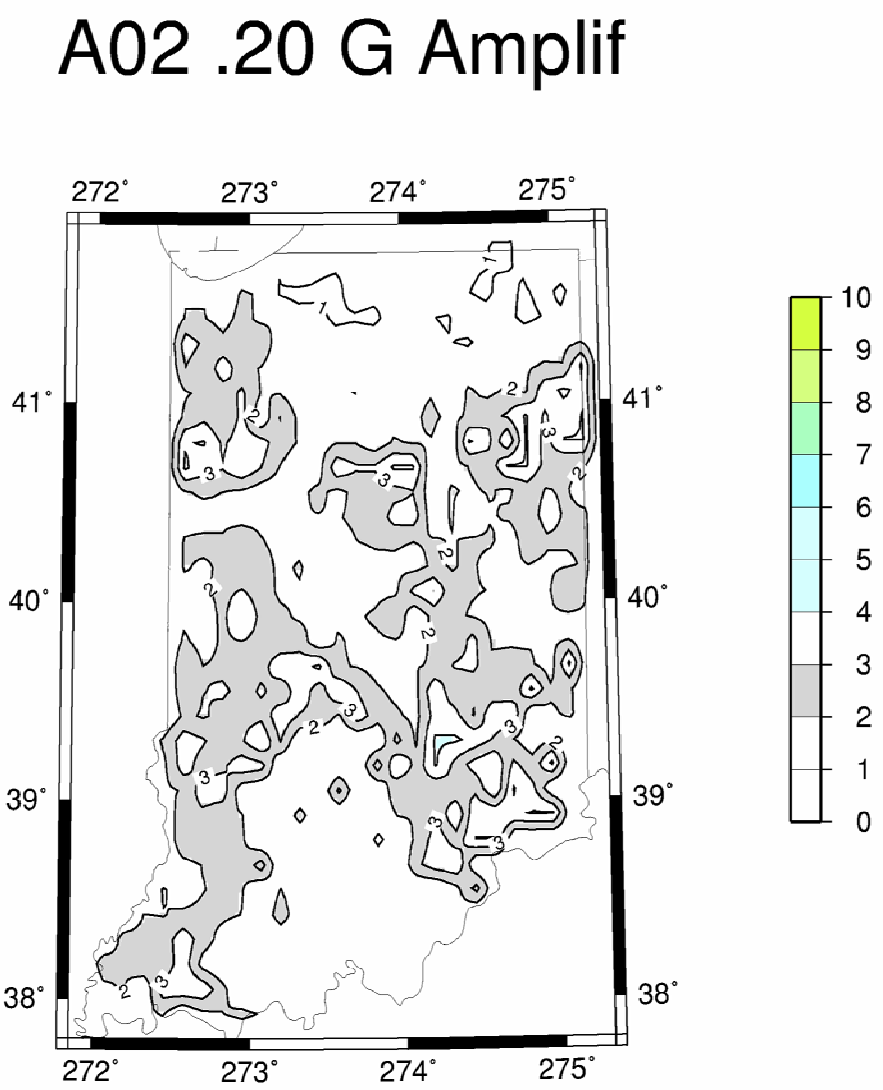

Figure 1-28 Map of amplification site response at 5 *Hz for input ground motion levels of 0.2 g.*

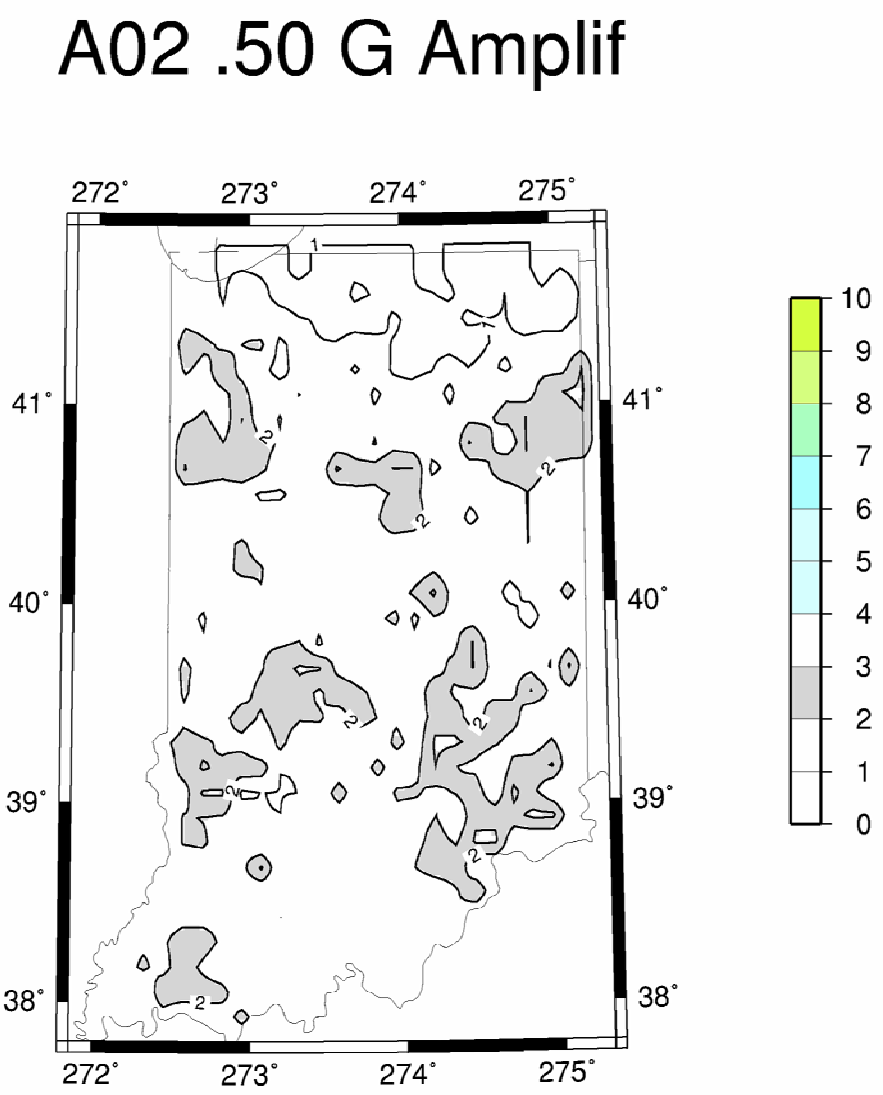

Figure 1-29 Map of amplification site response at 5 *Hz for input ground motion levels of 0.5 g.*

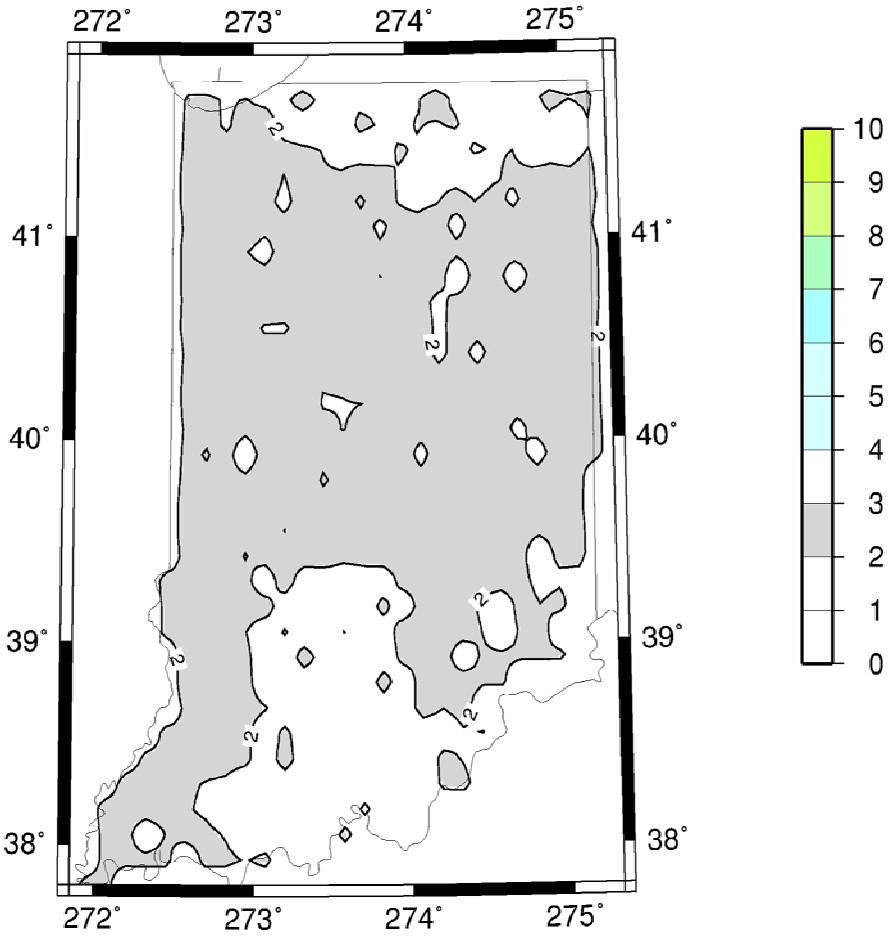

Figure 1-30 Map of amplification site response for *PGA for input ground motion levels of 0.05 g.*

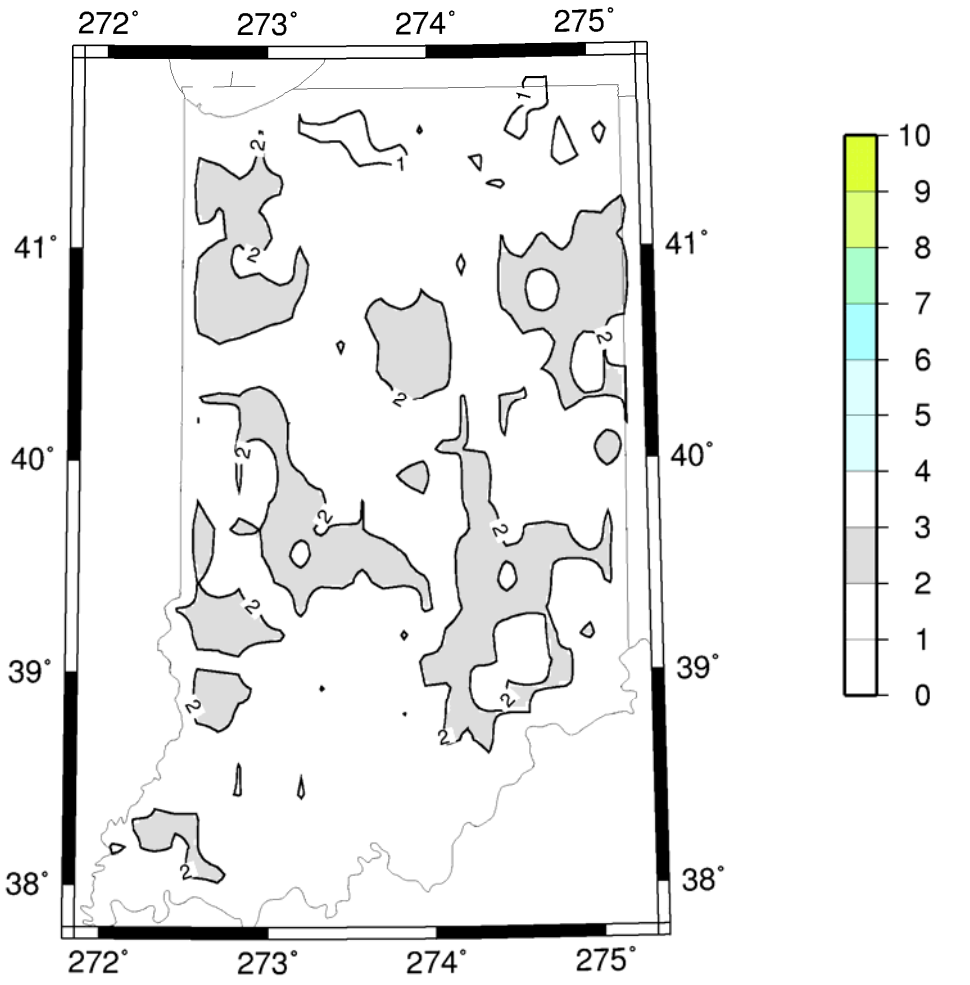

Figure 1-31 Map of amplification site response for *PGA for input ground motion levels of 0.2 g.*

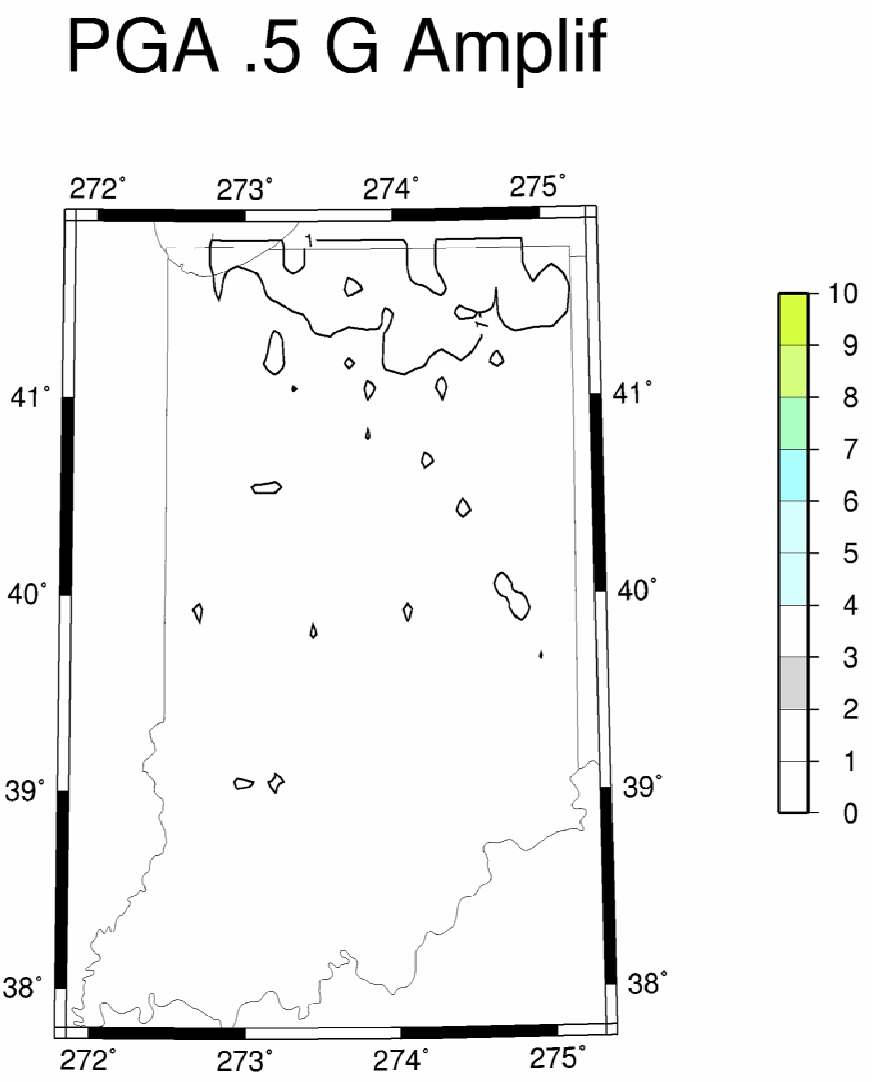

Figure 1-32 Map of amplification site response for *PGA for input ground motion levels of 0.5 g.*

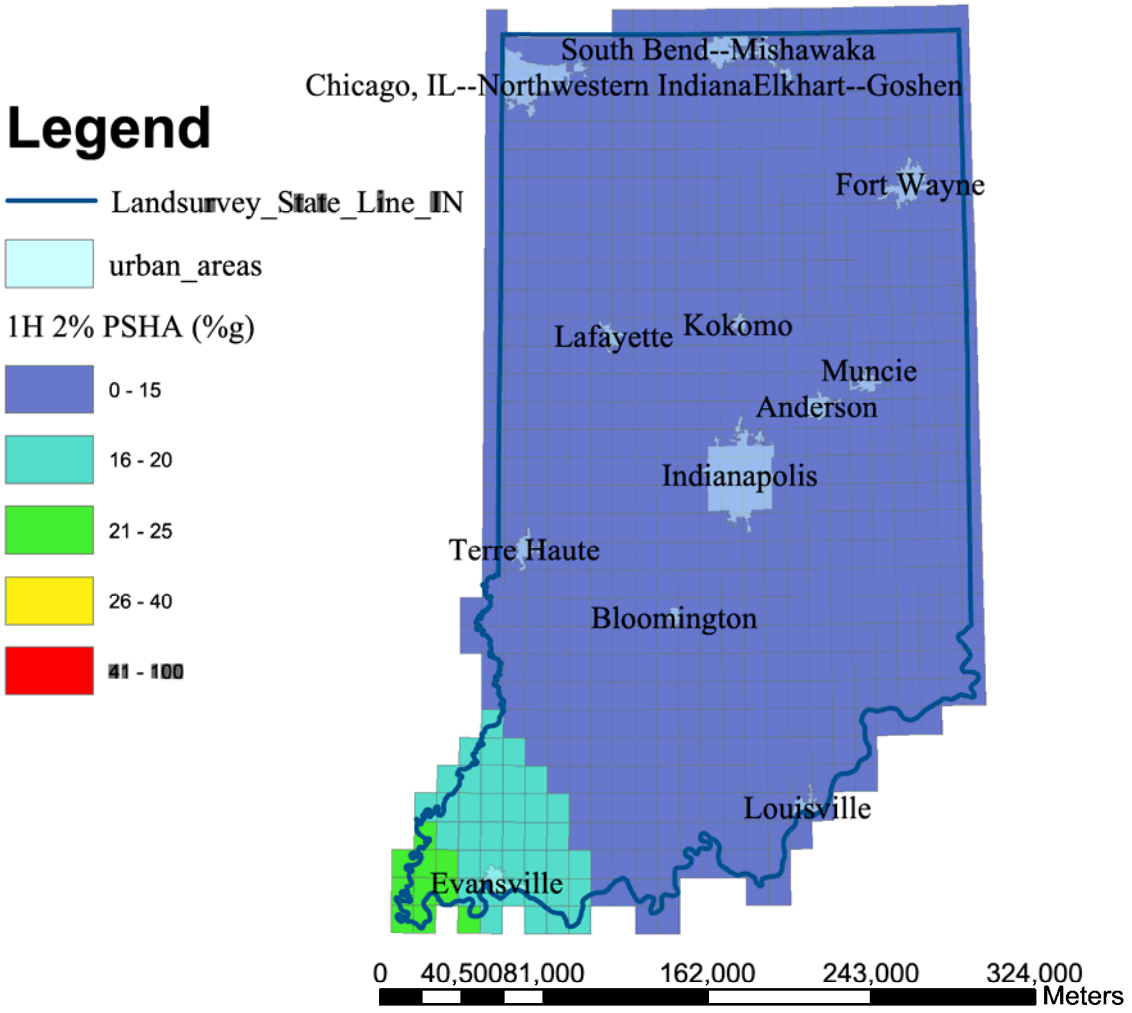

Figure 1-33 2002 USGS map of the probabilistic seismic hazard with 2% probability of exceedence in 50 years at *1* Hz spectral acceleration, which includes by default the site response for a NEHRP B/C site classification (gridded quadrangle version, for comparison).

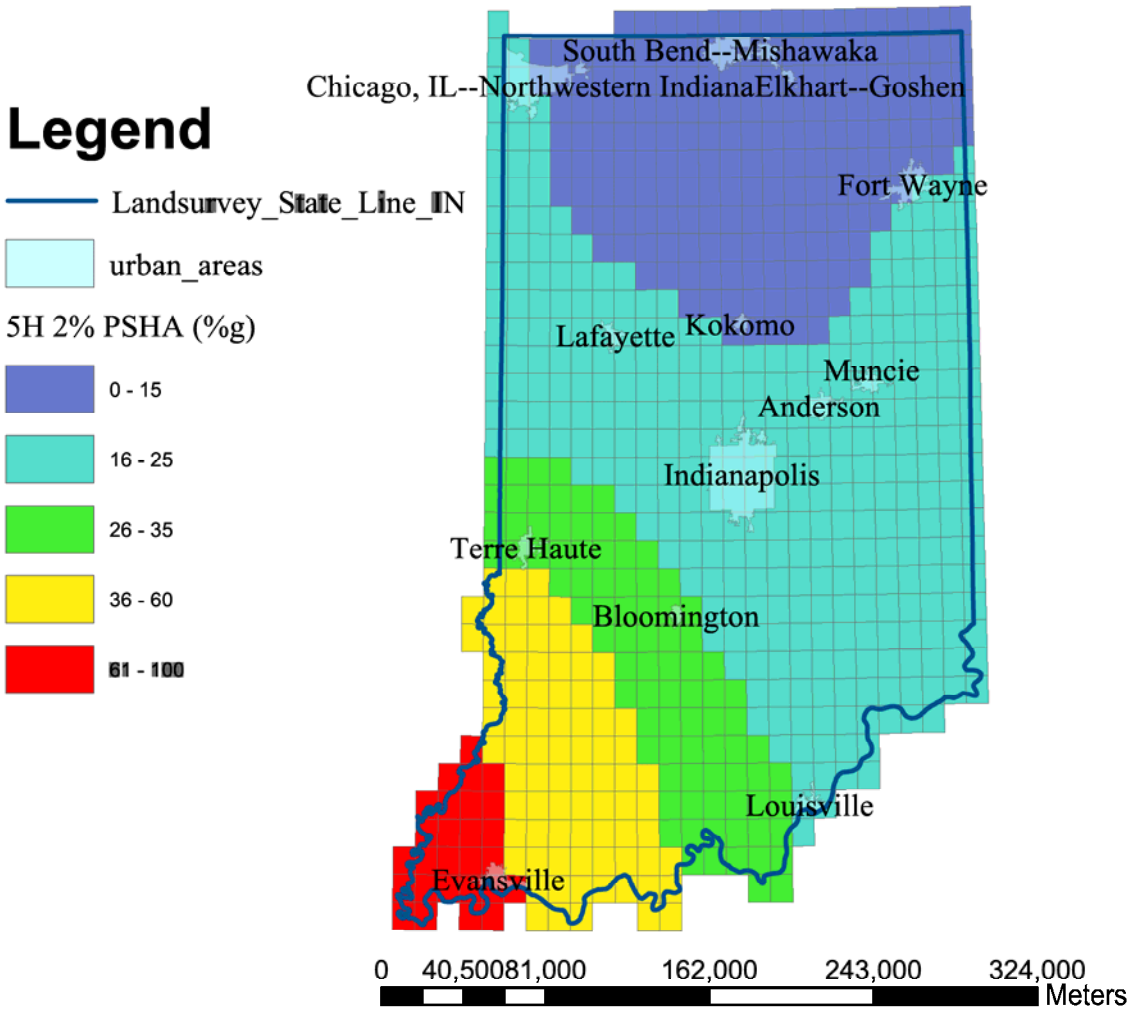

Figure 1-34 2002 USGS map of the probabilistic seismic hazard with 2% probability of exceedence in 50 years at *5 Hz spectral acceleration*, which includes by default the site response for a NEHRP B/C site classification (gridded quadrangle version, for comparison).

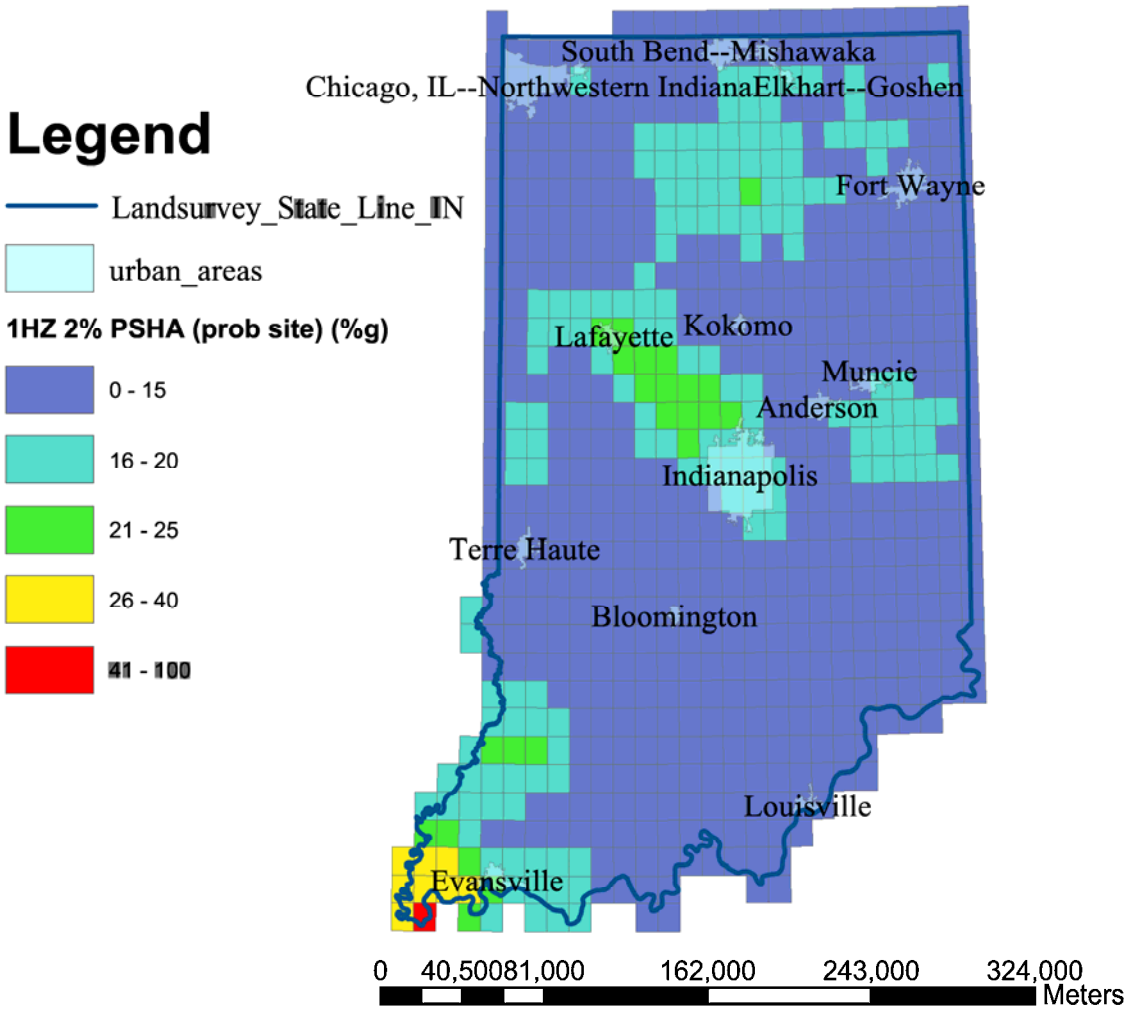

Figure 1-35 Map of the probabilistic seismic hazard with 2% probability of exceedence in 50 years at *1 Hz* spectral acceleration including the *probabilistically determined site response*. Comparison with the USGS PSHA map, which assumes a NEHRP B/C site classification, shows that there is high amplification of ground motions in the center and northeast of the state at 1 Hz due primarily to the extensive sediment thickness.

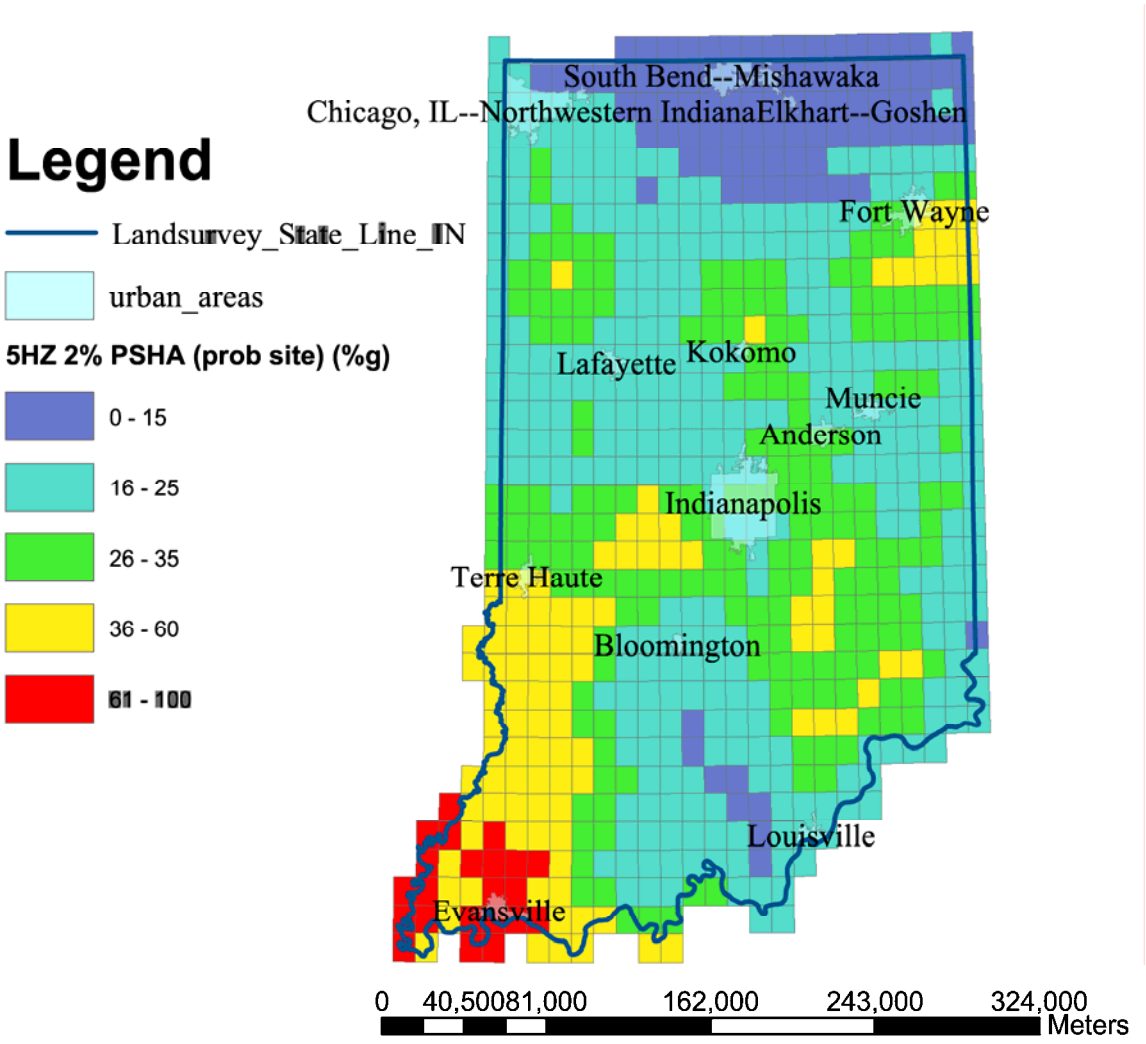

Figure 1-36 Map of the probabilistic seismic hazard with 2% probability of exceedence in 50 years at *5 Hz* spectral acceleration including the *probabilistically determined site response*. Comparison with the USGS PSHA map, which is calculated for a NEHRP B/C site classification, shows that there is high amplification of ground motions in the selected small regions of the state at 5 Hz due primarily to slow velocities in intermediate thickness materials with higher resonant frequency.

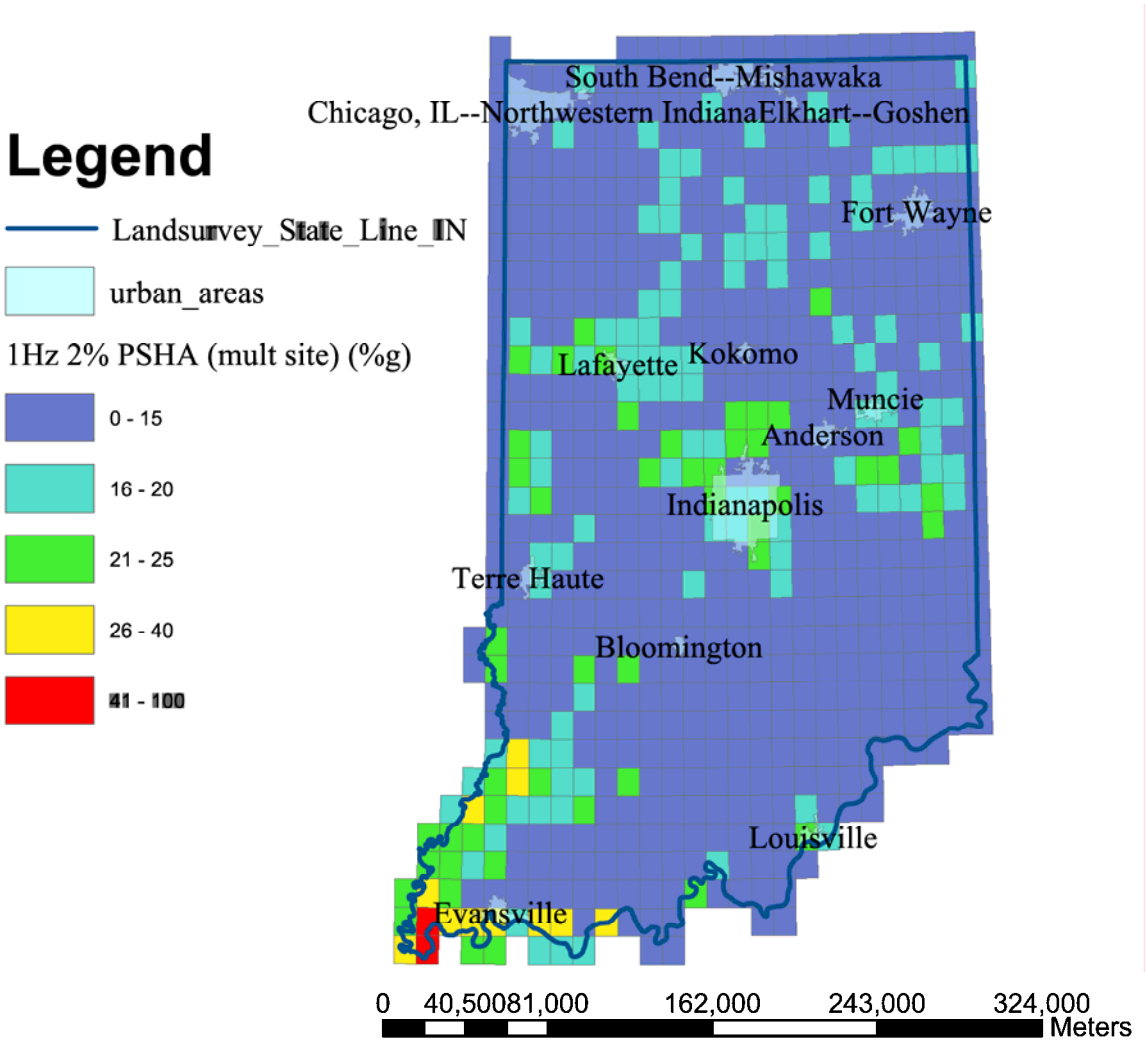

Figure 1-37 Map of the probabilistic seismic hazard with 2% probability of exceedence in 50 years at *1 Hz* spectral acceleration using a simplified method of *multiplication* of the USGS PSHA for a rock site by the site response amplification factor for the appropriate input ground motion level. This simplified method confirms that patterns produced in the probabilistic calculation.

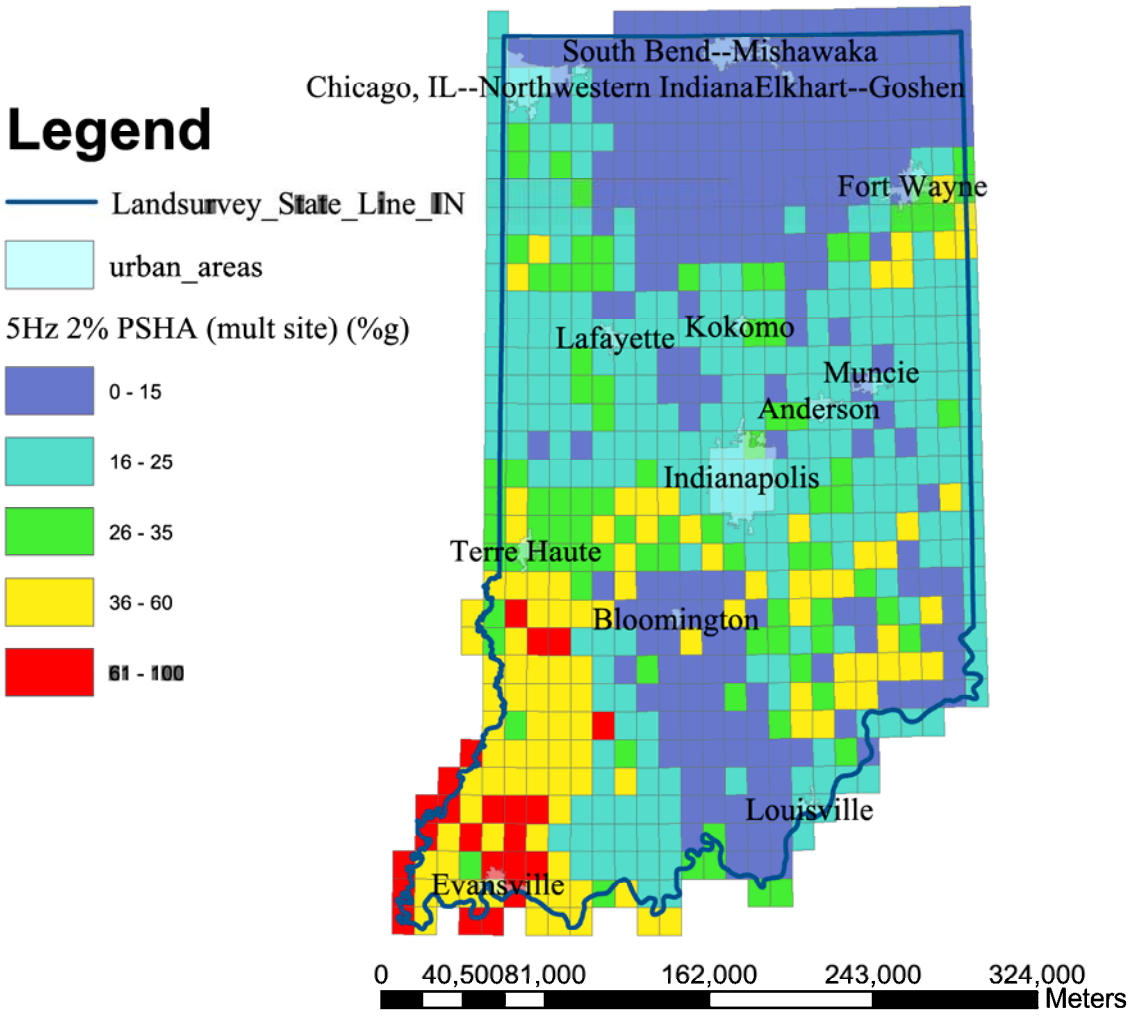

Figure 1-38 Map of the probabilistic seismic hazard with 2% probability of exceedence in 50 years at *5 Hz* spectral acceleration using a simplified method of *multiplication* of the USGS PSHA for a rock site by the site response amplification factor for the appropriate input ground motion level.

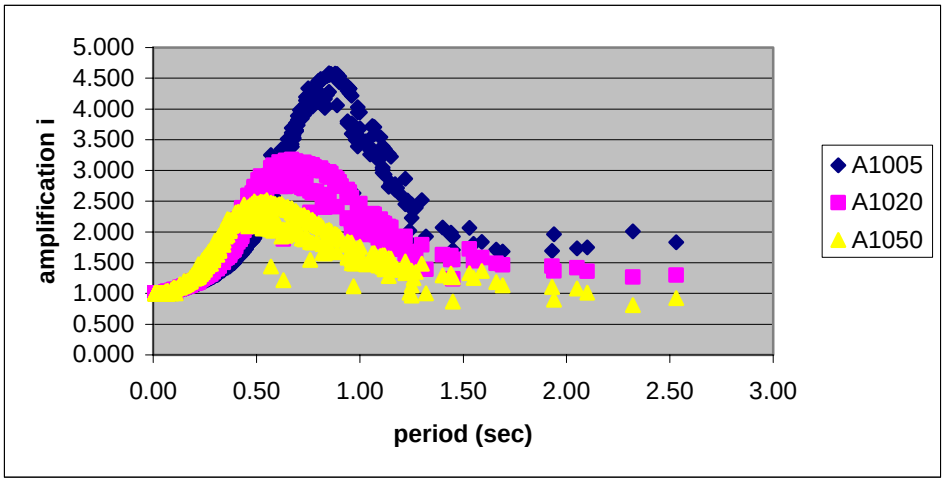

Figure 1-39 Site response amplification as a function of resonant period for each grid point in the 1 Hz spectral acceleration PSHA map, where the resonant period was calculated as T = 4Z2/Vs2 (Figure 1-20). This is used to validate the results, and demonstrates that the higher amplitudes do indeed occur where the surface geology is expected to produce a resonance. The curves illustrate the decrease in amplification for increasing ground motion level. The curves are resolvably different for different soil S-wave velocity.

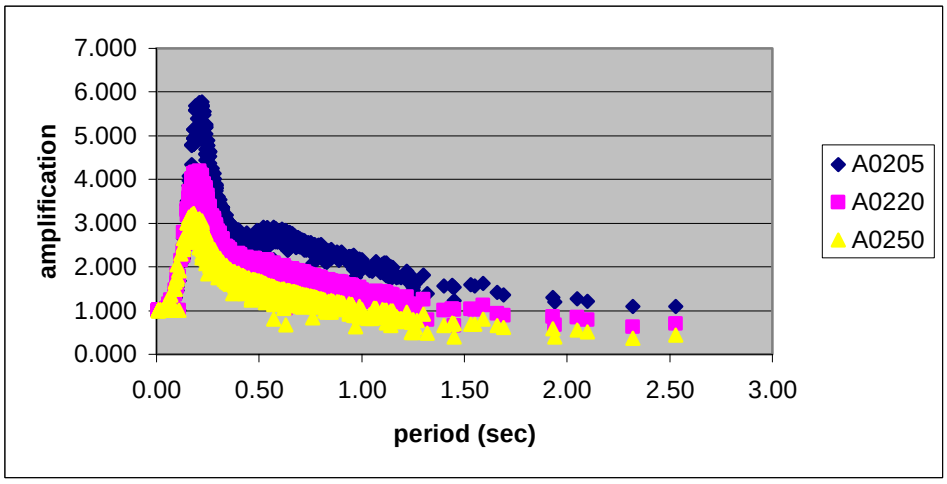

Figure 1-40 Site response amplification as a function of resonant period for each grid point in the 5 Hz spectral acceleration PSHA map, where the resonant period was calculated as T = 4Z2/Vs2 (Figure 1-20).

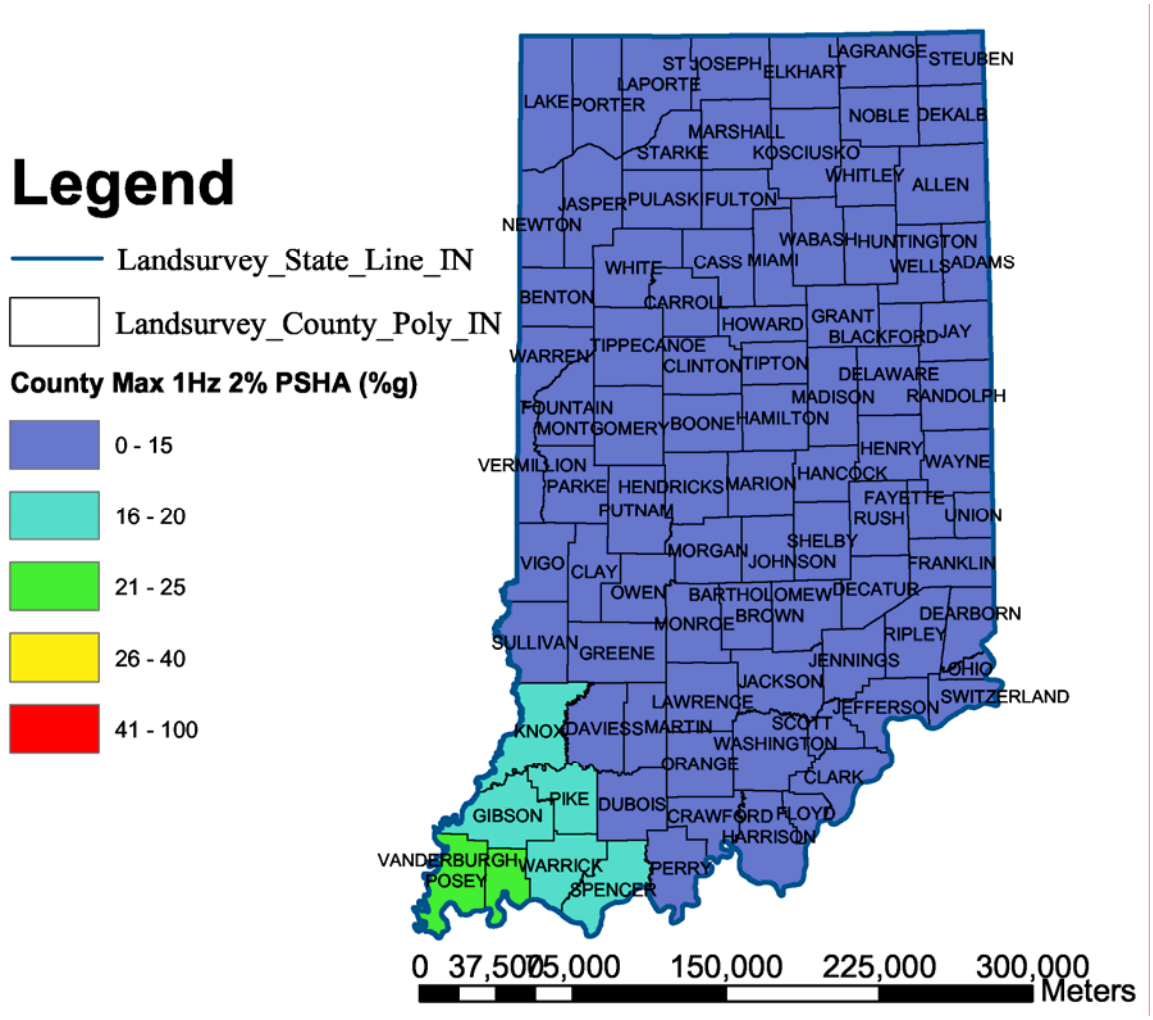

Figure 1-41 Map of the maximum seismic hazard level [*ATC/MCEER*, 2003] for each county for the 2002 USGS 1 Hz spectral acceleration PSHA maps.

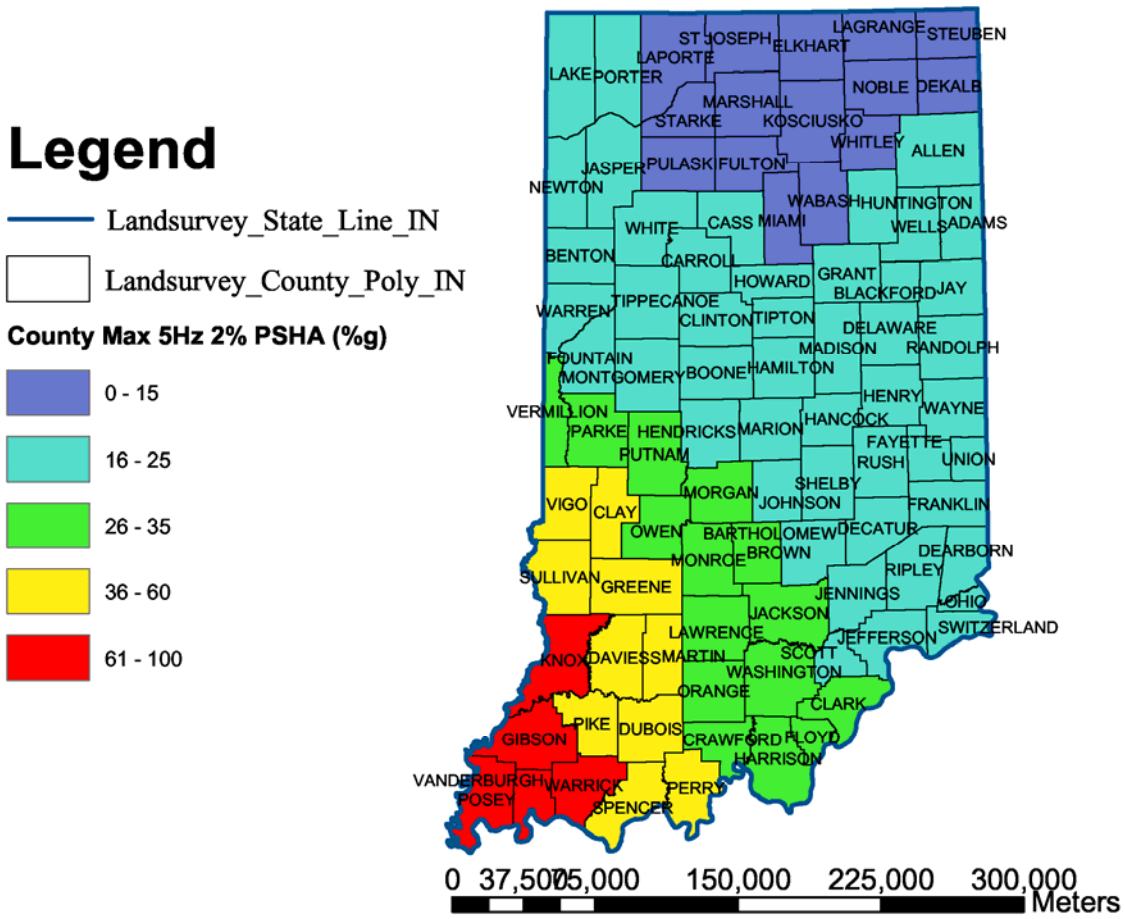

Figure 1-42 Map of the maximum seismic hazard level [*ATC/MCEER*, 2003] for each county for the 2002 USGS 5 Hz spectral acceleration PSHA maps.

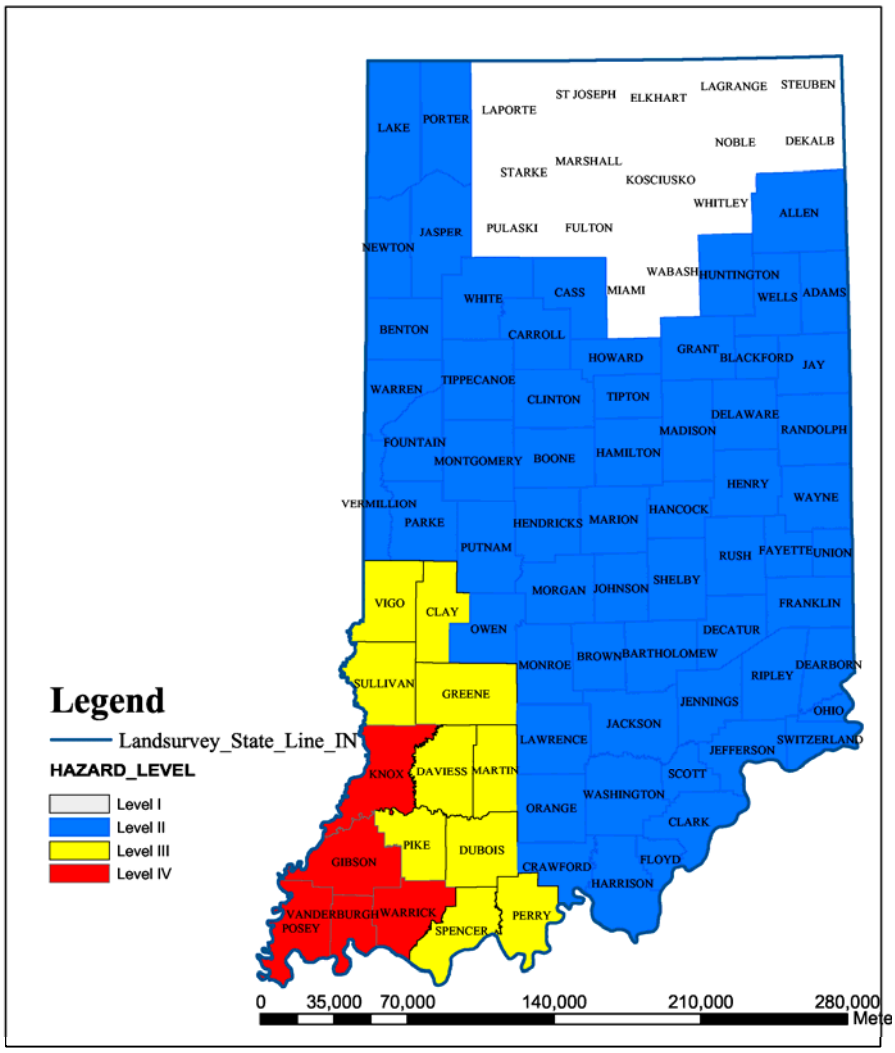

Figure 1-43 The design hazard level is defined as whichever is higher of the 1Hz or 5Hz hazard level [*ATC/MCEER*, 2003]. This map shows the level corresponding to that definition for the 2002 USGS probabilistic hazard map, *without the effects of site amplification*. This image cannot be considered an actual design map because it does not include actual site conditions.

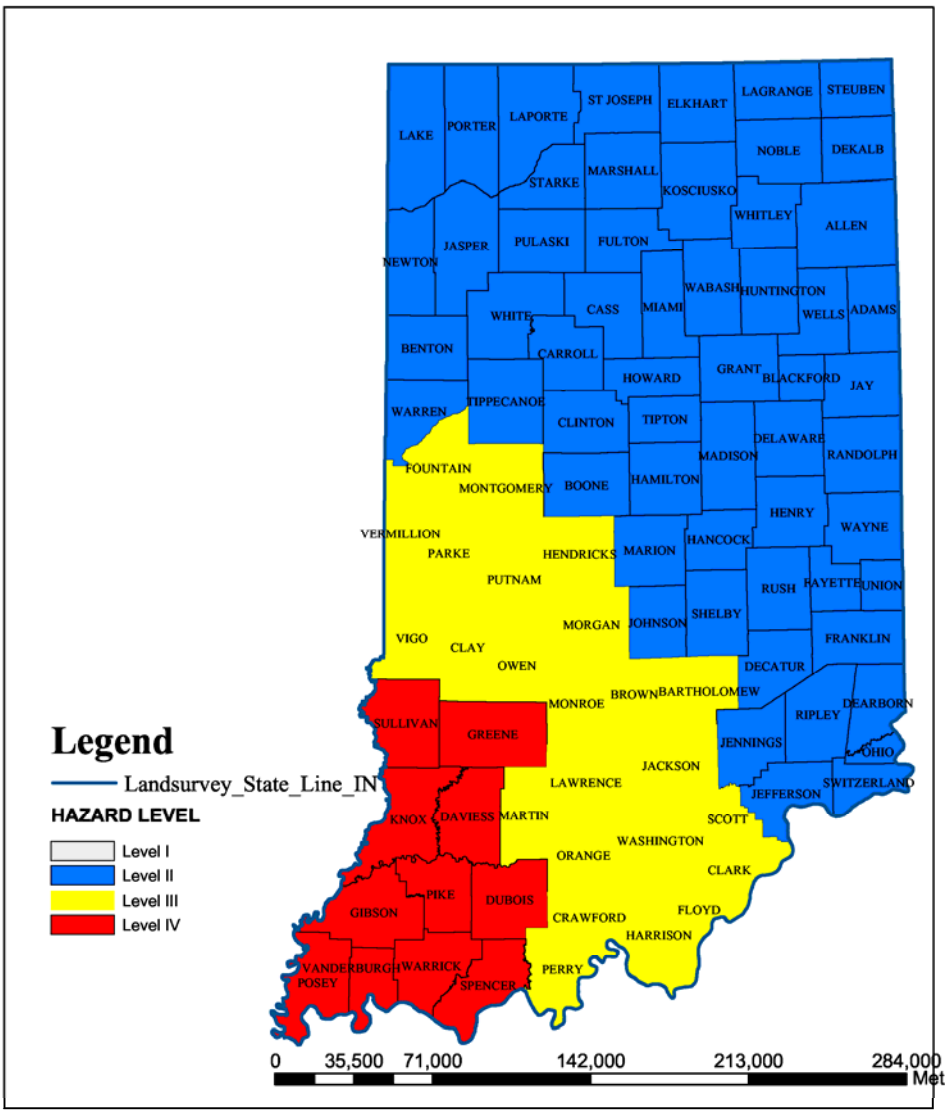

Figure 1-44 The design hazard level is defined as whichever is higher of the 1Hz or 5Hz hazard level [*ATC/MCEER*, 2003]. This map shows that hazard level for the 2002 USGS probabilistic hazard map, *with amplification factors for LRFD site class D*. This image cannot be considered an actual design map because it does not include actual site conditions.

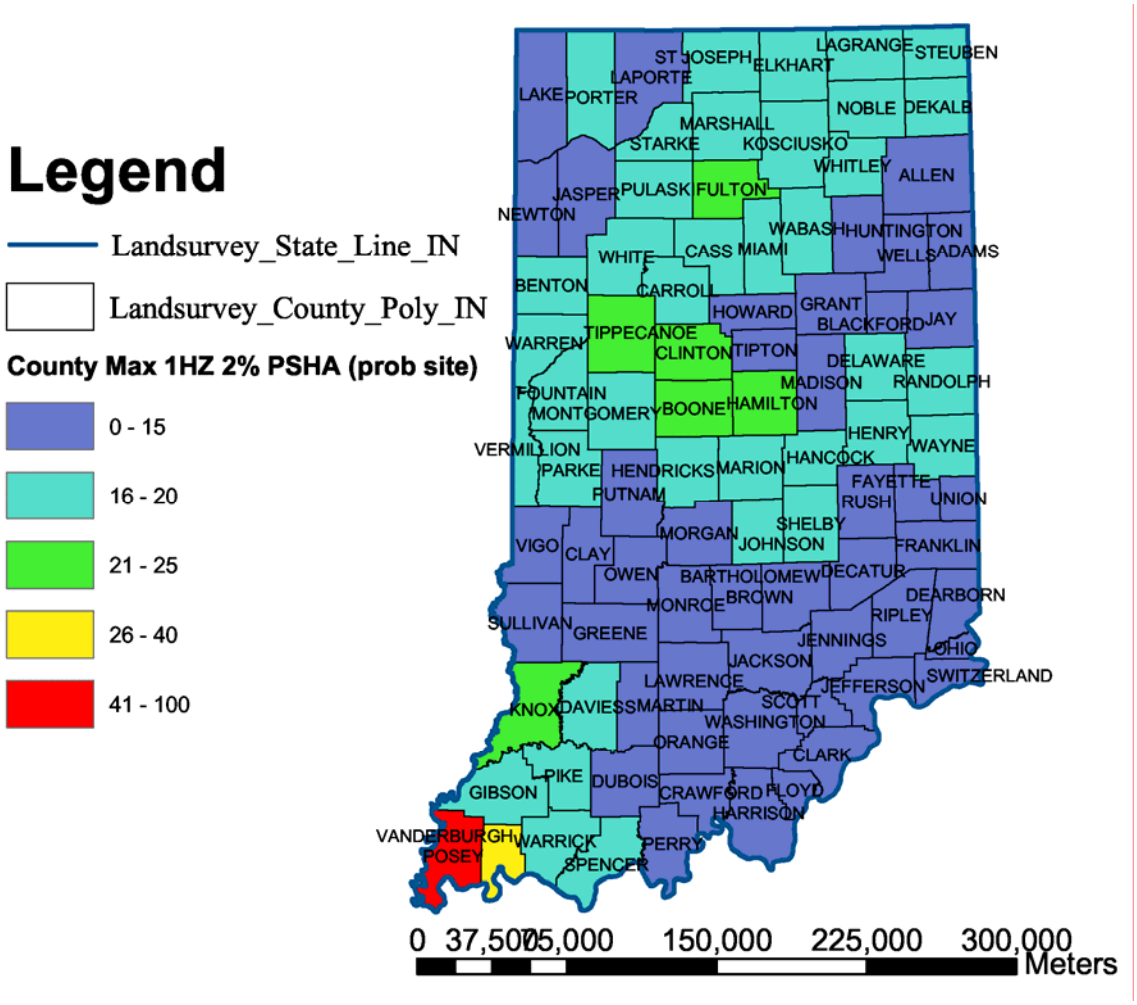

Figure 1-45 Map of the maximum seismic hazard level [*ATC/MCEER*, 2003] for each county if one assumed the 1 Hz PSHA results including probabilistic site response.

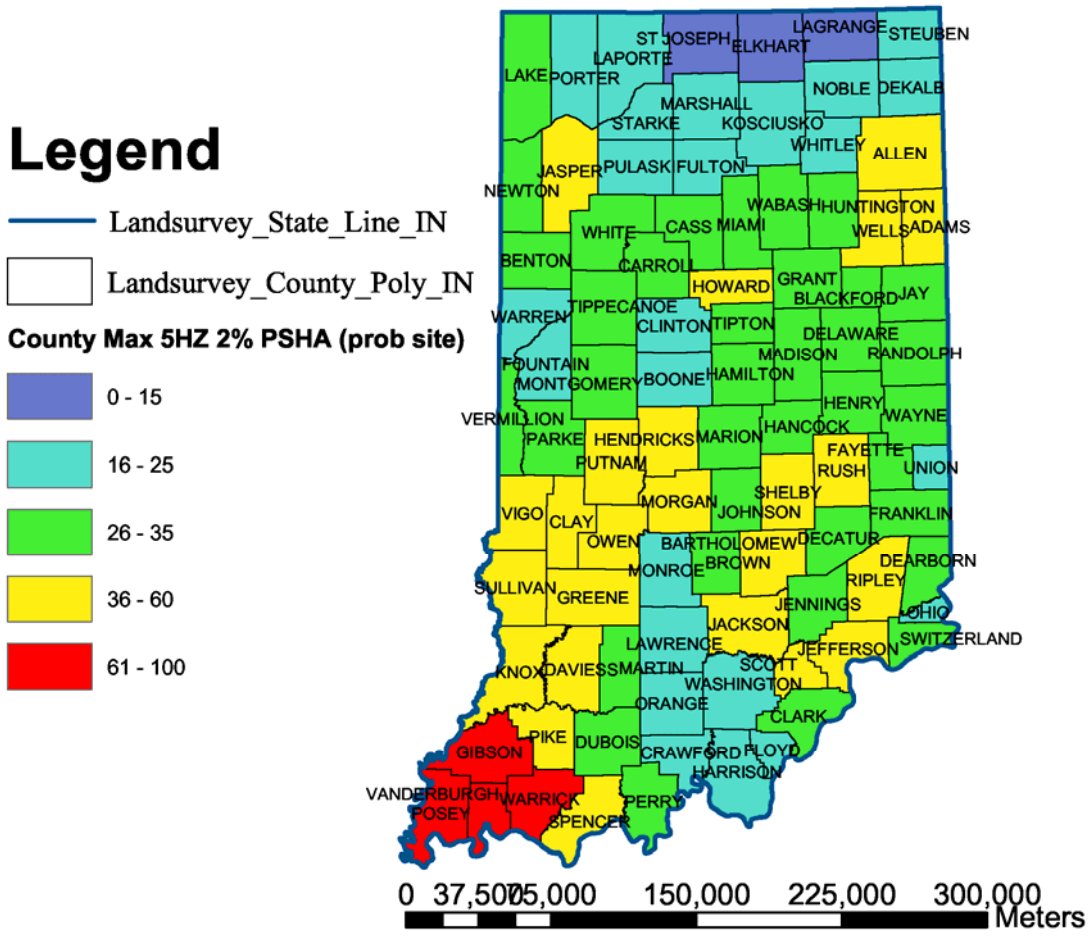

Figure 1-46 Map of the maximum seismic hazard level [*ATC/MCEER*, 2003] for each county if one assumed the 5 Hz PSHA results including probabilistic site response.

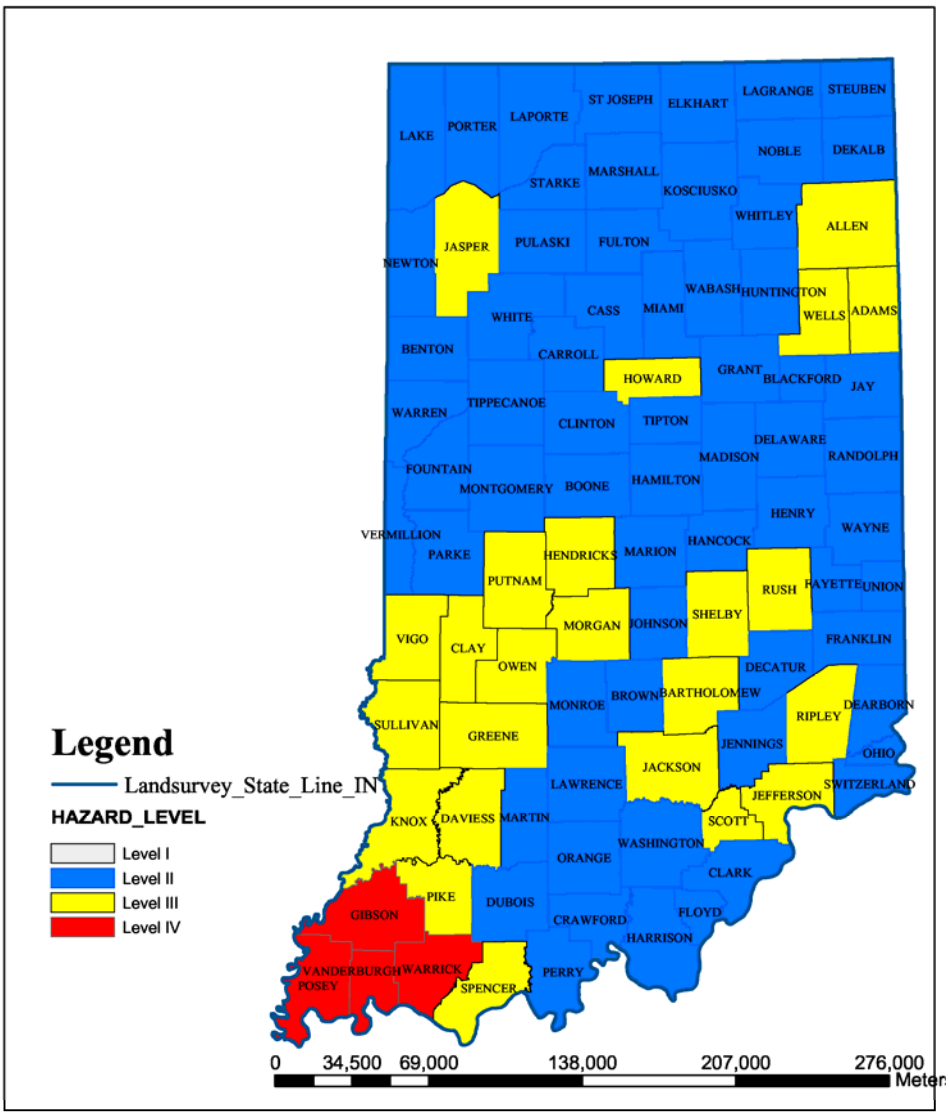

Figure 1-47 The final seismic hazard level is defined as whichever is higher of the 1Hz or 5Hz hazard level [*ATC/MCEER*, 2003]. This map shows that hazard level for the completely probabilistic site response. This image cannot be considered an actual design map because of the limitations discussed in section 1.7, however it gives a first approximation of the impact of the draft LRFD guidelines. The comparison with Figure 1-44 shows the predicted advantages of using a more detailed geologic description. This map is the prototype for the final preferred methodology for producing the seismic hazard maps.

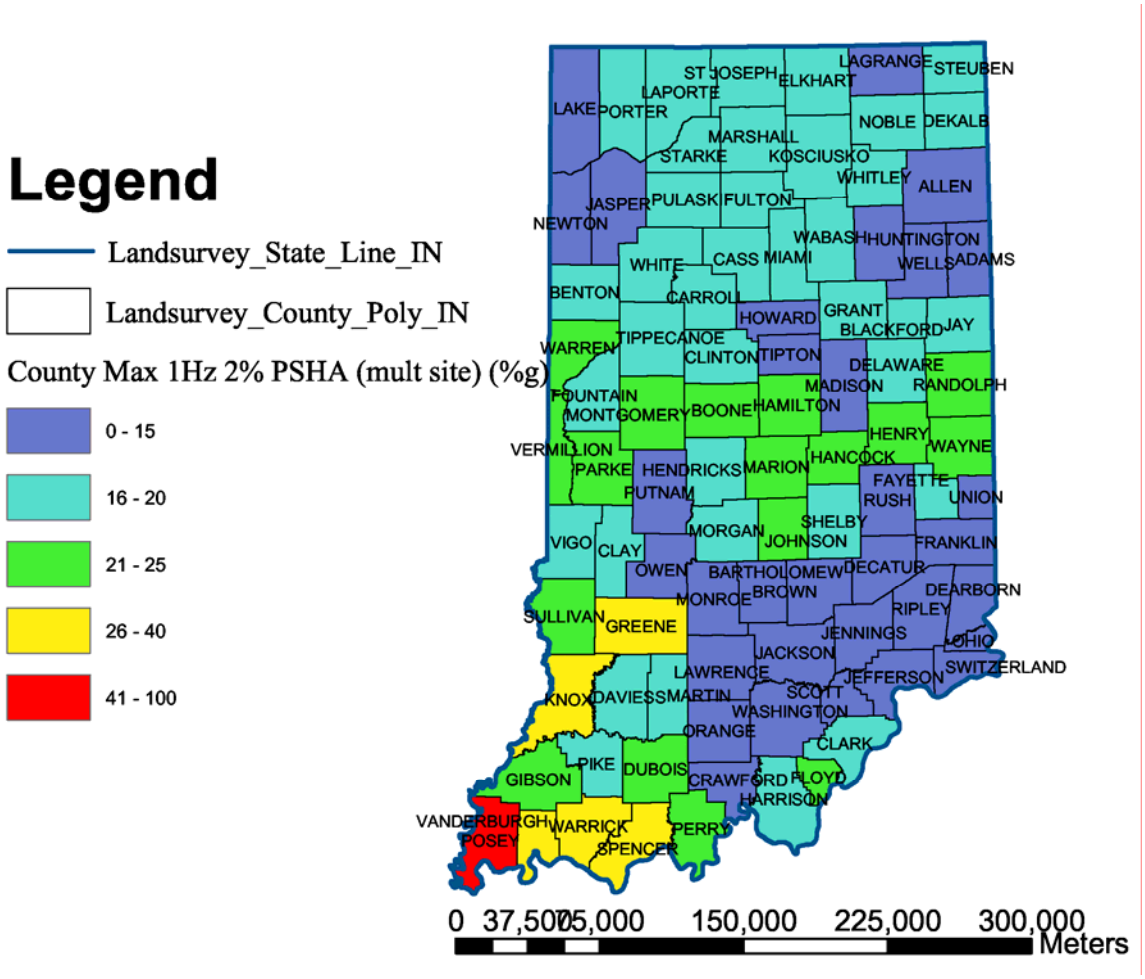

Figure 1-48 Map of the maximum seismic hazard level [*ATC/MCEER*, 2003] for each county if one assumed the 1 Hz PSHA results including simplified site response multiplication. Comparison with Figure 1-45 shows a similar pattern due to the strong regional geologic effects. Though this method is often applied in seismic hazard studies, the amplitude of the accelerations are less reliable because they do not take into account uncertainties in the knowledge of the near surface velocity profiles.

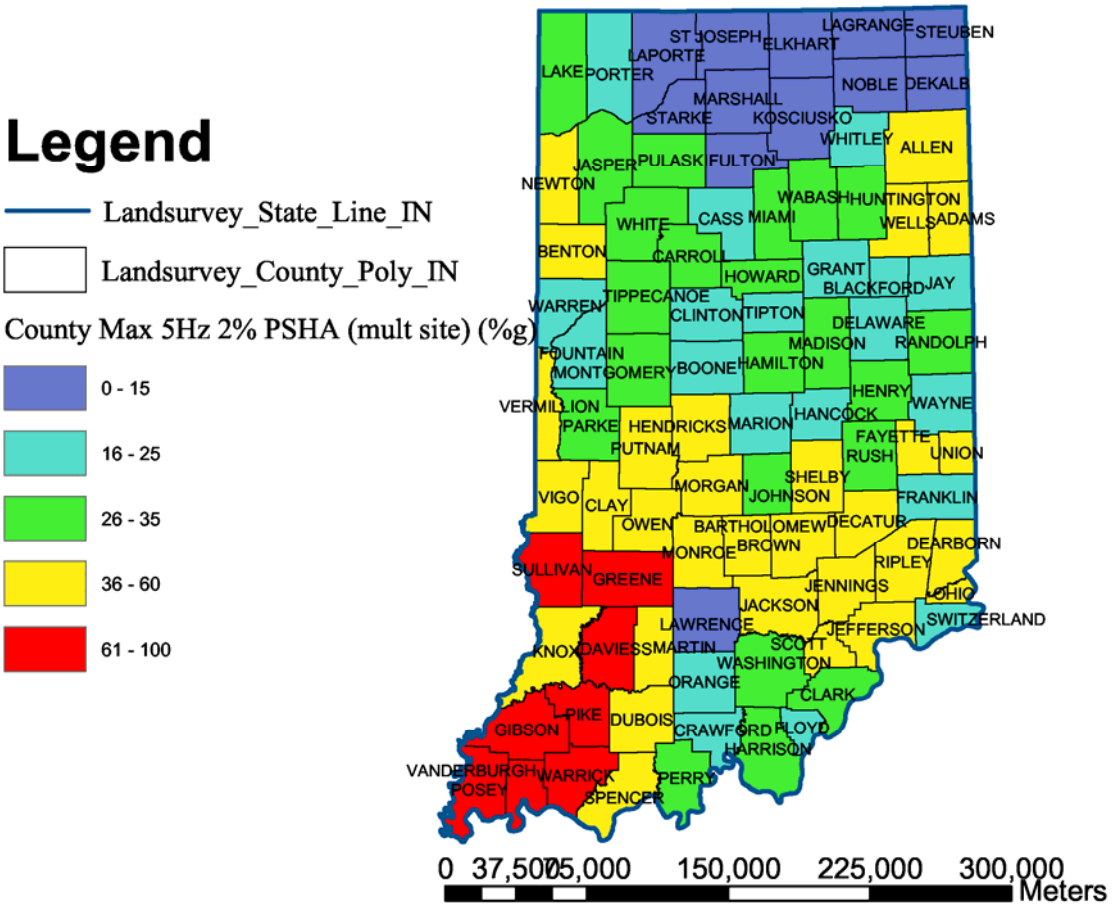

Figure 1-49 Map of the maximum seismic hazard level [*ATC/MCEER*, 2003] for each county if one assumed the 5 Hz PSHA results including simplified site response multiplication.

2 Shear Wave Measurement Methodology Comparison

2.1 Introduction

In order to implement a probabilistic hazard calculation that includes site effects for a large region such as the state of Indiana, it is necessary to develop a methodology to assign seismic velocities to surficial geologic units using a limited amount of shear wave velocity information in the near surface layer. We have analyzed the data from several methods and carried out a preliminary comparison of the data at a site near Pigeon Creek Bridge in Vanderburgh County. The types of data we have compared are 1) borehole shear wave velocity profiling using data collected by the Indiana Geological Survey (IGS) in the context of this project and previously collected shear wave profiles (Eggert, 1994) collected in a seismic hazard study commissioned by the city of Evansville 2) shear penetration test (SPT) data converted to Vs using empirical relations, 3) seismic refraction data and 4) estimates of Vs profiles using the Hardin and Drnevich equations [*Hardin and Drnevich*, 1972] using available geotechnical data. The uncertainties in the shear wave velocity data were estimated from all the available observations. We estimated the site amplification using Shake91 for a suite of velocity profiles with random variation of approximately 60 m/sec in the shear wave velocity and found that corresponds to an amplification factor for the PGA of approximately 6.8 +/- 0.7 for this site. The results illustrate for a particular case, the expected variation in the amplification factor due to the accuracy of the available shear wave data and also due to realistic horizontal variability in shear wave velocity and soil properties. Another important result is that it is evident that for the same soil profile, the amplification factor is much different for different input ground motion levels because of non-linear effects.

2.2 Downhole shear wave velocity profiles

Downhole shear wave velocity profiles using a three-component seismometer or cross hole measurements are the most accurate ways of characterizing the shear wave velocity in the upper 30 meters, the primary parameter affecting amplification. The Indiana Geological Survey made downhole shear wave velocity measurements in 28 boreholes across the state during the summer of 2003 to aid in assigning a velocity to the surficial geologic units. Measurements were taken at 2 m intervals from the base of the well, typically in bedrock, through the unconsolidated sediments. The units that were sampled are listed in Table 2-1, and Table 2-2. The distribution of sites was chosen to sample the principal geologic provinces in the state Figure 2-1. The wells were typically IDNR (Indiana Department of Natural Resources) monitoring wells or monitoring wells at INDOT sites. Examples of the retrieved velocity profiles from a site at Pigeon Creek (Figure 2-2) are shown in Figure 2-3, Figure 2-4 and Figure 2-5. Pigeon Creek was chosen as a test site because of the numerous types of S-wave data available there. The

borehole velocities clearly break down into two groups, with average velocities of 359 m/sec for glacial materials and 242 for nonglacial materials.

2.3 Local refraction surveys

Shallow seismic refraction is also useful for measuring the average shear wave velocity in the upper 30 m of sediments. We carried out measurements at 9 sites in the state using the Geometrics StrataView Exploration seismograph system and processing unit, with 110dB dynamic range. It is equipped with a 24 channel geophone cable with maximum offset of 500 meters with the capability of observing P-wave and S-wave energy on vertical and horizontal component geophones. The technique does not have the vertical resolution of borehole seismic profiles, but can sample deep layers much more efficiently and provides accurate averaged seismic velocities, and requires less permitting and preparation than borehole measurements. The 24 geophones were laid out in 100 m lines with .002 second sampling. The source was a 5 pound sledge hammer vertically striking a metal plate for P waves and horizontally striking a railroad tie coupled to the ground by the weight of a truck for the S-waves.

The travel times were picked from the recorded traces, spline interpolated, and then a slope was fit to individual segments of the travel time curve to provide a velocity. The choice of layer interfaces was subjectively chosen to provide the best fit. The errors in the data reduction procedure are estimated to be on the order of 10 m/sec. The layer velocities at each of the 9 sites are given in

Table 2-4. The average velocity is sensitive to the depth over which the layers are averaged. The Vp/Vs ratio has a large range, from 1.8 to over 4, which makes it difficult to use to for interpreting shear wave velocity from the large scale P-wave refraction dataset [*Rudman et al.*, 1973]. However, there is an indication that Vp/Vs is correlated with Vp (Figure 2-15). This means that if enough data is collected to establish the correlation more accurately, by means of classifying by type of sediments, it may be possible to exploit the rich P-wave refraction dataset for approximate shear wave velocities in the future.

2.4 SPT data from engineering drawings

Shear penetration test (SPT) data were collected from the INDOT records of bridge drawings (INDOT personal communication; Garcia, personal communication). We transformed the data to shear wave velocity using the following empirical relation [*Bobet et al.*, 2001; *Imai and Tonouchi*, 1982]

Eq 2-1

$$V_s = 97 \cdot N^{0.314} \quad \text{for clay}$$
$$V_s = 114 \cdot N^{0.217} \quad \text{for other soil types}$$

where N is the blow count number. The data for the Pigeon Creek site is shown in Table 2-3.

2.5 Hardin-Drnevich equations and specific soil characteristics

The value of shear wave velocity of near surface soils is one measurement of soil behavior when dynamically loaded. Currently, the shear wave velocity profile of a location may be obtained through field tests such as the standard penetration test (SPT), ASTM D1586, seismic refraction, ASTM D5777, or crosshole seismic testing, ASTM D4428/D4428M. Because each of these tests requires significant resources in terms of equipment and time in the field, an alternative method of approximating the shear wave velocity profile may be desirable for some applications. The following technique was implemented using bore log data to generate a shear wave velocity profile for the location at which the bore log was recorded.

Equation 1, the Hardin Equation [*Hardin and Drnevich*, 1972] is used to calculate the shear modulus of a soil at minimum strain.

Eq 2-2 $$G_{max}=SF(e)OCR^{K}(\sigma_o')^{n}Pa^{(1-n)}$$

In the above equation *S* refers to the "Stiffness Number" and is approximately to 625 [*Hardin*, 1978], *F(e)* is the function of void ratio discussed later in the spreadsheet explanation, OCR^{K} is the overconsolidation ratio raised to a coefficient, K, related to the plasticity index of the soil. σ_o' is the mean effective stress of the soil at the point of measurement, n is a coefficient equal to 0.5, and Pa is atmospheric pressure.

G_{max} is related to shear wave velocity by the following equation,

Eq 2-3 $$V_s = \sqrt{\frac{G_{\max}}{\rho}}$$

We have developed a spreadsheet that uses information collected on a bore log to calculate each variable in the Hardin equation as well as density to generate the shear wave profile of a specific location. The report in the appendix describes in more detail the method, with an example from the literature.

2.6 Intercomparison of data

We have performed an intercomparison of the different types of data in order to 1) describe the advantages and disadvantages of the different methods for acquiring a dense dataset in the future 2) estimate the variability of the shear wave velocity over a length scale that is below the limit of reasonable mapping efforts at the state in order to describe the most reasonable sampling density, and 3) to provide velocity data and uncertainty estimates for the preliminary probabilistic hazard calculation. Evansville was chosen because we have independent data from different measurement methods for comparison, at a bridge site near Pigeon Creek (Figure 2-2). Within a few kilometers there are 3 boreholes where shear wave velocity data were already available [*Eggert et al.*, 1994], 3 boreholes within 20 m where new S-wave profiles were taken, 3 different boreholes where detailed borelogs were available from engineering site studies with both SPT data and soil properties, and a refraction profile within several kilometers. The profiles are typically interbedded layers of gravel, sand and gravel, and silty or sandy loam, overlaying shale bedrock.

The comparison of the data is shown in Figure 2-17. Often the velocities within the profiles seem to be lower for silt and silty loam layers and higher for sand and gravel layers. However, the lateral variation in the thickness and depth of the different layers makes it difficult to correlate individual layers. Most of the standard deviation of the average velocities at each depth may be due to variations in the depth of the layers. A statistical approach for describing these profiles seems reasonable for such variable materials. The average velocity and standard deviation for each layer depth, taking into account all of the shear-wave velocity measurements, is shown in Figure 2-18. The standard deviation of the velocity is around 60 m/sec uniformly with depth until the bedrock is reached (Table 2-5). At bedrock, velocity uncertainties go up because of the variation in bedrock depth that control the depth of the large impedence contrast.

2.7 Uncertainties and their effect on amplification

The purpose of this study is to determine the uncertainties in site response amplification due to the uncertainties in the shear wave velocity profile. This calculation is the critical part of the probabilistic hazard calculation, because these uncertainties modify the rock site attenuation curve. We investigated this effect with a limited dataset prior to implementing the hazard calculation.

We created a suite of 4 random velocity profiles with mean and standard deviation given by the characteristics of the Pigeon Creek data (Table 2-5). We calculated the amplification factor for each of the profiles using SHAKE91 [*Idriss and Sun*, 1992]. The spectral response for the average profile with a range of input ground motion levels is shown in Figure 2-19. Note the broadening of the peak and shift towards lower frequencies for higher input ground motions. The calculation was run again with an input ground motion time series with two different levels of peak ground acceleration. The results for 0.1g and 0.2g are shown in Figure 2-20, Figure 2-21, and Table 2-6. In this example with an input ground motion of 0.1g, the resulting uncertainty in the output amplification factor is 0.3, for 5 Hz. If we use the amplification factor of 2.08 and an uncertainty of 0.3 we can calculate that for 35% of the range of ground motions in the seismic level II (ground motions of .15 to 0.35g), the one standard deviation uncertainty would put the ground motion into a different seismic level. For this reason it is critical to include the uncertainty in the amplification factor into the probabilistic calculation.

2.8 Conclusions

We have collected and compiled 28 new borehole shear wave velocity profiles, and 9 new refraction profiles. We carried out a detailed comparison in order to 1) describe the advantages and disadvantages of the different methods for acquiring a dense dataset in the future 2) estimate the variability of the shear wave velocity over a length scale that is below the limit of reasonable mapping efforts at the state in order to describe the most reasonable sampling density, and 3) to provide velocity data and uncertainty estimates for the preliminary probabilistic hazard calculation.

The data included in the comparison included the new borehole and refraction profiles, previously collected shear wave profiles (Eggert, 1994) from a seismic hazard study commissioned by the city of Evansville, shear penetration test (SPT) data converted to Vs using empirical relations, and estimates of Vs profiles using the Hardin and Drnevich equations [*Hardin and Drnevich*, 1972] using available geotechnical data. The uncertainties in the shear wave velocity data for the particular site studied, near Pigeon Creek, are 60 m/sec almost uniform with depth to bedrock. Running ground motion simulations with SHAKE91, we find that an uncertainty of 60m/sec in this type of profiles produces uncertainty in the output amplification factors less than 0.5.

Table 2-1 Borehole shear wave velocities grouped by geological formation

Lagro

Town	Shear Velocity	Average Velocity (m/s)
Salamonia	360	
Portland	356	
Muncie	294	337

Trafalger

Town	Shear Velocity	Average Velocity (m/s)
Lafayette	325	
Lafayette	348	
Lafayette	394	
Lafayette	380	
Frankfort	383	366

Midwestern Fluvial

Town	Shear Velocity	Average Velocity (m/s)
Sullivan	159	
Carlisle	158	158
East Mt Carmel	199	
Pimento	215	
Farmersburg	200	
Oaktown	263	
Decker	219	
Frichton	238	222

Seymore

Town	Shear Velocity	Average Velocity (m/s)
Teppco	310	
Rumpke	274	292

Northwest Glacial

Town	Shear Velocity	Average Velocity (m/s)
Gary (bedrock?)	616	616
St. Joseph	256	
Laporte	241	249

South Central

Town	Shear Velocity	Average Velocity (m/s)
Bloomington (bedrock)	1176	1176
Mooresville	316	
Martinsville	335	
Martinsville	295	315

Evansville

Town	Shear Velocity	Average Velocity (m/s)
Pigeon Creek	238	
Pigeon Creek	230	
Pigeon Creek	225	231

Table 2-2 List of borehole shear-wave velocity measurements made by the IGS in the summer 2003.

Glacial	Shear Velocity (m/s)	NEHRP site class
Salamonia	360	C
Portland	356	D
Muncie*	294	D
Lafayette	325	D
Lafayette	348	D
Lafayette	394	C
Lafayette	380	C
Frankfort	383	C
Gary (bedrock)	616	C
St. joseph	256	D
Laporte	241	D
AVERAGE	359	
Non Glacial	**Shear Velocity (m/s)**	
Teppco	310	D
Rumpke	274	D
Mooresville	316	D
Martinsville	335	D
Martinsville	295	D
Pigeon Creek	238	D
Pigeon Creek	230	D
Pigeon Creek	225	D
Sullivan**	159	E
Carlisle**	158	E
East Mt. Carmel	199	D
Pimento	215	D
Farmersburg	200	D
Oaktown	263	D
Decker	219	D
Frichton	238	D
AVERAGE	242	
Bedrock	**Shear Velocity (m/s)**	
Bloomington ^	1176	B

Table 2-3 SPT data from 3 holes at Pigeon Creek bridge site with calculated shear wave velocity.

T.B.#B-1

Pigeon Creek Boring Data

	elevation	thickness (m)	depth (m)	soil type	N	V (m/s)	GL
	114.35			grond Level			
1	113.44	0.91	0.91	42	15	227.0201	
2	112.83	0.61	1.52	44	23	259.6296	
3	111.91	0.92	2.44	43	11	205.9534	
4	107.19	4.72	7.16	44	9	191.0985	GL
5	103.99	3.2	10.36	44	8	182.6169	
6	100.94	3.05	13.41	43	15	227.0201	
7	100.18	0.76	14.17	43	18	240.396	
8	99.11	1.07	15.24	42	32	287.9976	
9	96.37	2.74	17.98	43	19	244.5121	
10	92.4	3.97	21.95	4	11	203.973	
11	88.14	4.26	26.21	52			
	sum	26.21					

2= clay
21=stiff silty clay
22=hard silty clay
23=silty clay
3=silt
31=stiff silt
32=dense silt
33=clayey silt
34=stiff clayey silt
4=sand
41=stiff clay silty sand
42=gravel sand
43=silty or sandy loam
44=gravel
45=clay loam
51=sandstone
52=shale
*=grouting

T.B#B-2 114.79

1	114.18	0.61	0.61	43	21	252.3182	
2	113.57	0.61	1.22	43	6	170.2595	
3	110.68	2.89	4.11	42	4	145.8656	
4	110.07	0.61	4.72	*			
5	108.69	1.38	6.1	45	10	187.8905	
6	102.29	6.4	12.5	43	9	189.9369	
7	101.68	0.61	13.11	43	12	211.658	
8	99.55	2.13	15.24	*			
	sum	15.24					

T.B#B-6

	114.77	thickness	depth(m)	soil type	N	V	GL
1	108.67	6.1	6.1	43	11	207.8931	
2	107.15	1.52	7.62	43	2	120.5855	
3	101.51	5.64	13.26	43	5	160.786	
4	97.7	3.81	17.07	43	9	191.0985	GL
5	96.94	0.76	17.83	4	13	214.3885	
6	95.72	1.22	19.05	43	15	227.0201	
7	92.52	3.2	22.25	43	18	238.279	
8	90.72	1.8	24.05	52	120	436.1488	
	sum	24.05					

Table 2-4 P-wave and S-wave velocity data from seismic refraction at 9 sites.

P-wave Velocity Profile							
Station	**Latitude**	**Longitude**	**z0**	**z1**	**vp0**	**vp1**	**vp2**
vann	37.96	-87.52	0.97	8	189.3	405.2	1672.5
nepac	41.103	-86.403	1.62	10	213.6	1548.9	2068.5
swpac	38.741	-87.491	0.98	4	225.5	541.9	2292.6
tpac	40.295	-86.884	2.08	206	2159.4		
ppac	41.445	-86.939	6.97	306	2708.6		
sipac	38.453	-86.684	1.87	240	2427.6		
fpac	38.888	-86.563	1.43	11	223.2	1339.3	4113.8
dpac	40.26	-85.15	1.14	7	255.3	879.1	4765.0
sepac	39.034	-85.529	1.45	6	183.6	1742.3	5008.8

S-wave Velocity Profile							
Station	**Latitude**	**Longitude**	**z0**	**z1**	**vs0**	**vs1**	**vs2**
vann	37.96	-87.52	0.13	14	146.3	185.7	357.1
nepac	41.105	-86.403	1.52	6	113.0	292.0	449.3
swpac	38.741	-87.491	6.21	14	144.2	527.6	1593.5
tpac	40.295	-86.884	1.6	13	101.8	364.6	590.2
ppac	41.445	-86.939	23.5	192	1340.7		
sipac	38.453	-86.684	2.13	169	803.3		
fpac	38.888	-86.563	1.07	12	136.1	297.5	2226.3
dpac	40.26	-85.15	1.13	9	103.2	300.0	2757.7
sepac	39.034	-85.529	1.74	8	140.0	447.9	2977.1
cherryln	40.43775	-86.9462	0.96	16	116.3	322.6	555.6

Average Speeds down to 10 meters					
Station	**latitude**	**longitude**	**Ave Vp**	**Ave Vs**	**Vp ave/ Vs ave**
vann	37.96	-87.52	609	185	3.29
nepac	41.105	-86.403	1336	323	4.14
swpac	38.741	-87.491	1610	290	5.55
tpac	40.295	-86.884	1753	323	5.43
ppac	41.445	-86.939	1034	192	5.39
sipac	38.453	-86.684	2018	668	3.02
fpac	38.888	-86.563	1180	280	4.21
dpac	40.26	-85.15	2036	639	3.19
sepac	39.034	-85.529	2738	936	2.93
cherryln	40.43775	-86.9462		275	

Average Speeds down to 15 meters					
Station	**latitude**	**longitude**	**Ave Vp**	**Ave Vs**	**Vp ave/ Vs ave**
vann	37.96	-87.52	963	196	4.91
nepac	41.105	-86.403	1580	365	4.33
swpac	38.741	-87.491	1838	452	4.07
tpac	40.295	-86.884	1889	371	5.09
ppac	41.445	-86.939	1592	192	8.29
sipac	38.453	-86.684	2155	713	3.02
fpac	38.888	-86.563	1891	677	2.79
dpac	40.26	-85.15	2946	1345	2.19
sepac	39.034	-85.529	3495	1616	2.16
cherryln	40.43775	-86.9462		290	

Average speeds down to 30 meters					
Station	**latitude**	**longitude**	**Ave Vp**	**Ave Vs**	**Vp ave/ Vs ave**
vann	37.96	87.52	1318	276	4.78
nepac	41.105	85.403	1824	407	4.48
swpac	38.741	87.491	2065	1023	2.03
tpac	40.295	86.884	2024	480	4.22
ppac	41.445	86.939	2150	441	4.88
sipac	38.453	86.684	2291	758	3.02
fpac	38.888	86.563	3003	1452	2.07
dpac	40.26	85.15	3855	2051	1.88
sepac	39.034	85.529	4252	2297	1.85
cherryln	40.43775	-86.9462		369	

Table 2-5 Average and standard deviation of the shear wave velocity for all measurements made at the Pigeon Creek site. The random profiles are those generated from the average profiles with a random number generator assuming the standard deviation of the actual measurements. These random profiles are used in the simulations examining the effects on amplification.

Depth (m)	Standard dev.	Average	Random1	Random2	Random3	Random4
2	65.1	208.6	252	182	202	215
4	55.2	192.5	186	215	229	192
6	64.1	213.3	240	240	257	166
8	88.6	231.4	313	151	301	155
10	66.2	218.1	256	214	220	171
12	69.3	224.7	177	205	255	220
14	61.7	277	281	230	309	222
16	50.4	242.4	249	213	258	239
18	62.8	259.3	277	243	260	202
20	30.4	252.2	270	266	230	271
22	97.7	320	371	244	311	242
24	240.3	472.2	482	418	542	608
26	524.6	837.1	1361	359	928	1053

Table 2-6 Amplification factor and uncertainties for a suite of four random profiles with the same statistical variation as was found at the Pigeon Creek site and for input ground motion levels of 0.1g and 0.2g.

Period(s)	0.1g	Avg Fa	σ Fa	0.2g	Avg Fa	σ Fa
0.00	0.10	1.57	0.14	0.20	1.25	0.08
0.10	0.27	1.15	0.17	0.54	0.69	0.14
0.20	0.18	2.08	0.30	0.37	1.32	0.24
0.50	0.09	6.77	0.65	0.19	3.68	0.63

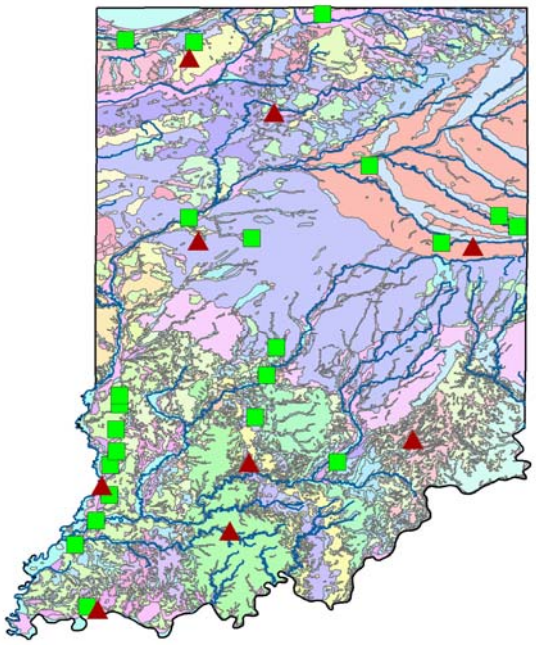

Figure 2-1 Map of locations of IGS downhole shear wave velocity profiles (green squares) and refraction measurements (red triangles).

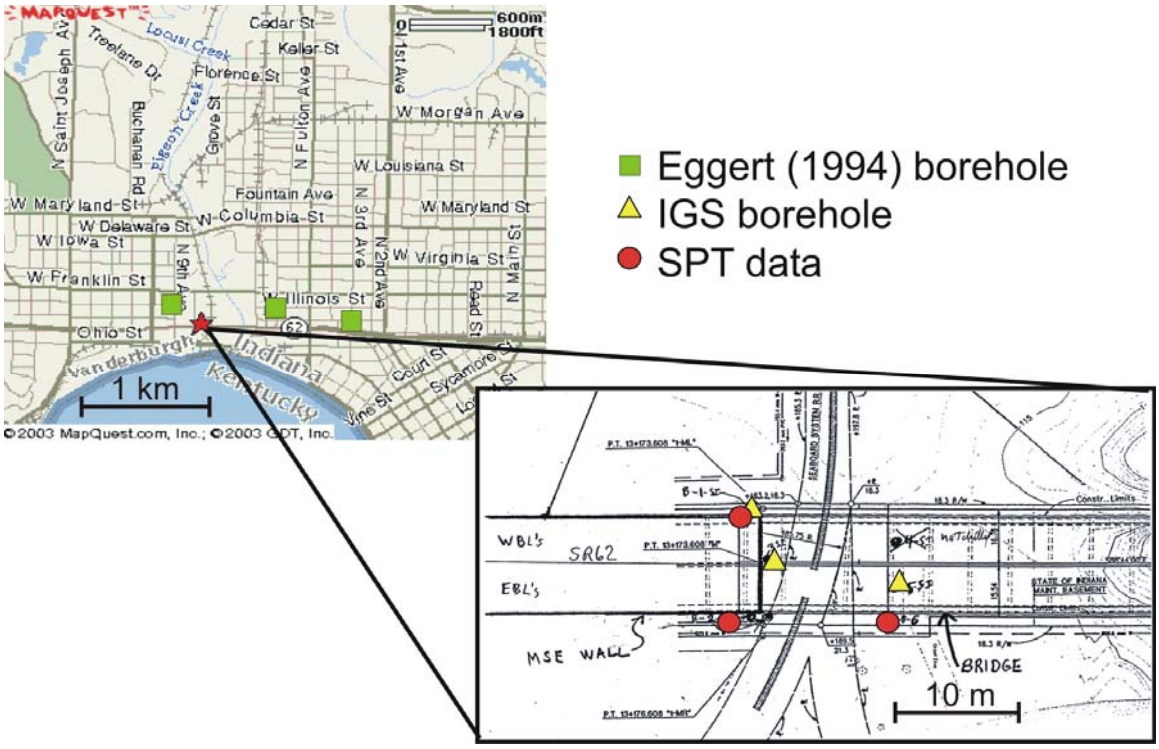

Figure 2-2 Sites used in the intercomparison of multiple datasets from the Evansville region.

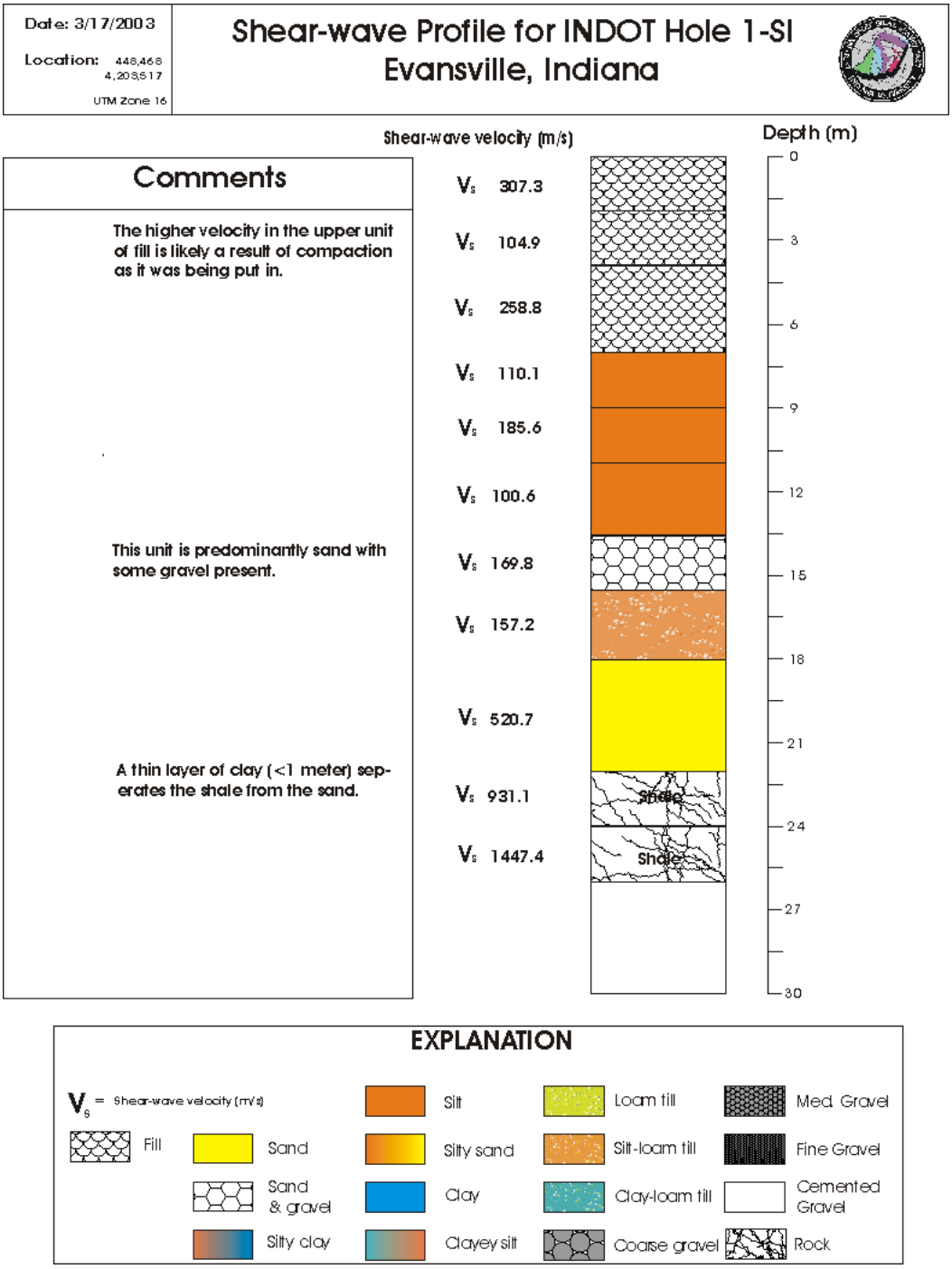

Figure 2-3 Shear wave velocity profile from borehole 1-S1 at Pigeon Creek.

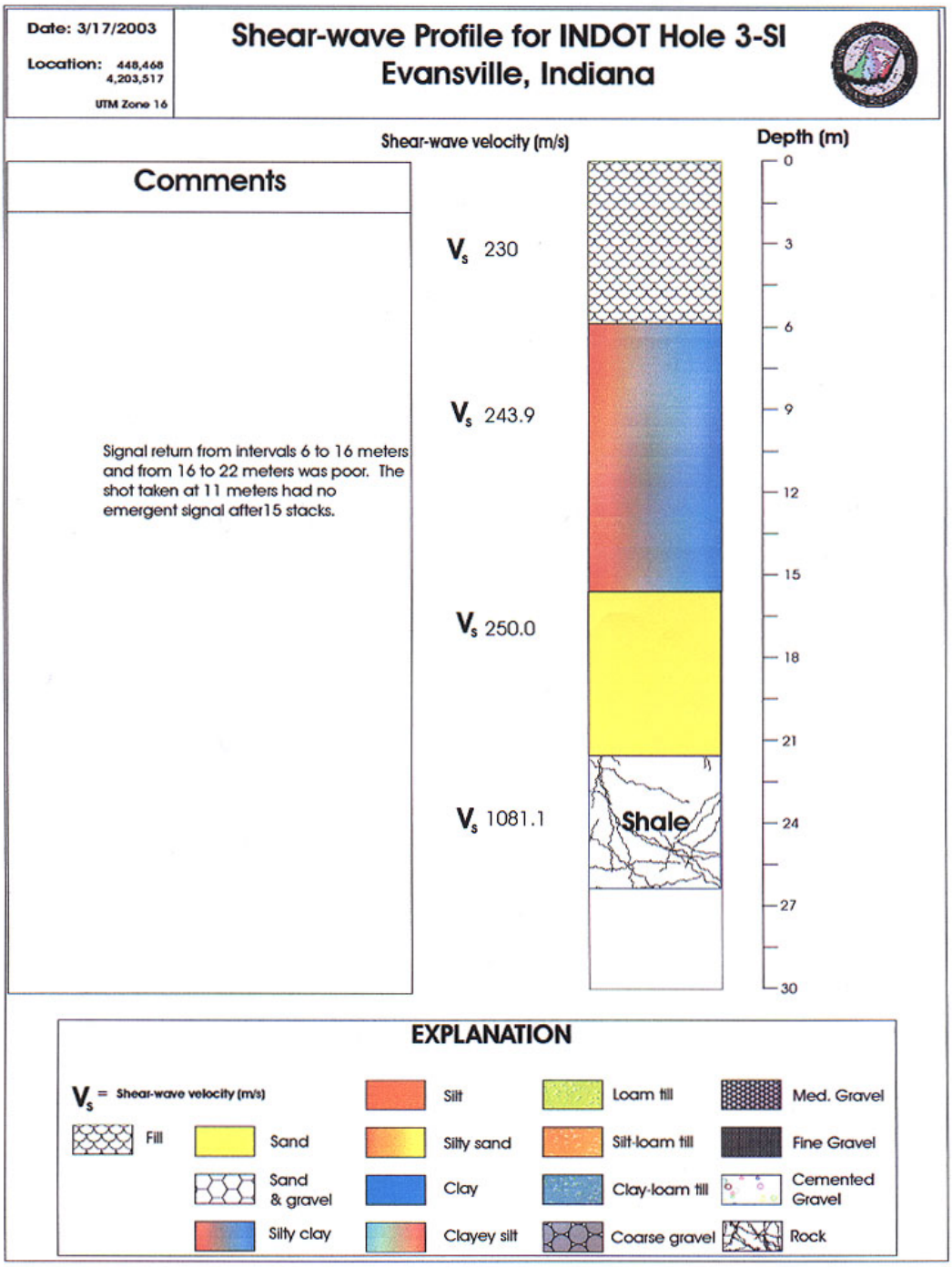

Figure 2-4 Shear wave profiles from borehole 3-S1 at Pigeon Creek.

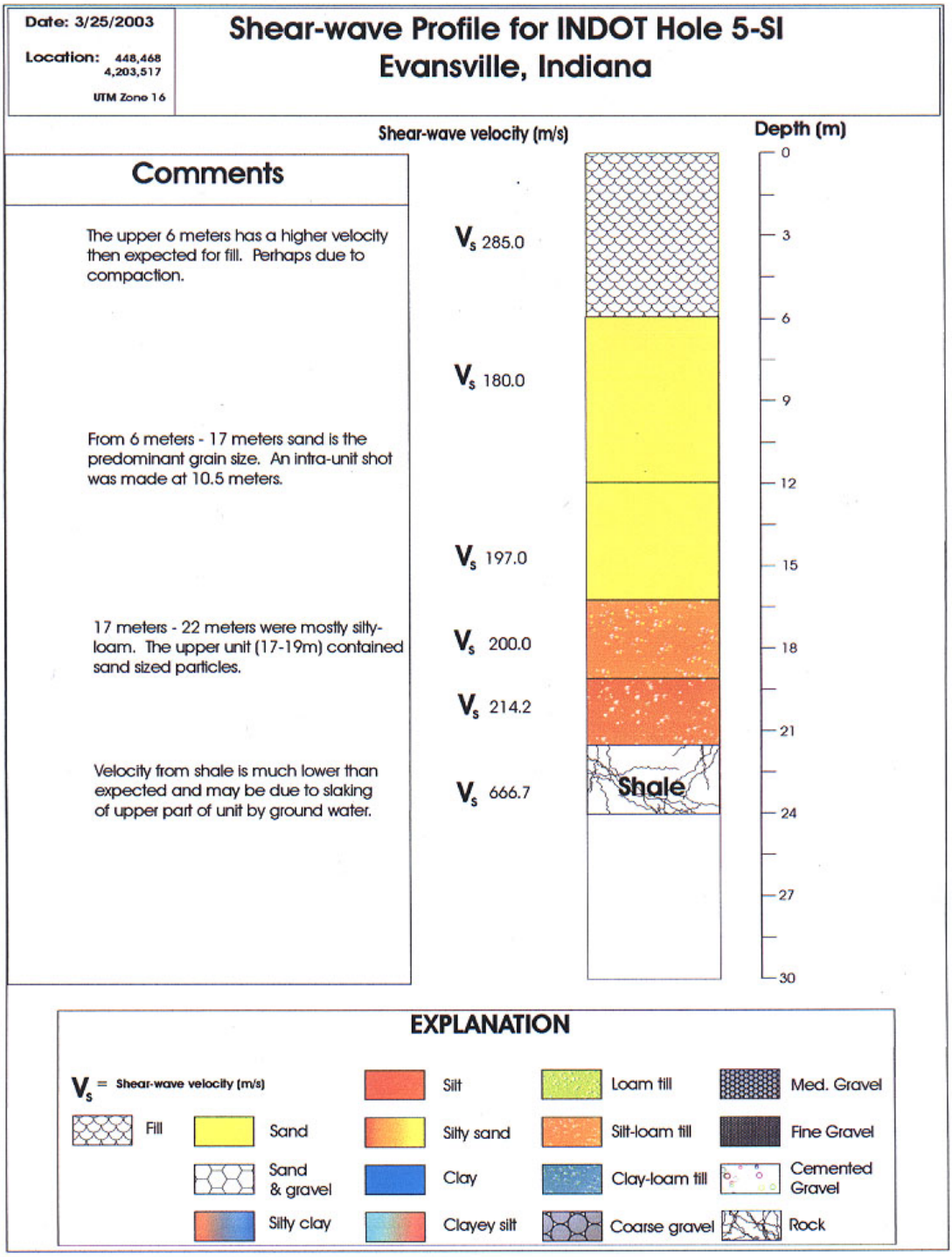

Figure 2-5 Shear wave profiles from borehole 5-S1 at Pigeon Creek.

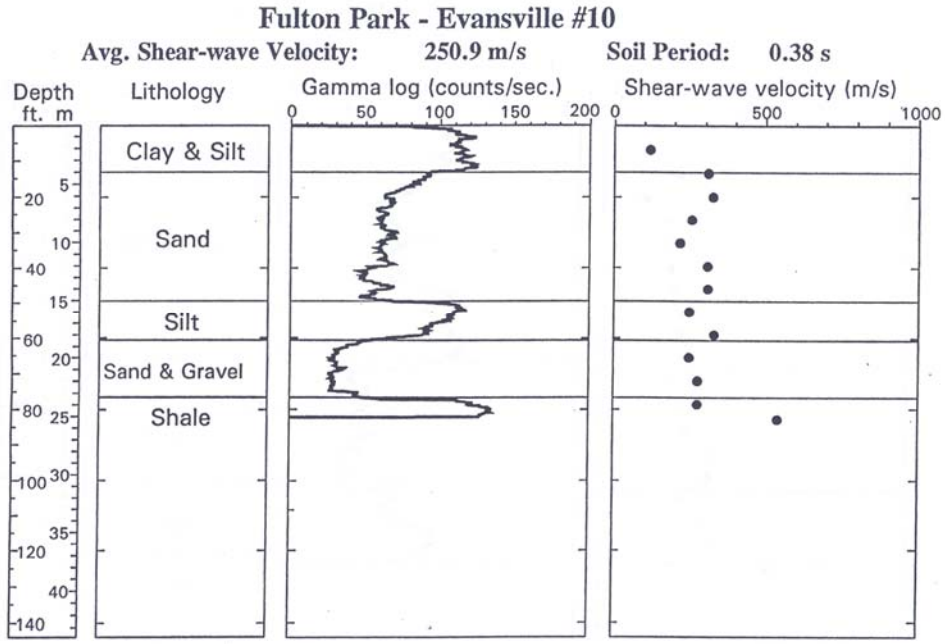

Figure 2-6 Shear wave profile EV10 from a site near Pigeon Creek [*Eggert et al.*, 1994]

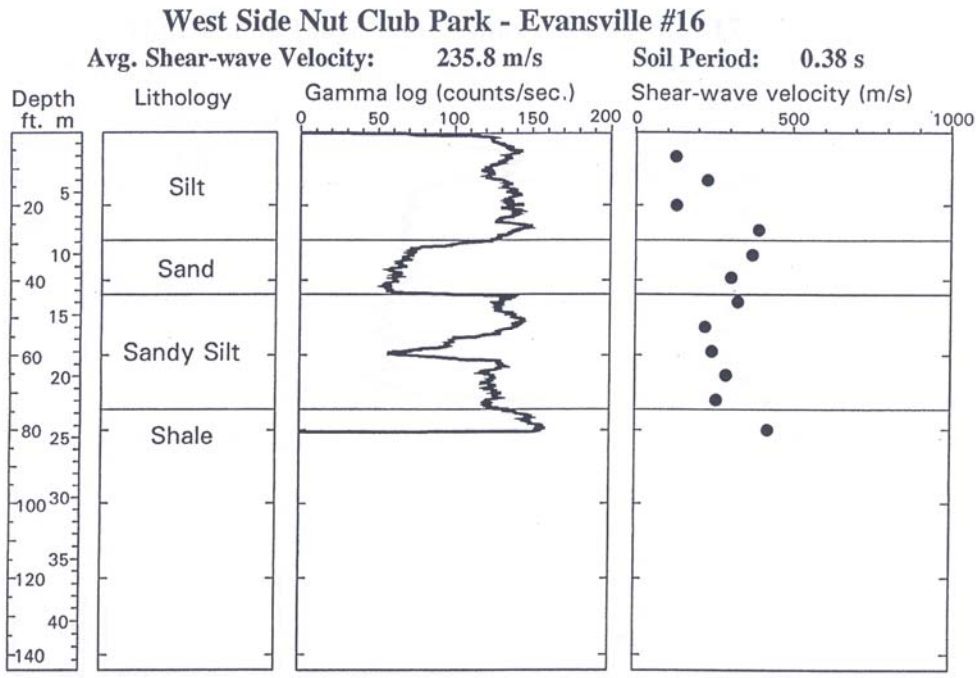

Figure 2-7 Shear wave profile EV27 from a site near Pigeon Creek [*Eggert et al.*, 1994]

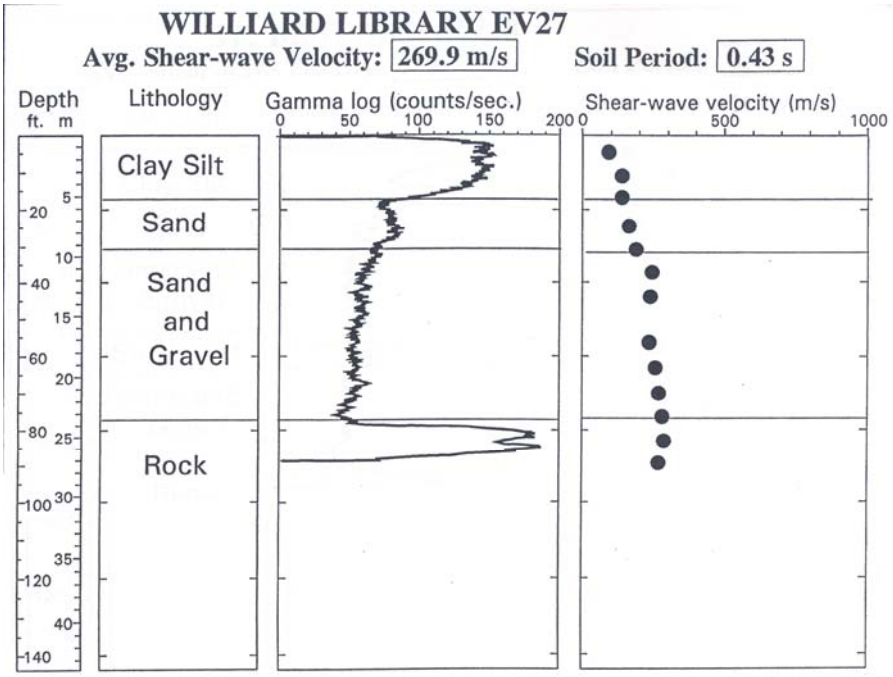

Figure 2-8 Shear wave profile EV27 from a site near Pigeon Creek [*Eggert et al.*, 1994]

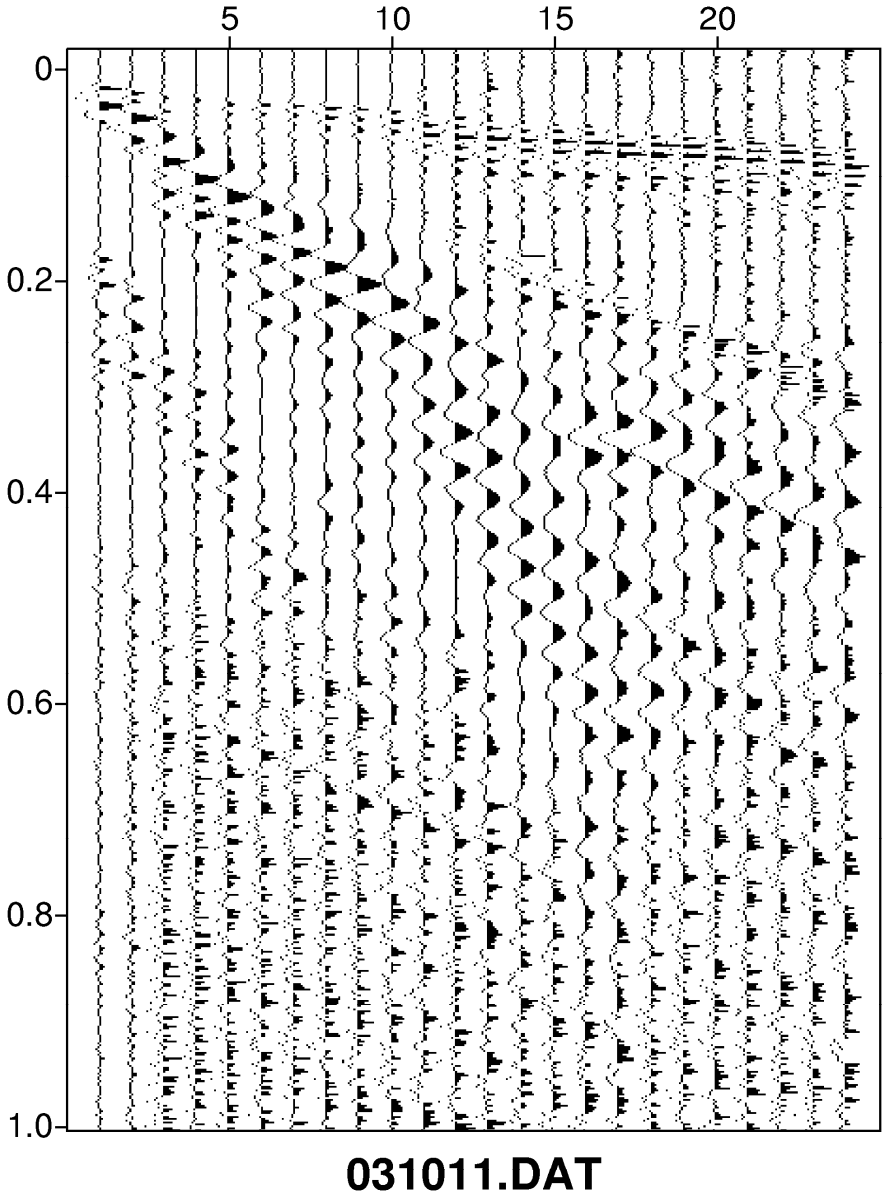

Figure 2-9 Example of P-wave refraction data from the Cherry Lane site. Trace number is on the x-axis, with each trace 5m apart. Time in seconds is on the y axis.

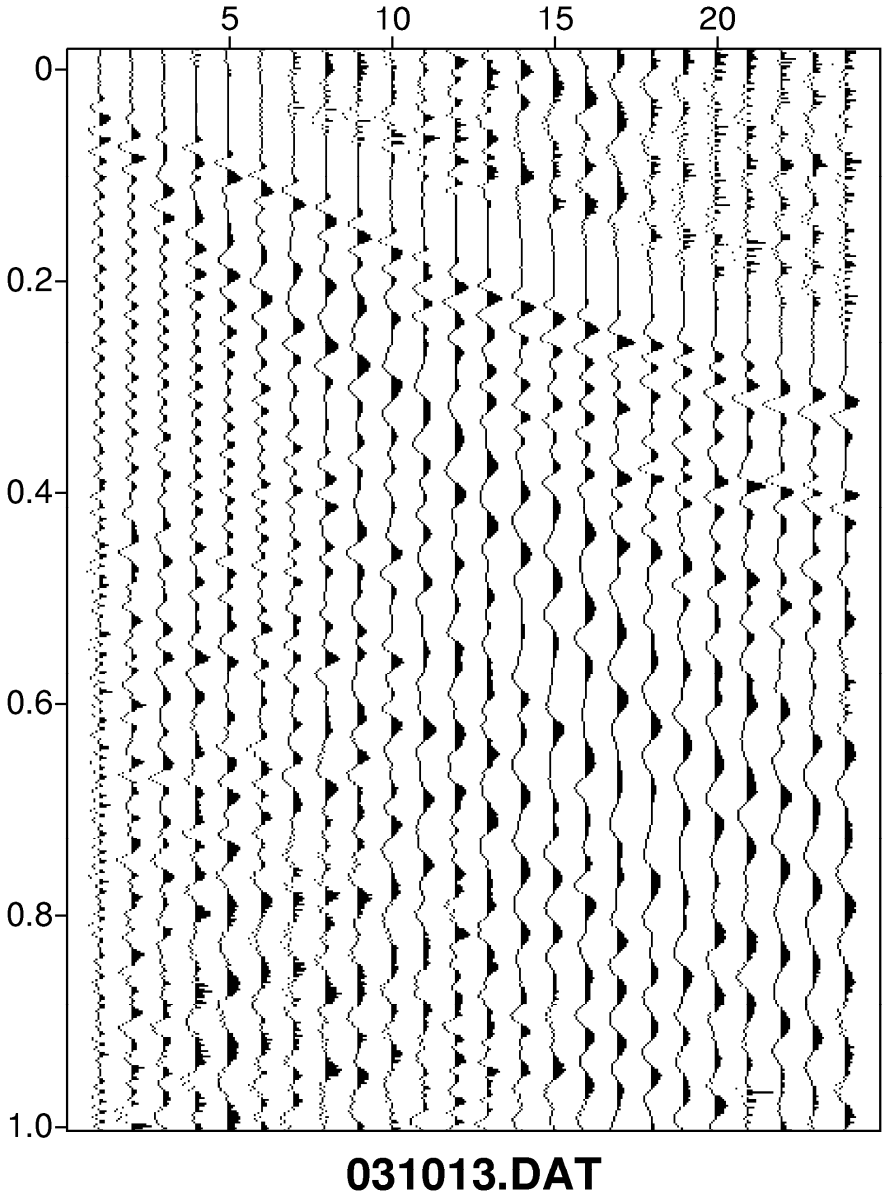

Figure 2-10 Example of S-wave refraction data from the Cherry Lane site. Trace number is on the x-axis, with each trace 5m apart. Time in seconds is on the y axis.

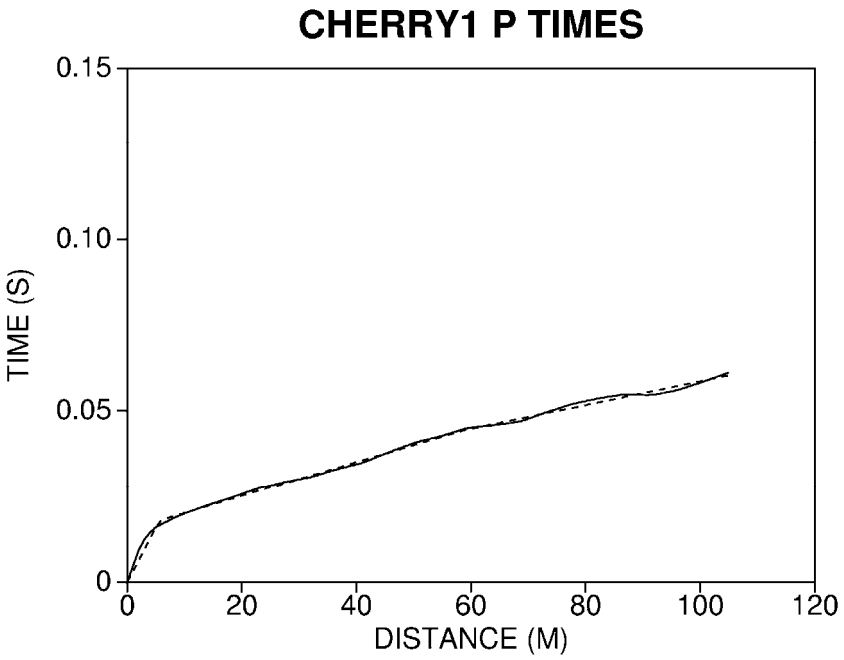

Figure 2-11 Travel-time curve from picked P-arrivals of refraction record section

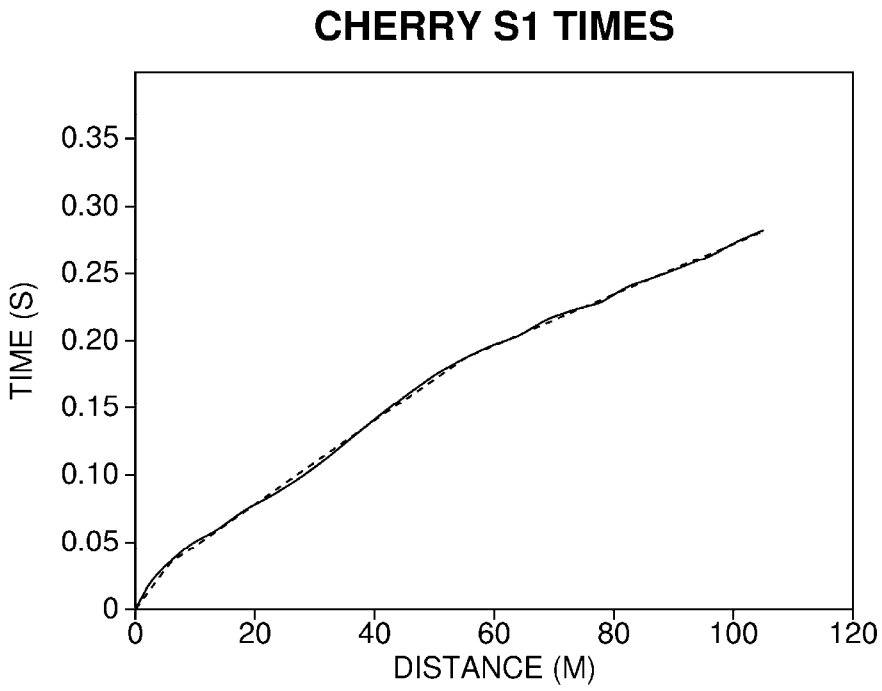

Figure 2-12 Travel-time curve from picked S-arrivals of refraction record section

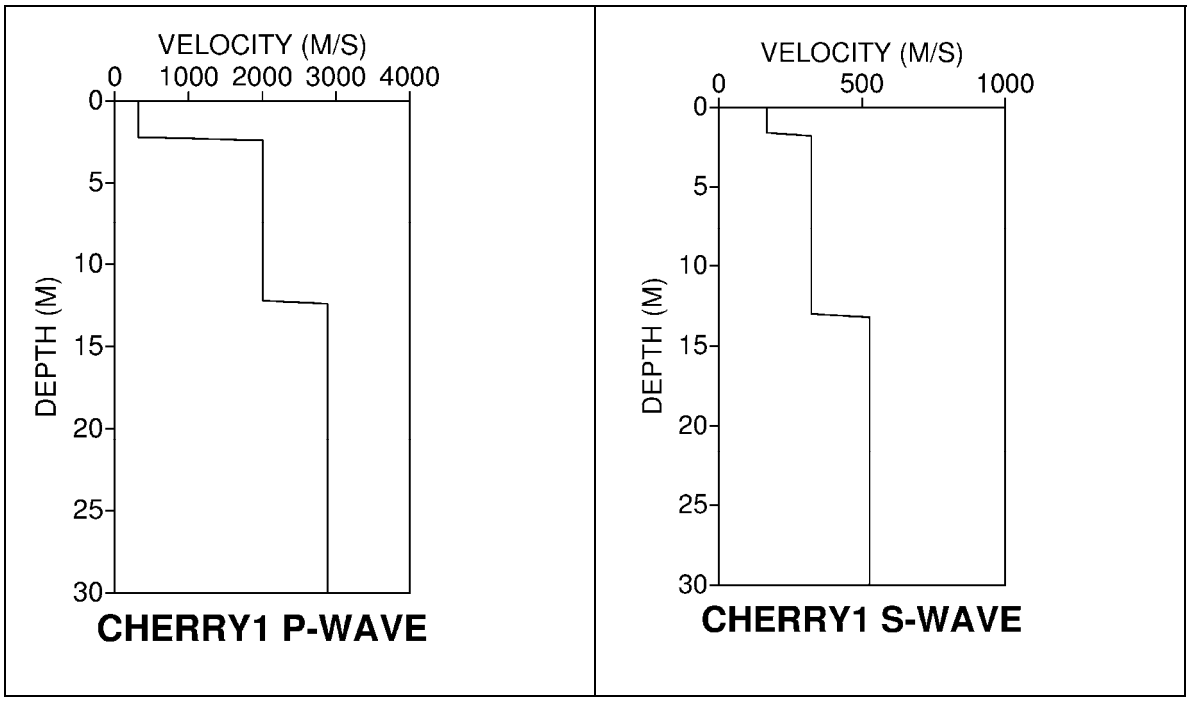

Figure 2-13 P-wave and S-wave velocity profile from seismic refraction at Cherry Lane site.

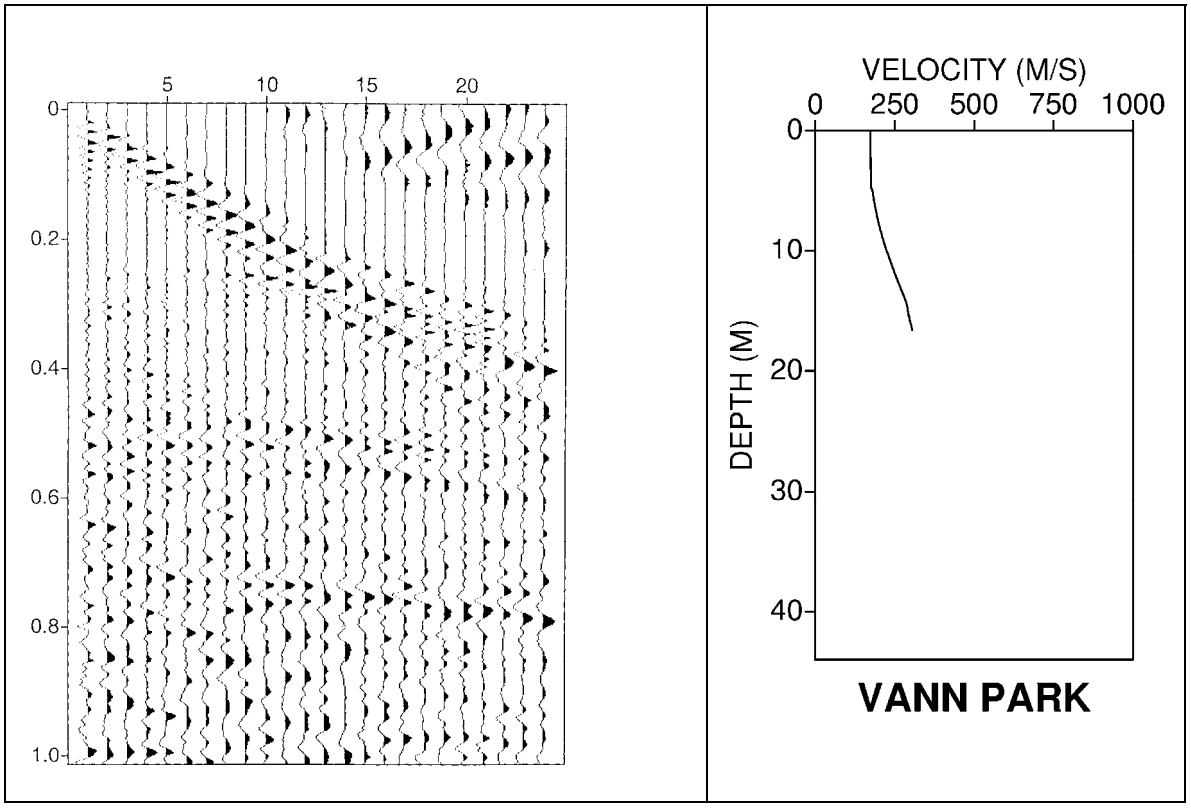

Figure 2-14 S-wave refraction data and S-wave velocity model from Vann-Pollock Park, a site in Evansville within 5 km of Pigeon Creek. Trace number is on the x-axis, with each trace 5m apart. Time in seconds is on the y axis.

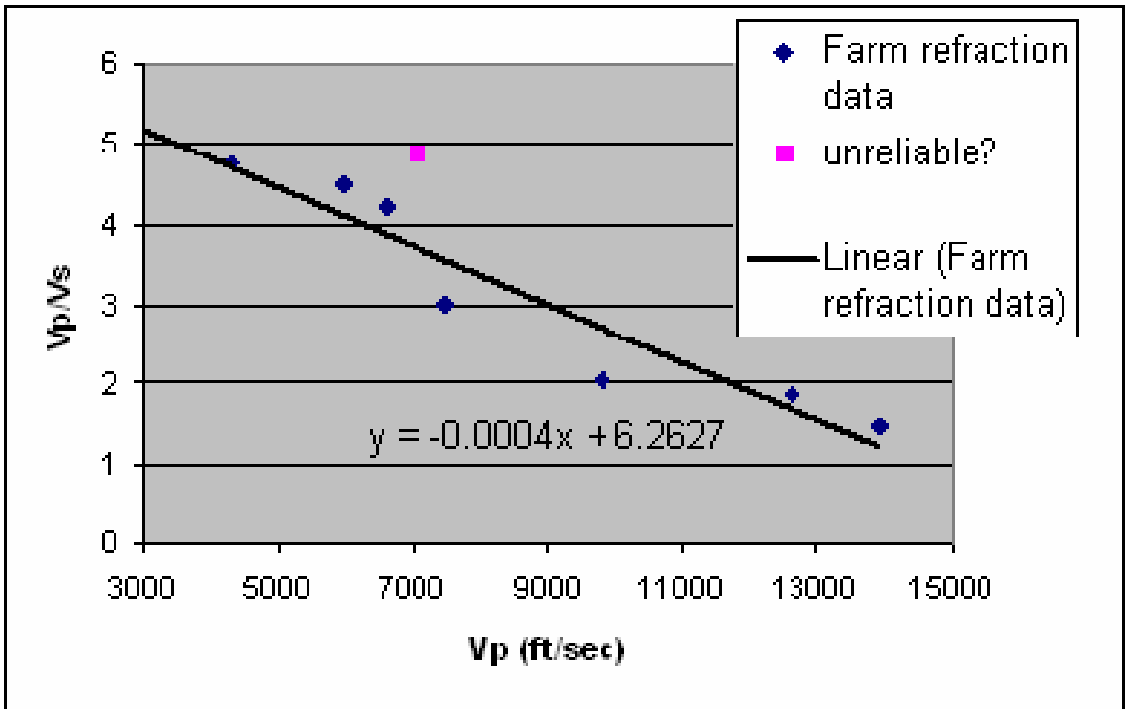

Figure 2-15 Correlation between Vp/Vs ratio and Vp from the entire seismic refraction dataset. With more data, this curve may be sufficiently accurate to use for establishing a mapping from the deep P-wave refraction dataset to S-wave velocity.

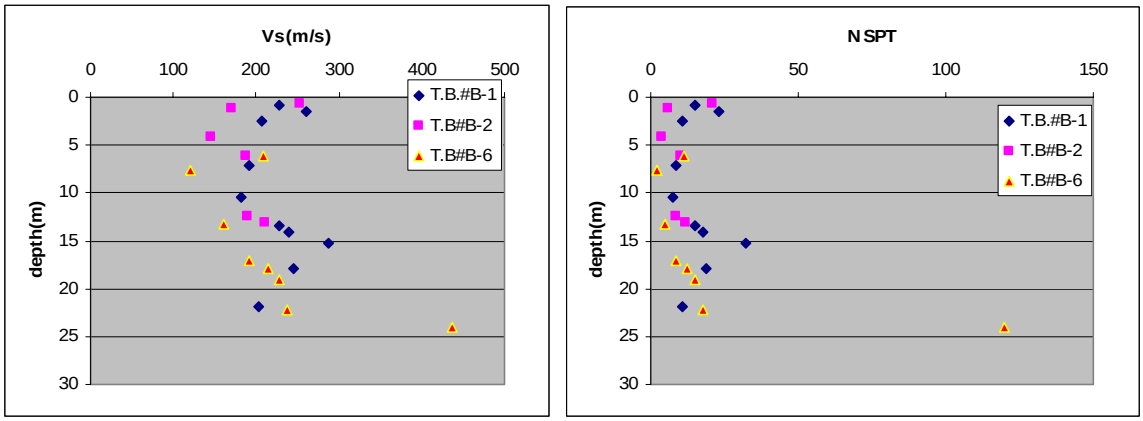

Figure 2-16 SPT derived shear wave velocity profiles (left) and blowcount number profiles (right) for 3 bore logs from the Pigeon Creek bridge site.

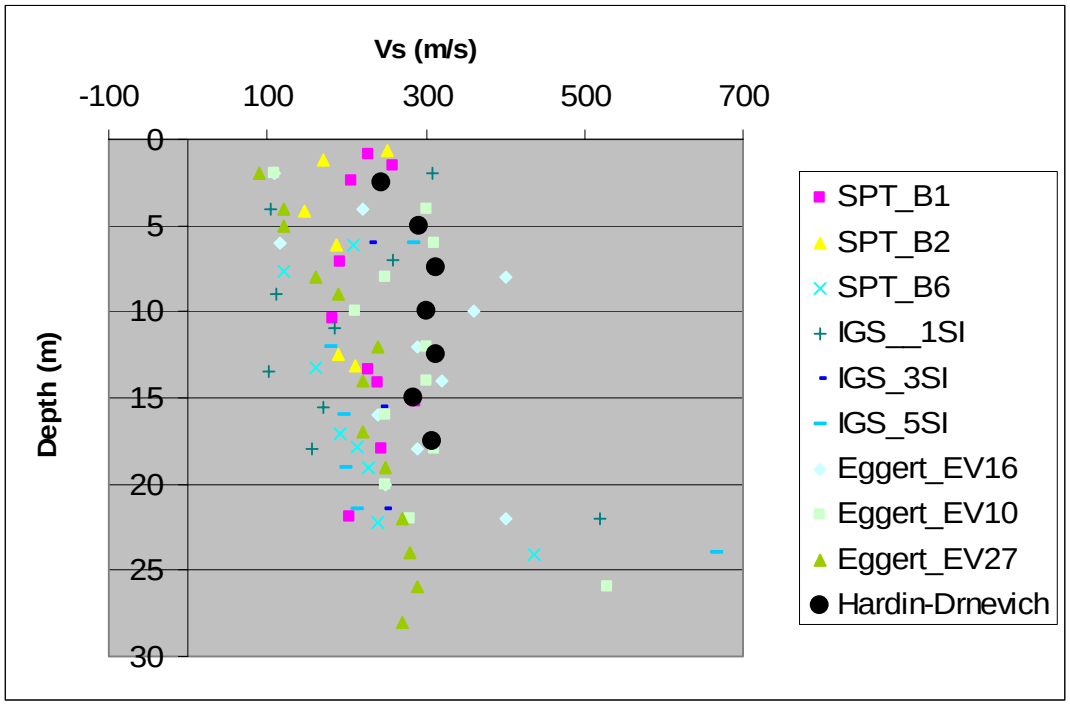

Figure 2-17 Comparison of shear wave velocity values, SPT points are calculated from SPT blowcount profiles, IGS and [*Eggert et al.*, 1994] points are from downhole shear wave velocity measurements, Hardin-Drnevich points are calculated from geotechnical soil characteristics. All sites are within 1 km (see map Figure 2-2).

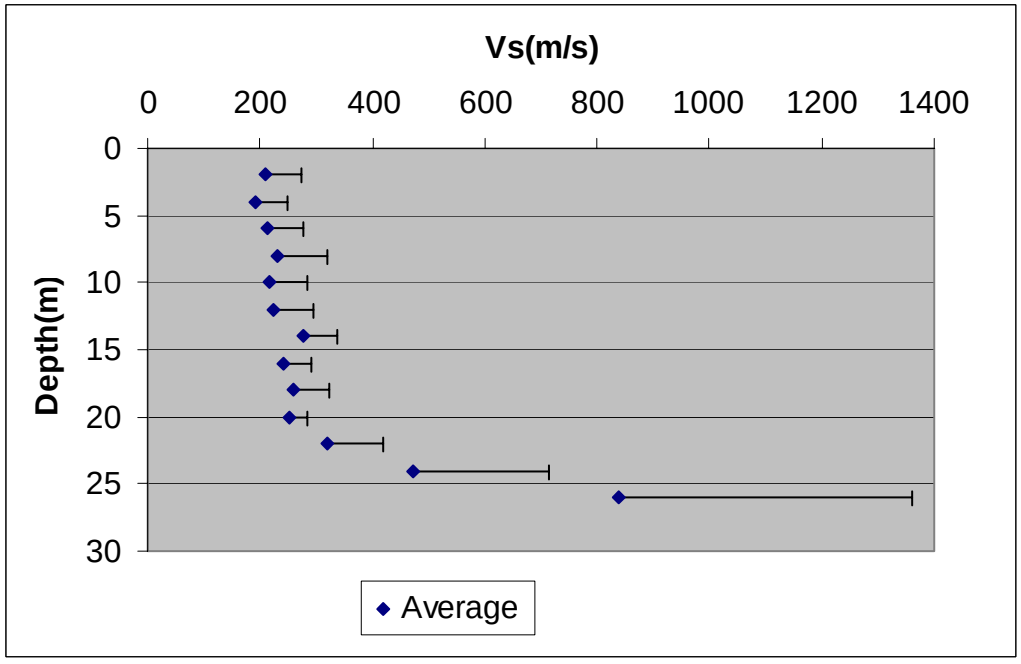

Figure 2-18 Average shear wave velocity profile for Pigeon Creek. All measurement types and sites were included in the average. Standard deviation error bars are also shown, that indicate the variability among the estimates.

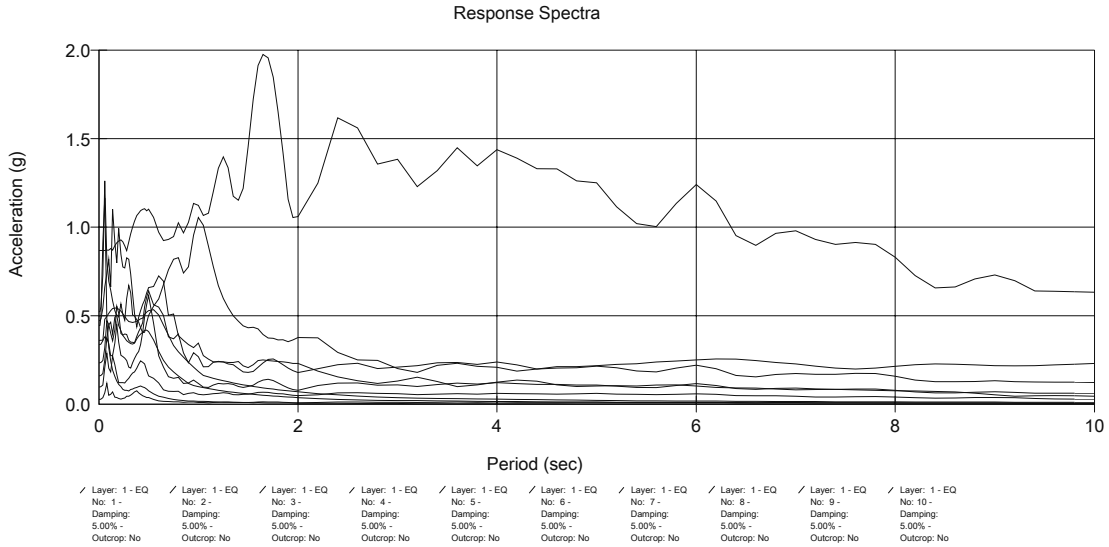

Figure 2-19 Response spectra were calculated from the average shear wave velocity profile in Figure 2-18 for 10 different input ground motion levels. Note the broadening of the peak and shift towards lower frequencies for higher input ground motions.

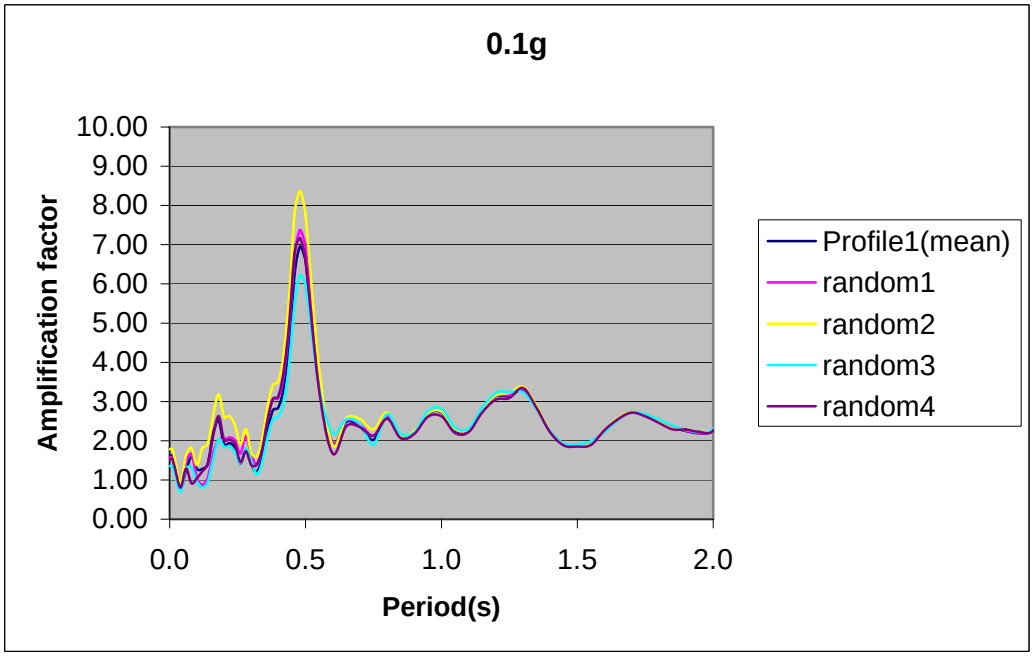

Figure 2-20 Amplification factor for a suite of four random profiles with the same statistical variation as was found at the Pigeon Creek site. The input ground motion PGA was 0.1 g.

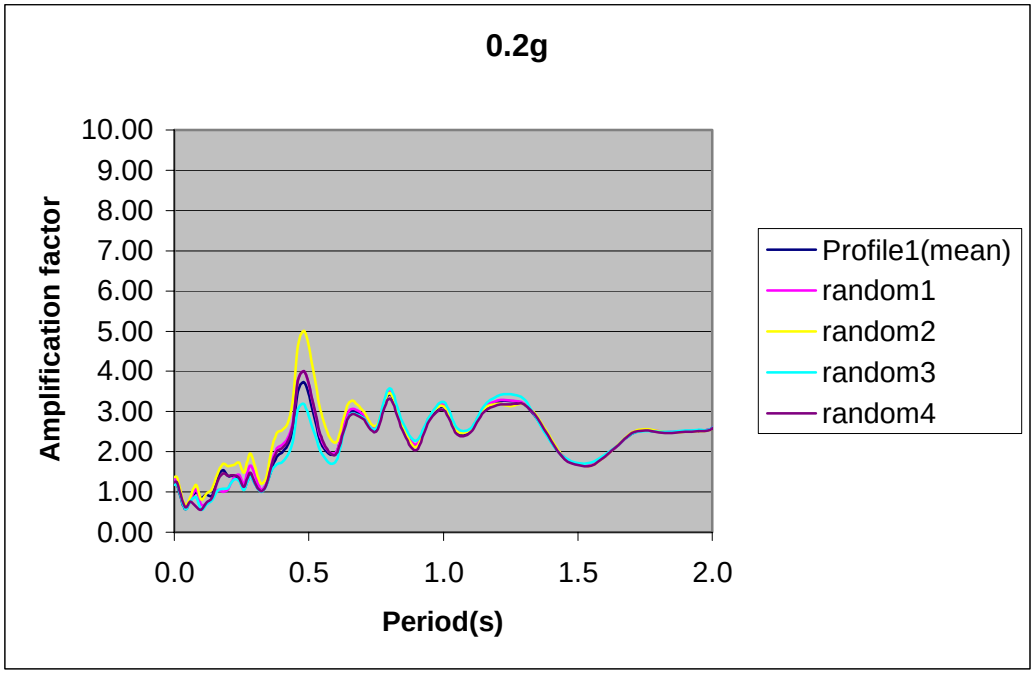

Figure 2-21 Amplification factor for a suite of four random profiles with the same statistical variation as was found at the Pigeon Creek site. The input ground motion PGA was 0.2 g.

3 Implications of Recent Seismicity – the June 18 Darmstadt earthquake

3.1 Introduction

The June 18, 2002 earthquake (M_b=5.0, M_w=4.5) that occurred near Evansville in Darmstadt, Indiana is the largest felt earthquake in Indiana since 1968 and the second largest felt earthquakes in the last 100 years. Investigations of moderate felt earthquakes such as this and recent smaller earthquakes provide necessary data for improving seismic hazard estimates in the future. The rate of occurrence of earthquakes provides one constraint on the recurrence rate of earthquakes in the background source regions that are used in the probabilistic seismic hazard models. The location of small earthquake occurrence provides information on fault locations in the source zones, which faults are active, and the thickness of the seismogenic crust, all of which are parameters contributing to the characteristic source model in the hazard calculation. Strong ground motion recordings provide information that may be used to improve attenuation curves that determine the distance dependence of ground motion in the probabilistic seismic hazard models. Felt intensity data provides corroboration of patterns reported in historical records of past large earthquakes. Because of low seismicity rates in the Midwest, it is necessary to glean the maximum of information from any moderate earthquake occurrence. We report here on earthquakes that have occurred during the first year covered by the project, and discuss the implications of that seismicity for hazard estimation.

3.2 Seismotectonic setting

The Wabash Valley Seismic Zone (WVSZ) is a set of high angle normal faults cutting the sediments in the southern edge of the Illinois Basin within the Wabash Valley (Figure 3-1). [*Braile et al.*, 1982; *Braile et al.*, 1986] proposed that this region and the New Madrid seismic zone are underlain by a failed rift in the north American continent during the late Precambrian, when mafic rocks intruded into the base of the extending crust leaving a large scale signature in the gravity and magnetic data in the central US. Repeated reactivation of the zone has occurred in the Phanerazoic, stimulating theories that recent activity in the New Madrid Fault Zone and Reelfoot Rift is related to reactivation of this ancient rift. The geometry of the WVSZ has been investigated with seismic reflection data [Sexton et al., 1986], revealing subsurface graben and rift related structures that extend to the basement. Proprietary seismic data provided additional evidence for dip-slip faulting in the region and evidence for significant strike-slip displacements on the major faults bounding the graben structures [Bear et al., 1997]. The concentration of seismicity in the Wabash Valley area [*Nuttli*, 1979; *Nuttli*, 1983] (Figure 3-2), along with the occurrence of several sizeable earthquakes in the past several years including the June 10, 1987 M 5.2 event [Hamburger and Rupp, 1988] and the mb = 5.5 event of 9 November 1968, which was felt over 23 states and parts of Canada [Stauder and Nuttli, 1970] indicate that the fault zone is active. Paleoseismic evidence exists for two large prehistoric earthquakes with moment magnitude (MW) between 7.1 and 7.5

occurred in the lower Wabash Valley between 6,100 and 12,000 years ago [*Munson et al.*, 1995; *Obermeier*, 1996], and as many as seven significant earthquakes (M > 6.5) in the last 20,000 years. These data are the motivation for including the Wabash Valley Seismic Zone in the region of the United States for which a higher maximum magnitudes background source model is used in the USGS 2002 probabilistic seismic hazard maps.

3.3 The Darmstadt earthquake

The June 18, 2002, Darmstadt earthquake was the most significant recent earthquake in the vicinity of the Wabash Valley seismic zone. It was located about 20 km west of Evansville (Figure 3-3), and was widely felt in parts of Illinois, Indiana, Kentucky, Michigan, Missouri, Ohio, Tennessee, West Virginia and Wisconsin (Figure 3-4). The quake caused minor damage in the immediate area of the event, which included broken window glass, objects thrown off shelves, and cracked chimneys representative of maximum Modified Mercalli (MM) intensity VI. The event was well recorded by the PEPP network (Figure 3-5), providing arrival times at short distances for precise earthquake location. The regional network of 3-component broadband digital seismographic stations provided high quality recordings of the earthquake out to epicentral distances of almost 600 km, which were then used to retrieve precise source parameters by analysis of the complete waveform [Kim, 2003] (Figure 3-6). Kim reported that the quake occurred on a steeply dipping fault at a depth of about 18 km. The source mechanism is predominantly strike-slip along near-vertical nodal planes (dip= 82° and strike= 28°). This North-northeast trending fault plane is consistent with previous earthquake mechanisms from the midcontinent region, and with the estimated regional stress orientation.

Following the June 18, 2002 earthquake, researchers and staff from the Lamont, Indiana University, Purdue University and CERI, University of Memphis, jointly worked and deployed portable digital seismographs around the epicenter. The aftershock monitoring lasted for about three weeks. We captured an aftershock of ML=1.2 that occurred on June 25, 2002 (Figure 3-7). The local network stations were in the distance range 5 to 8 km from the epicenter and hence, provided data to determine an accurate epicenter and focal depth (19 km) for this small event which would otherwise have gone undetected [Hamburger et al., 2002]. The location of the event confirms a very thick crust in the seismogenic zone, and also provides support for associating this earthquake with the Caborn fault, one of the mapped fault structures in the Wabash Valley seismic zone.

The close proximity of the mainshock and aftershock epicenters to the trace of the compound Caborn fault (Figure 3-3), and good agreement between the strike and dip of that fault and the source mechanism of the mainshock, suggest that the mainshock also may have occurred on that fault (Kim et al., 2003). The 2002 quake raises questions concerning the nature of the seismogenic layer in the Wabash Valley seismic zone and its seismic potential.

3.4 Earthquake rates

In addition to the Darmstadt earthquake, there have been two other earthquakes felt in Indiana in the past year: January 3, 2003 magnitude 2.9 near New Haven, IL (Figure 3-8

and Figure 3-9), and the June 6, 2003 magnitude 4.0 near Bardwell, KY (Figure 3-10 and Figure 3-11). All of these earthquakes included in the earthquake cataolog contribute to our understanding of seismic hazard. The primary catalog used for the central and eastern US is [Seeber and Armbruster, 1991], which is a refinement of the EPRI (1986) catalog [EPRI, 1986]. It is supplemented with the PDE catalog from 1985-95 and with early events not reported in [Seeber and Armbruster, 1991], and was adjusted for improved assignment of magntidues [Mueller et al., 1996]. The catalog is complete above magnitude Mb=3.0 since 1976. The number of events above a given magnitude is shown in the frequency-magnitude curve in Figure 3-12 [*Frankel et al.*, 1996].

Recent short term seismicity rates in the last year for the central US appear to be consistent with the levels used in the seismic hazard calculations. Incompleteness of the catalog may contribute to significant uncertainty in Indiana, however. Figure 3-13 shows a magnitude frequency relation that extends to lower magnitudes, made possible by a sensitive seismic array deployment [*Pavlis et al.*, 2002] in 1996 that show that more smaller events are occurring than expected for the magnitude frequency distribution, and more data is required to determine the slope of the curve more accurately. Statistically, given these rates, two magnitude 5 or greater events are expected to occur in a 10 year period. Recordings from such events would be valuable additions to the database for future strong motion hazard estimate validation if equipment is operating at that time. This has important implications for our discussions in the following chapter on recommendations for network monitoring.

3.5 Attenuation Curves

Attenuation curves that describe the acceleration as a function of distance from the source are necessary for projecting probabilistic seismic hazard. These attenuation curves are based on years of data collected from as many earthquakes as possible world wide. The attenuation curve for the western US is relatively well known because of the large number of recordings available for events up to magnitude 7.5. The attenuation curve is characterized separately for each magnitude range of earthquakes. These attenuation curves are not representative of characteristic of crustal properties of the central and eastern US, as evidenced by the much larger felt area for the New Madrid event than the same size event in the western US. There is not as much data available for the central and eastern US, so that it is critical that any earthquake there is recorded by as many stations as possible and those data are continually added to the growing database of records from which these attenuation curves are constructed.

The June 18, 2002 event provided observations at 5 sites of the Kentucky Seismic and Strong-Motion Network and the U.S. Army Corps of Engineers (ACE) strong-motion stations These records provide a useful data set to augment the strong-motion database in the central and eastern United States. Below we summarize recent results from [*Wang et al.*, 2002] on the implications of the ground motion levels recorded at these sites have for attenuation curves in the central US.

The two free-field sites of the Kentucky Seismic Network, HIKY and RIDG were 200 and 245 km from the epicenter, respectively. HIKY observed a peak ground acceleration of 0.021 g and RIDG observed 0.004 g. Three ACE stations located at dams, J.T.Myers,

Newburgh, and Patoka, at distances of 30, 35, and 110 km respectively observed peak ground accelerations of 0.098 g, 0.059 g, and 0.063 g. These sites are all NEHRP classification C or D. In order to compare them to attenuation relations valid for hard rock sites, it is necessary to compensate for the effect of the soils. The ground motion at HIKY and J.T.Myers were corrected by a factor of 1.5, and the sites RIDG, Newburgh and Pakota were corrected by a factor of 2.0. The corrected ground motions are plotted on Figure 3-14 along with the hard rock ground-motion (NEHRP soil classification A) predicted from several attenuation relationships developed for the central and eastern US [*Atkinson and Boore*, 1997; *Campbell*, 2003; *Toro et al.*, 1997] for an $M_{w=}4.5$ earthquake. The values for 4 sites are slightly higher than those given by the ground-motion attenuation relations. With only five sites it is not possible to state conclusively that the attenuation relations underestimate the true motion, however it does indicate that the attenuation relations merit continued study as more data are acquired in the future.

3.6 Conclusions

The June 18, 2002 Darmstadt earthquake (M_b=5.0, M_w=4.5) was the largest felt earthquake in Indiana since 1968 and the second largest felt earthquakes in the last 100 years. Data from this earthquake was used to provide additional information on seismic hazard. The mainshock was able to be precisely located in depth because of the dense distribution of PEPP network sensors surrounding the event. High quality broadband digital instruments provided data for modeling of the full earthquake waveform so that a more accurate moment magnitude M_w and depth could be determined. Temporary stations that we installed directly after the event provided a lower detection threshold and dense data for precise location of a magnitude 1.2 aftershock. With this data, the precise location of the causative fault can be interpreted [*Hamburger et al.*, 2002; *Kim*, 2003]. In particular, the accurate depths indicate that source models for rupture in the Wabash Valley should extend to at least 19 km depth. This large fault area should be taken into account in characteristic earthquake models in the future. The Indiana PEPP network recorded two additional felt events, a magnitude 2.9 in the Wabash Valley and a magnitude 4.0 near Bardwell, KY. The number and magnitudes of these events is consistent with the magnitude-frequency relationship for events in the Central and Eastern US, but the detection level is unreliable for some of these small events. Statistically, given these rates, two magnitude 5 or greater events are expected to occur in a 10 year period. Uncertainties in the magnitude frequency relation would be reduced if small events recorded by PEPP were routinely incorporated into the USGS catalogs used for the seismic hazard estimates. Strong ground motion recordings from the Darmstadt earthquake suggest that PGA values are slightly higher than current ground-motion attenuation relationships for a magnitude 4.5 event in the central and eastern United States [*Wang et al.*, 2002]. These attenuation relations are used in the 2002 USGS seismic hazard maps [*Atkinson and Boore*, 1997; *Toro et al.*, 1997] and subsequent studies [*Campbell*, 2003; *Campbell and Bozorgnia*, 2003]. The result is inconclusive due to the limited number of strong motion stations recording the event, but does make a significant contribution to the accumulating strong motion database for the central and eastern US.

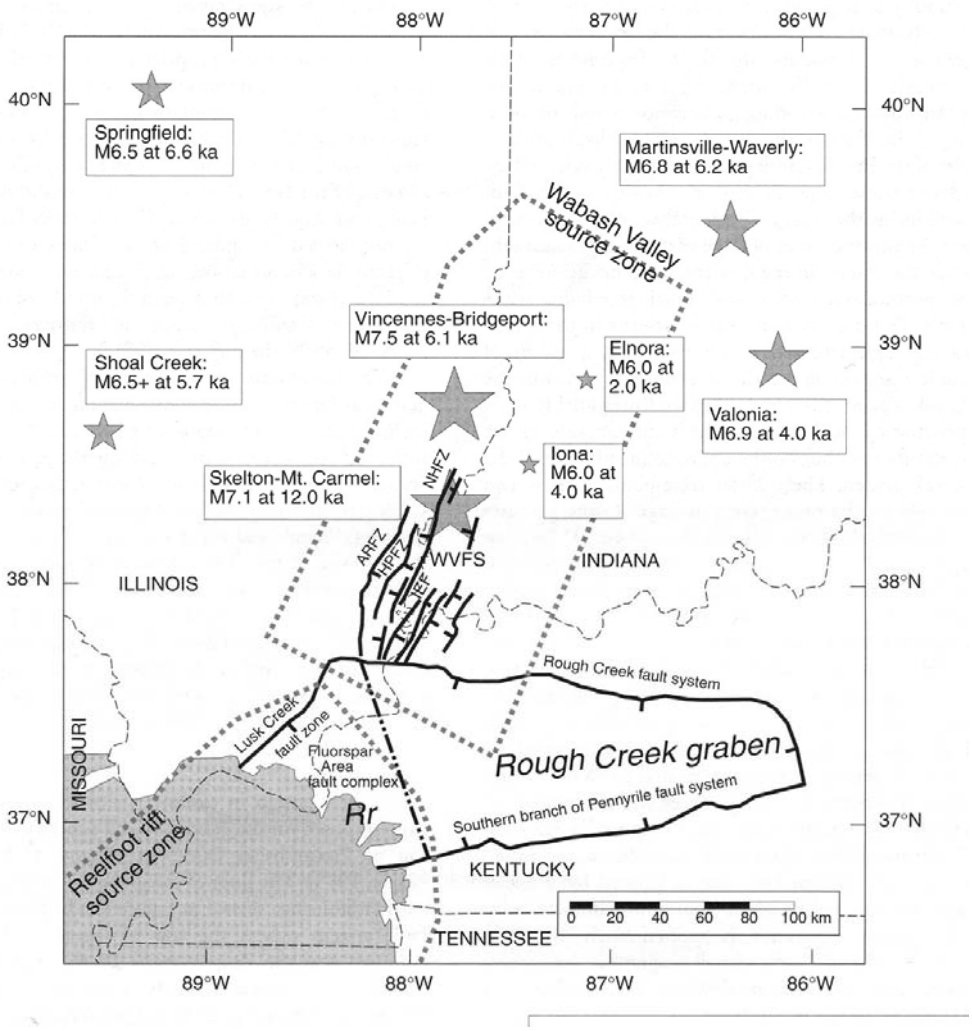

Figure 3-1 Prehistoric seismicity and structural tectonic map from [*Wheeler and Cramer*, 2002] illustrating the source regions used in the 2002 USGS probabilistic seismic hazard maps [*Frankel et al.*, 2002].

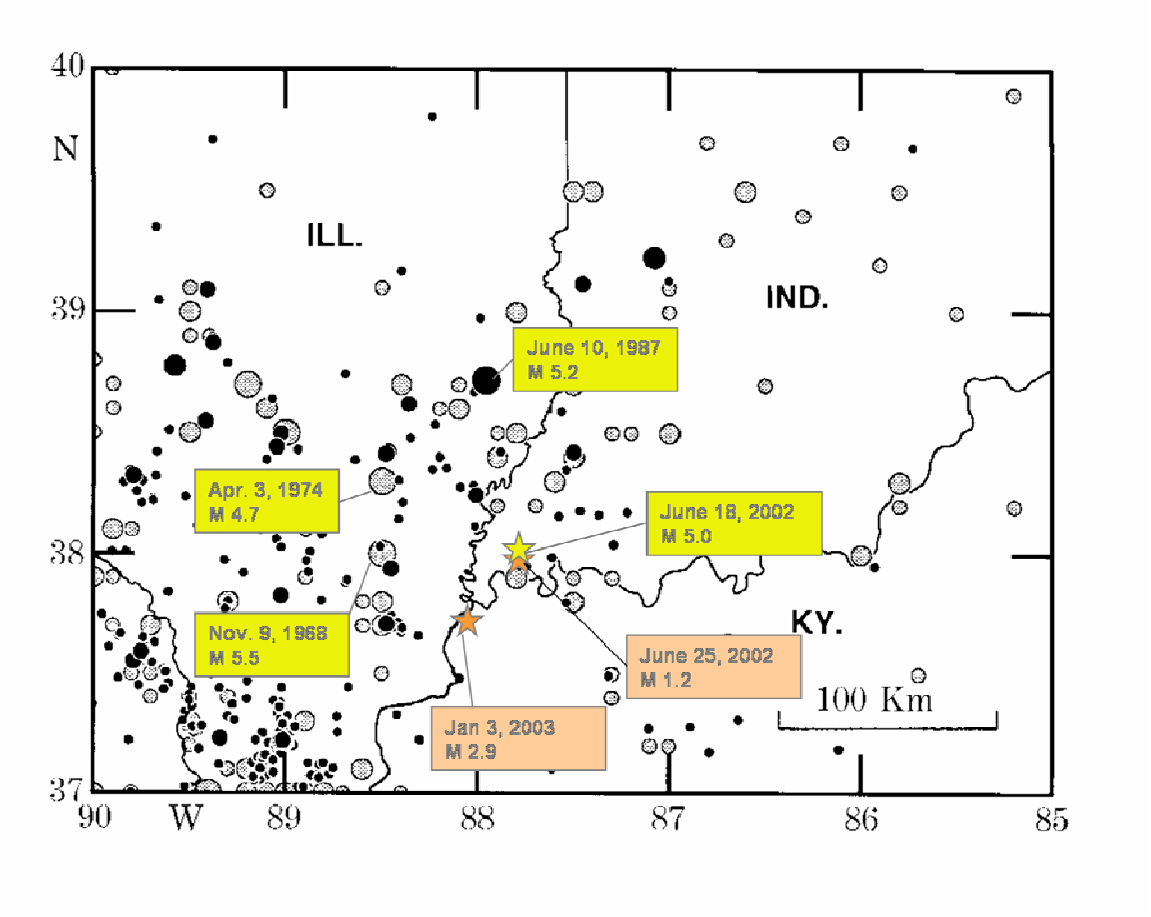

Figure 3-2 The largest earthquakes felt in Indiana since 1970 when operational monitoring began. In orange are the two additional earthquakes that we investigate in this research.

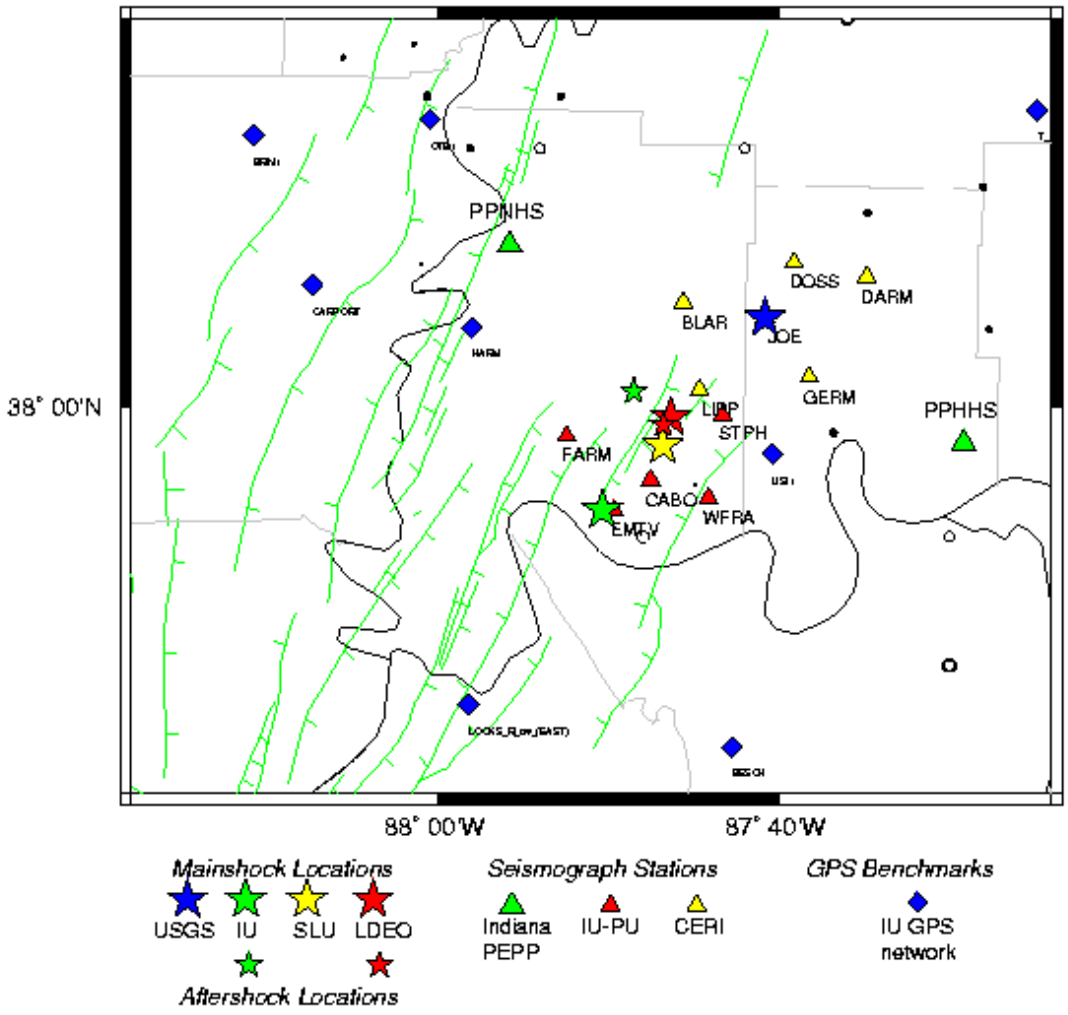

Figure 3-3 Map of June 18, 2002 mainshock, and June 25, 2002 aftershock and the location of the PEPP network stations and temporarily deployed aftershock monitoring stations that recorded the event. Earthquake locations that include all the local data (red stars) are more accurate than the original USGS location (blue star).

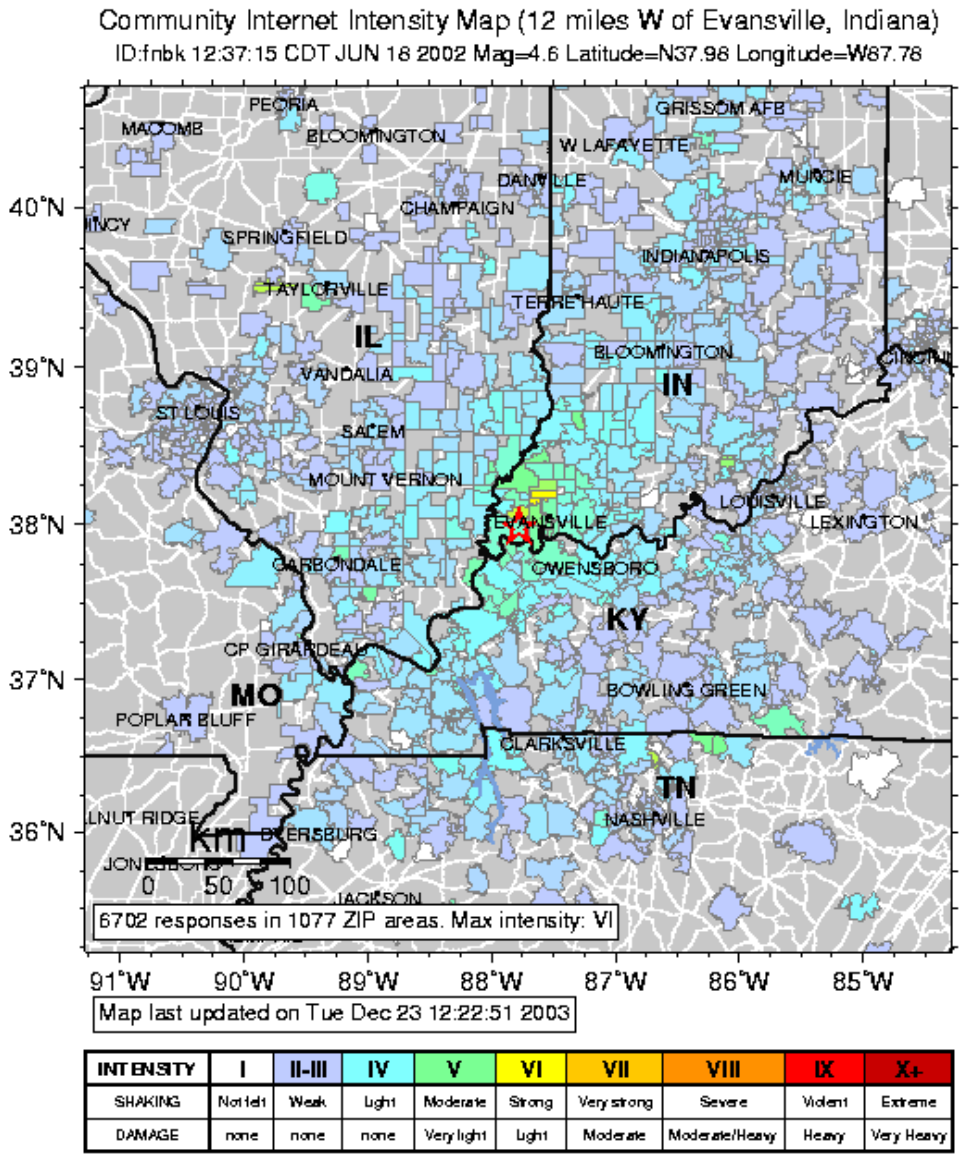

Figure 3-4 Intensity map of the felt area of the Darmstadt earthquake. The quake was felt as far north as Lafayette and Muncie.

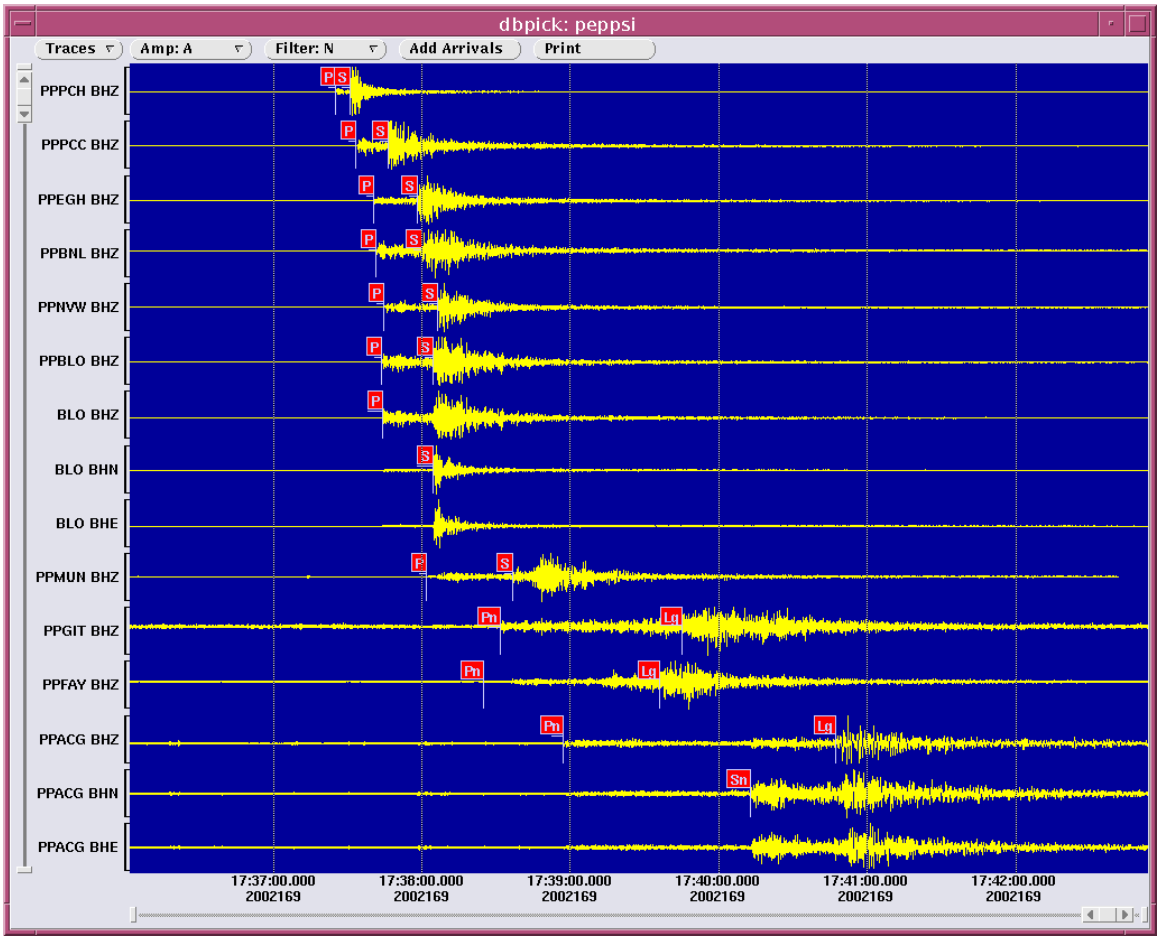

Figure 3-5 Seismic arrival times picked from PEPP seismic network stations for the June 18, 2002 Darmstadt earthquake. Derivation of seismic wave propagation times from these events and others will validate shear wave velocities from the statistical model.

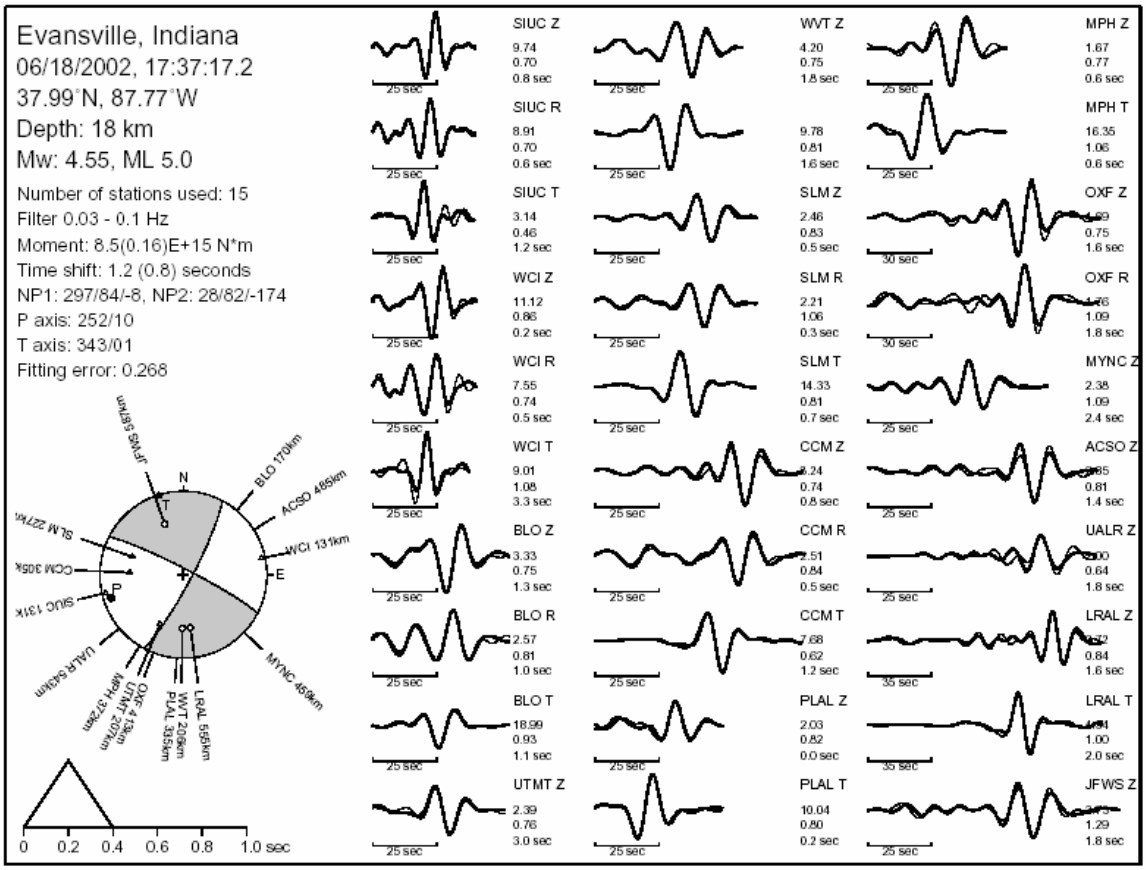

Figure 3-6 Moment tensor solution for moment-magnitude, fault plane orientation, and depth of the event derived from broadband digital recordings, taken from [*Kim*, 2003].

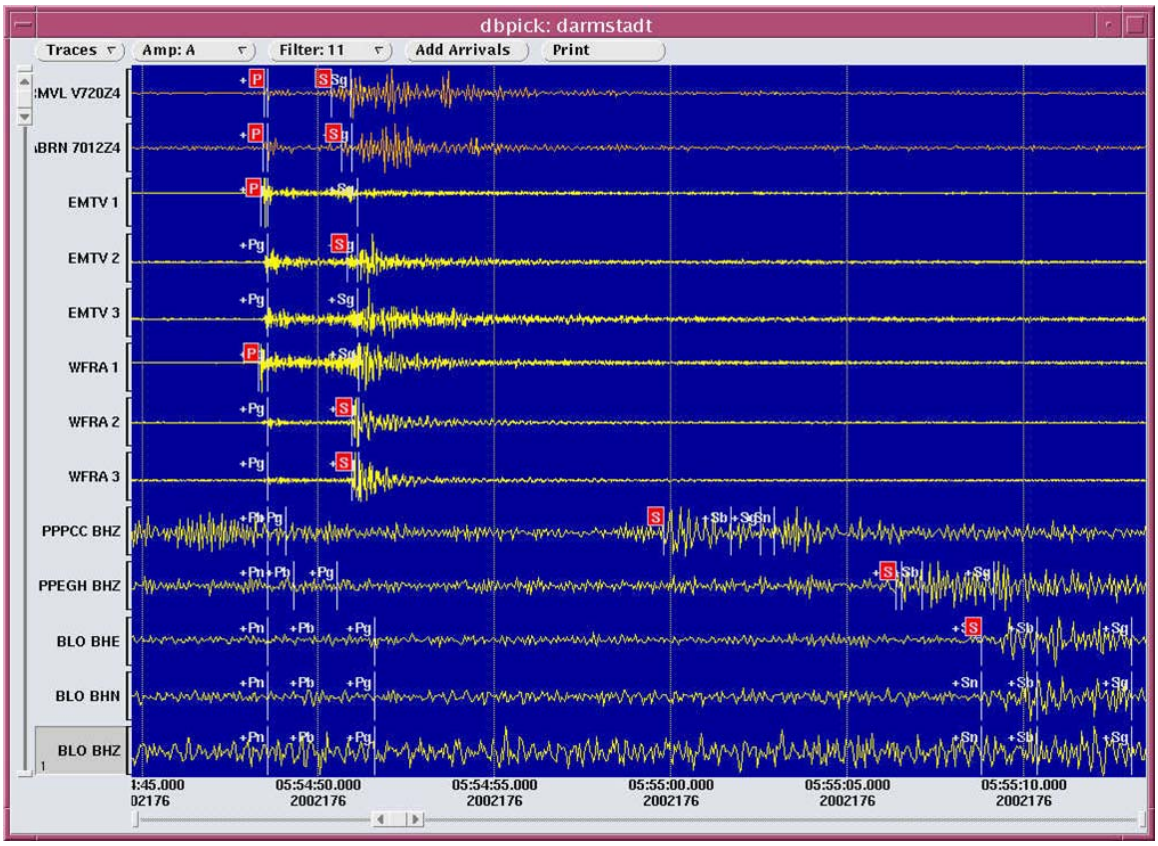

Figure 3-7 Recordings from the June 25, 2002 aftershock of the Darmsdadt earthquake from the PEPP seismic network.

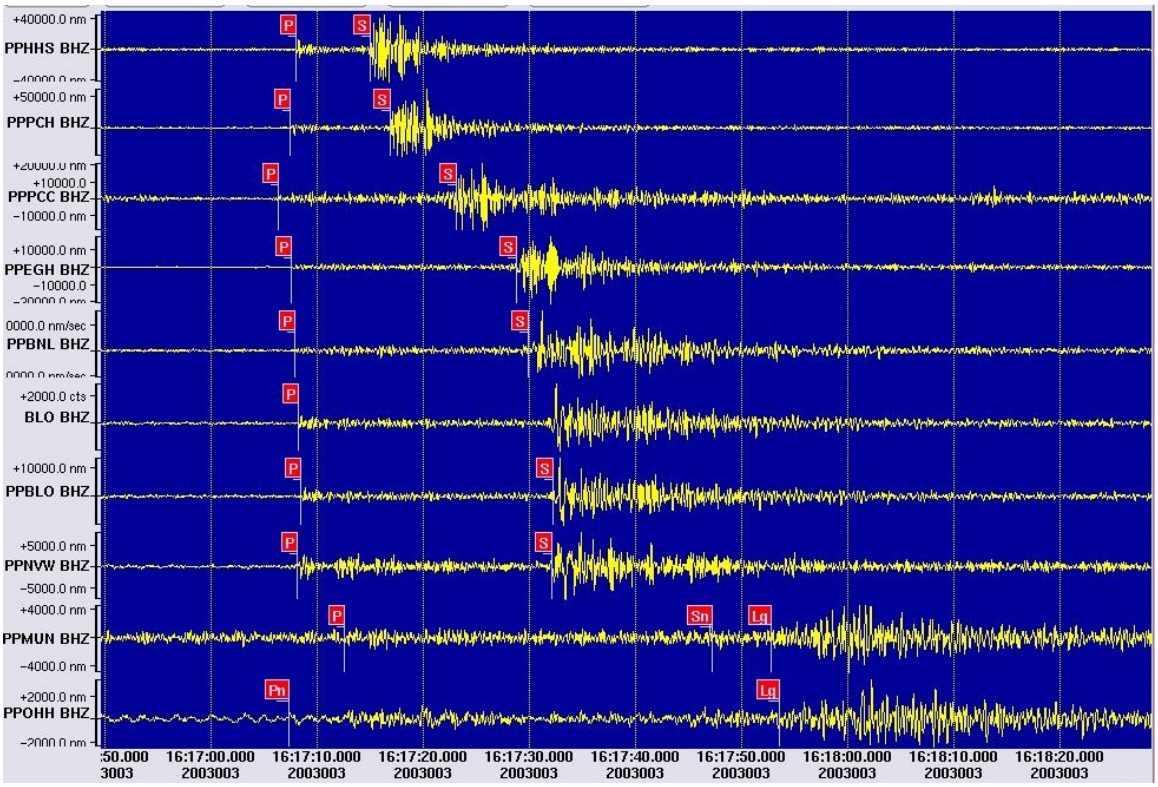

Figure 3-8 PEPP network recording of the Jan 3, 2003 M 2.9 Wabash earthquake.

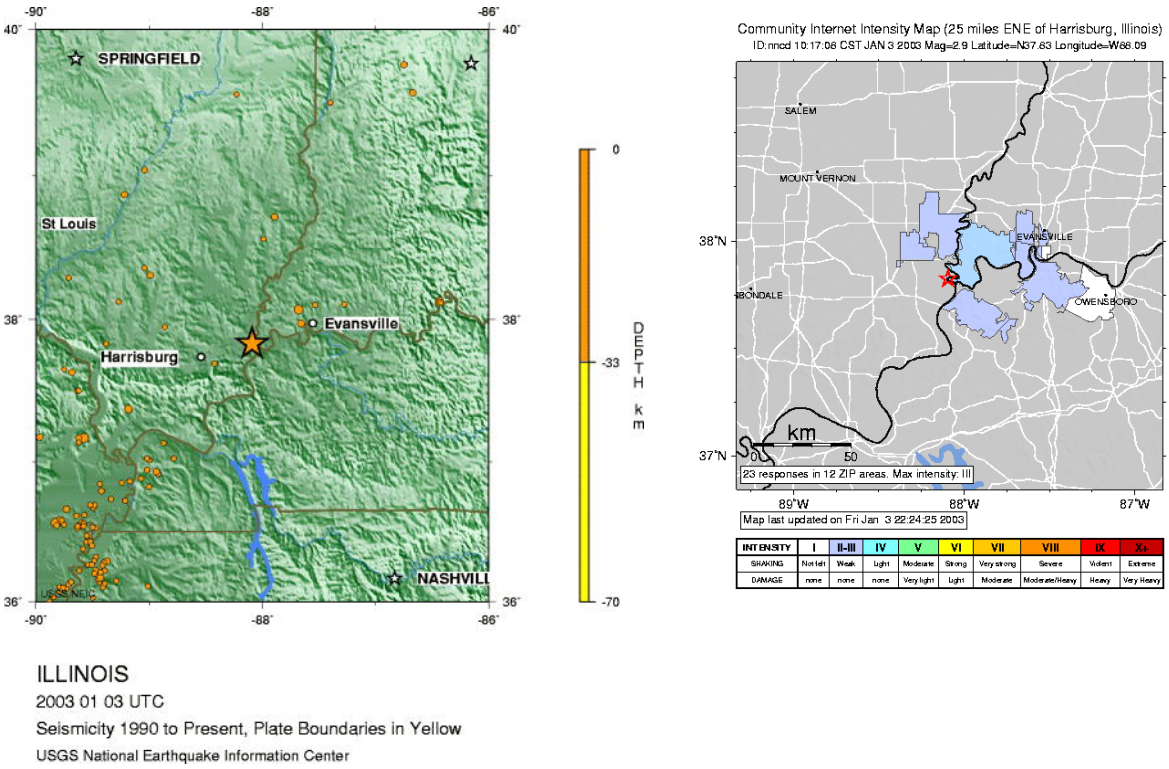

Figure 3-9 Location and felt intensity from the Jan 3, 2003 M 2.9 Wabash earthquake [*USGS*, 2003]

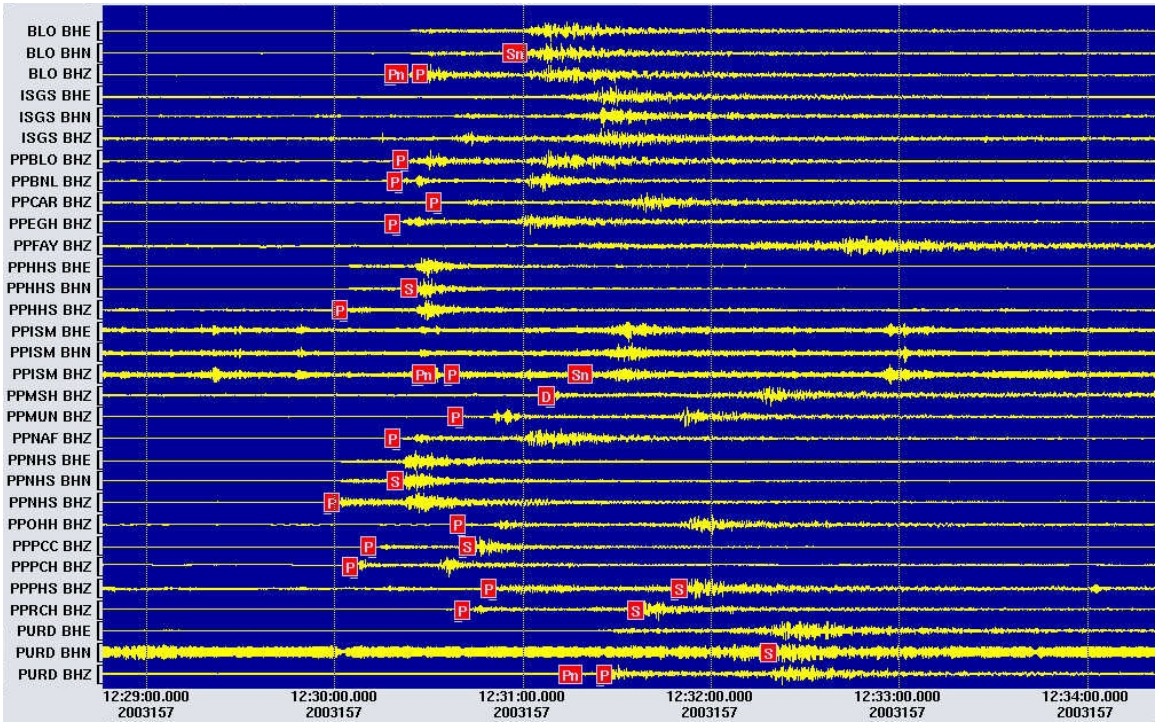

Figure 3-10 PEPP Network seismic recordings and arrival times for the June 6, 2003 M = 4.5 Bardwell, KY earthquake.

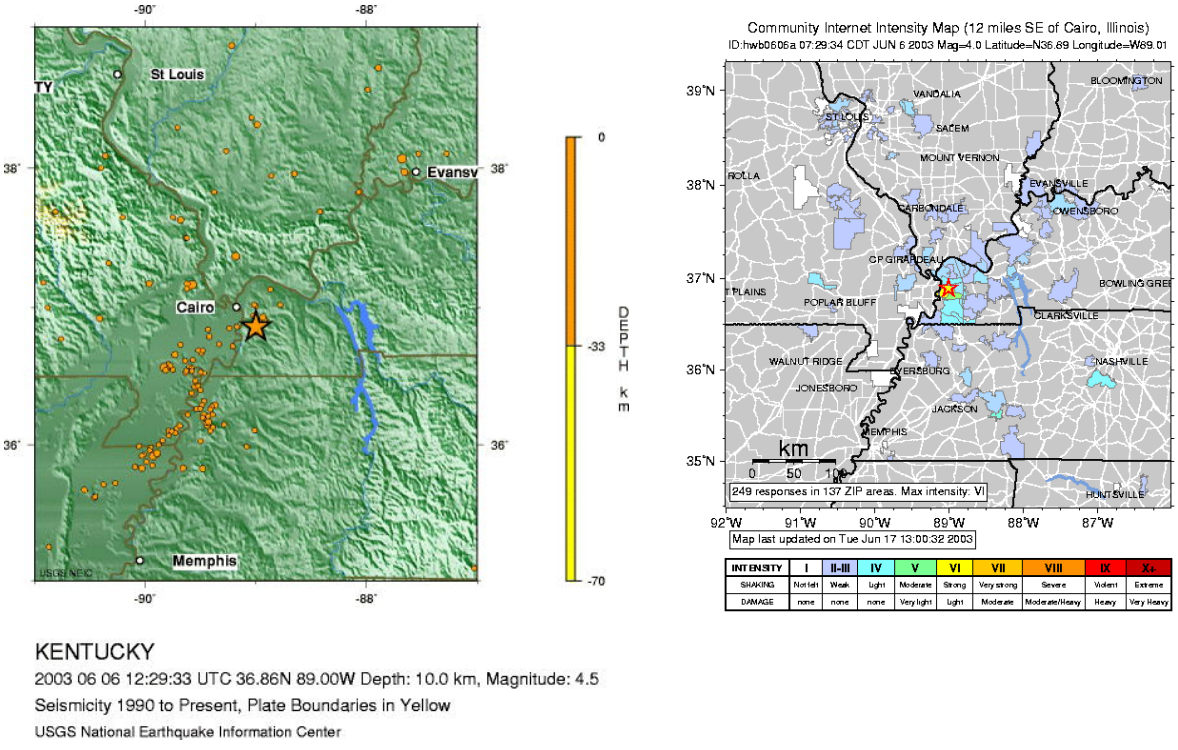

Figure 3-11 Location and felt intensity from the June 6, 2003 M 4.5 Bardwell, KY earthquake [*USGS*, 2003]

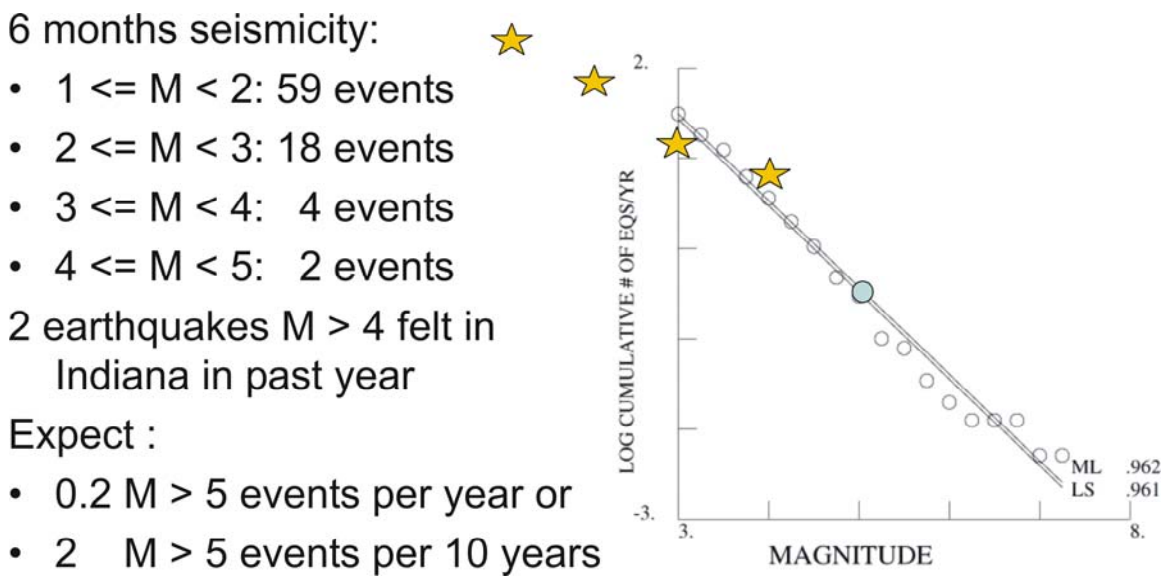

Figure 3-12 Recent short term seismicity rates for the central US appear to be consistent with the levels used in the seismic hazard calculations (figure modified from [*Frankel et al.*, 1996]). Incompleteness of the catalog may contribute to significant uncertainty in Indiana, however.

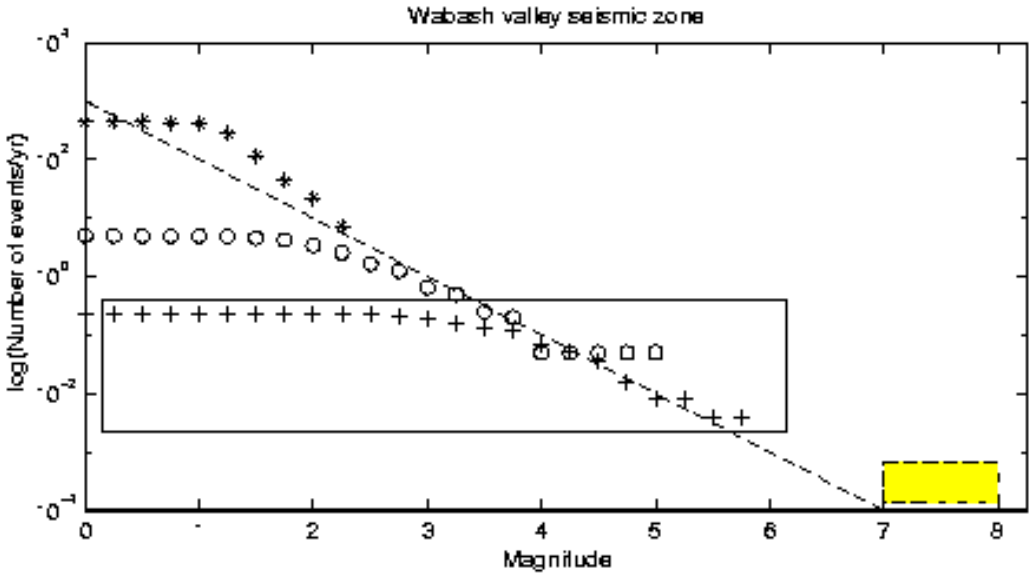

Figure 3-13 Magnitude frequency relation determined for very small Wabash valley events (* symbols) from a temporarily deployed array in the Wabash Valley, from [*Pavlis et al.*, 2002].

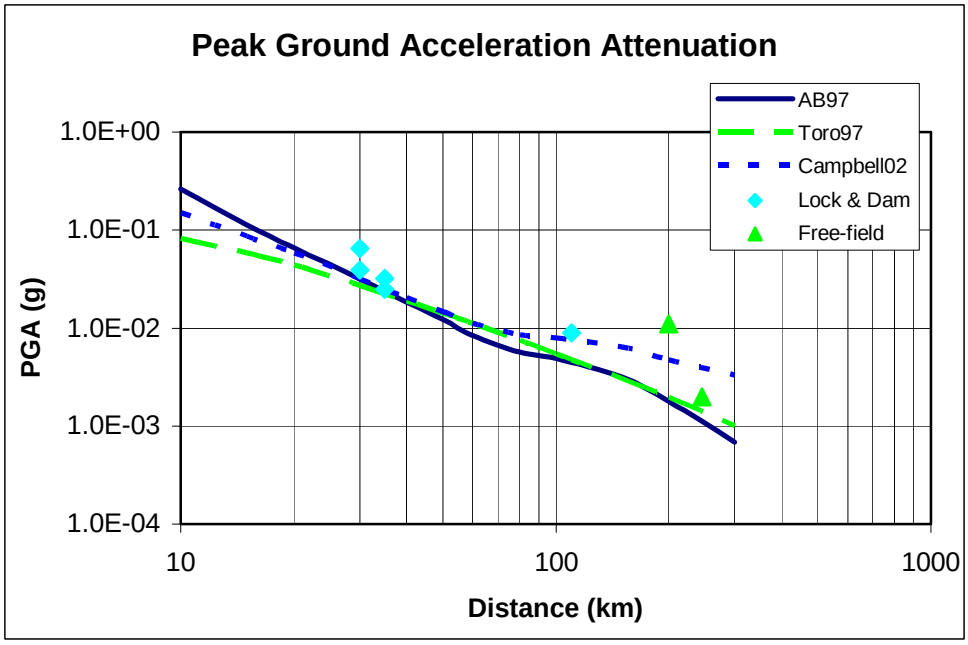

Figure 3-14 PGA data for the June 18, 2002 earthquake compared with the attenuation relations of [*Atkinson and Boore*, 1997], [*Toro et al.*, 1997], and [*Campbell*, 2002] for an M_w=4.5 earthquake, from [*Wang et al.*, 2002].

4 Analysis of Seismic Monitoring Capabilities and Recommendations

In this section we provide recommendations on cost-effective means for augmenting the seismic monitoring capability in the state. This last provision will ensure that data from Indiana is included in future nationwide evaluations of seismic hazard, thus reducing the ambiguity in adopting engineering guidelines developed solely with data from other states.

4.1 Introduction

The objectives of monitoring weak motion (velocity seismometers) and strong motion (accelerometers) are the following. Detection of small earthquakes with weak motion sensors makes it possible to determine seismicity rates appropriate for Indiana, including the Illinois basin, the Wabash Valley, and the background seismicity level in Indiana. Mapping of these small earthquakes localizes the faults responsible for the hazard and their depth extent, something which affects their seismogenic potential. Strong motion monitoring provides the ultimate ground truth observational data for realistic ground motion levels to determine site effects and attenuation curves. In this way, predictions of shaking effects on structures and soil response can be calibrated. Both weak and strong motion sensors are useful for providing accurate information to emergency response agencies and INDOT operational services for maintaining lifeline support during an earthquake, but this use requires real-time data transmission and analysis. This is because weak motion sensors are critical for determining the location precisely, and strong motion sensors are critical for estimating the likely amount of damage.

The current status of seismic monitoring in Indiana is that the PEPP (Princeton Educational Physics Program) Seismic network, originally installed as an educational resource for Indiana schools, has taken on a large part of the responsibility for seismic monitoring in the state. More detailed information on the PEPP network is provided below. The PEPP network is, of course, by no means the only monitoring resource in the region. It can be properly viewed as a densification of national-level resources deployed in the Cooperative New Madrid Seismic Network (http://www.eas.slu.edu/Earthquake_Center/NM/). Stations WCI, BLO, and SIUC (CNMSN and USNSN) are within the study area of this project. Data from these stations are often merged with the PEPP data to produce a comprehensive data set for detailed analysis. Data is also available from the Kentucky real-time network, which also includes digital real-time strong motion sensors. Neighboring educational seismic networks 'Michseis' (http://www.geo.lsa.umich.edu/MichSeis/) and 'Ohioseis' (http://www.ohiodnr.com/OhioSeis/) also provid information about neighboring areas of Ohio and Michigan. The USGS / Center for Earthquake Research and Information plays the operational role of near real time monitoring for the entire Central and Eastern US, however very few of the PEPP network stations are integrated into this operational system to date because of the demand for real-time data transmission from the stations. A map of currently operating stations in the region is shown in Figure 4-1 and Figure 4-2,

though it must be stressed that the data from these stations is not all available simultaneously for analysis in real-time in a coordinated manner.

4.2 The PEPP Network

The Indiana University PEPP Earthquake Science program, initiated in 1996 by IU geophysics professors Michael Hamburger and Gary Pavlis, has brought the science of earthquake seismology into some 25 public schools in Indiana, Illinois, Ohio, and Kentucky. PEPP, for *Princeton Earth Physics Project*, is part of a nationwide educational initiative whose aim is to combine state-of-the-art seismological research with hands-on classroom training for high-school students in physics and the earth sciences. Initiated in 1992 by Princeton University seismologists Guust Nolet and Robert Phinney, and supported by funding from the National Science Foundation, the PEPP project has become a major nationwide educational program with nearly 100 participating schools across the country. The PEPP program has forged a new partnership among university-based academic researchers and high-school teachers and students. The Indiana PEPP website (http://www.indiana.edu/~pepp/) contains additional information about the program.

In addition to its educational contributions, the PEPP program has provided an important new resource for the research seismology community. In spite of its position on the northern periphery of the New Madrid seismic zone, our state has remained, until recently, one of the most poorly instrumented areas of the U.S. midcontinent. Thus, the development of the Indiana PEPP seismic network answered an important need for earthquake hazard mitigation in the state. Our broadband seismic network routinely records earthquakes from our area and from across the globe, as well as from artificial sources such as quarry and strip-mine blasting. The PEPP seismic network is currently the densest concentration of broadband seismic stations in the eastern U.S. We have been obtaining reliable, continuous data from this network for approximately three years that are archived on a mass storage system at Indiana University. These data have been only examined piecemeal for special studies (*e.g.,* in the aftermath of felt earthquakes).

Both Indiana University and Purdue University were collaborators with Princeton in the original PEPP experiment, but since 1999 IU has taken over technical support for all the PEPP schools in the nation and have integrated the Purdue stations into a single, integrated Indiana seismic network. An important change in network data flow we initiated at that time was the use of Internet data transmission from schools to a central recording computer at Indiana University. We use a system that uses the commercial seismic recording software SCREAM (from Guralp Systems) on a local PC, which transmits data to our central computer where it is processed in near-real time by a system running Antelope (http://www.brtt.com). Prior to this innovation schools used a DOS-based program developed by Princeton and they only uploaded segments of data from teleseismic events when requested by an automated data request from Princeton. Consequently, data prior to 1999 are limited to teleseismic events participants chose to upload to Princeton. Since then we have steadily increased the number of schools streaming data to us in real time. Approximately 20 stations currently send us data continuously by this mechanism and we are working to increase this number. In addition, many of the stations

that cannot get data to us in real time have a significant archive of digital data stored locally on various media. We are actively working to obtain copies of these data and to assimilate them into our database.

Most of the capital equipment for the Indiana PEPP network came from PEPP with matching support by participating schools in the form of computer equipment dedicated to running the station. Sensors at all original PEPP schools are vertical-component, Guralp PEPPV instruments. The network also includes six 3-component PEPP-T or CMG-40 3-component instruments. In addition, we expect to add several new PEPPV stations to the network in the next year through other funding sources. These instruments provide quality broadband recordings of local earthquakes, blasts, and teleseismic events (for additional examples see http://www.indiana.edu/~pepp). Timing precision of these data is generally excellent due to the use of GPS clocks at all sites.

4.3 Summary of operational status

Currently the operational detection level is magnitude 3.5, the size of earthquakes necessary to trigger stations in the relatively sparse network that is routinely processed in an operational manner at CERI. There are more than 20 single component broadband PEPP instruments across the state, and the quality of the individual instrumentation at these sites in Indiana, which is the largest up front cost, is very high and sufficient for a level of detection in the low 2 magnitude range. Five state of the art broadband three-component stations are providing information on earthquake sources at regional distances. Two digital strong motion sites exist, WVIL in the Wabash Valley and USIN in Evansville. Two to three Army Corps of Engineers strong motion sites exist in the state, primarily at dam sites, but the reliability of their operation is questionable after they failed to report any data after the June 18, 2002 event. Maintenance for the existing sites is primarily provided by Indiana University and USGS staff, though the period for which IU had funding for this activity ceased in summer 2003.

4.4 Recommended Upgrades

Some important points were made in the previous section in regards to motivation for upgrades to the monitoring operations. Primarily the argument was made for having in place an adequate strong motion network given the average recurrence times of one magnitude 5 earthquake every 10 years. The recording of these events are critical for ground-truthing the probabilistic seismic hazard estimates. The new results from the seismic hazard estimates incorporating site effects show that there may be significant amplification in the central part of the state, near Indianapolis, due to thick sediments filling in ancient bedrock valleys. These areas are high priority sites for installation of new strong motion instrumentation. Additionally, the majority of the weak motion stations are single component, thus providing no information on shear wave velocity.

Bridge decks, abutments, and free-field sites near bridges are often monitored with strong motion instruments to provide data on shaking levels and information for validating bridge design decisions. In the southwestern part of the state, (in the area south of I-70

and west of I-65), there are a number of new bridges and/or bridges getting major rehabilitation. These bridges, especially the new I-69 bridges especially near the Evansville area, should be considered for such monitoring as part of any strong motion network upgrade, since it is of particular advantage to INDOT. Real time monitoring systems are feasible for such a task, if desired.

Thus some recommendations for updating the monitoring capability are justified at this point. Because of the backbone of reliable weak motion and broad band seismometers, the situation could be greatly improved at reasonable cost. Concerning seismological equipment, we recommend 1) upgrading all stations to 3-component sites to measure shear wave propagation characteristics, and 2) installing digital strong motion instruments, especially in urban areas that coincide with the potential for relatively high amplification as revealed in this study. Concerning technical operations, we recommend 1) implementing a real time data exchange with CERI, who can assume a large load of the operational tasks at little additional expense, 2) install robust real-time connections at the schools hosting the equipment, 3) implement an automatic event associator that can efficiently integrate data coming from many local operational centers into a coherent product. Note this associator has recently become available and does not require new development, only implementation. Concerning maintenance, the cost and resources required here are adequately covered. Concerning operations, it is clear that additional personnel are required, at least a ¼ time analyst, either at CERI or IU to create and maintain the operational processing of the data, which has currently fallen far behind. Funding for these operations through the PEPP program ceased in 2003. Another reason operations are lagging is the mixture of coal mining blasts and small earthquakes unique to Indiana that complicates the analysis task. This leads to the final recommendation concerning some level of research, in particular for automating blast/earthquake discrimination. This is important in assuring that the hazard level assumed in probabilistic assessments is not artificially elevated because of misidentification of blasts as earthquakes.

4.5 Resources

Resources for improvements to the monitoring capabilities would naturally come from a wide spectrum of sources, and some current opportunities exist that promote initiation of these improvements. In particular, the new Advanced National Seismic System has been initiated particularly as an urban strong motion measurement program. The objectives are 100 strong motion sites in the central and eastern US region. This is a logical resource for requesting strong motion sensors, as previously noted, in regions with exceptionally amplified ground motion that coincide with urban areas. Though it is a national network, priorities for the location of strong motion sites are decided at a regional level. USGS/CERI resources are available if the key technical issues are resolved, such that upgrades, logistical support, real-time earthquake alerts, and SHAKE MAP (a real time tool for reporting ground motions for emergency management) could be easily and rapidly implemented. Because the USGS internal research program has initiated a 5 year research plan that includes Evansville seismic hazard as a national priority, funds that are not normally directed towards this region are available during the current time period for completing a highly detailed seismic hazard mapping project in Evansville that would be

of great use to INDOT. The USGS external research program mirrors the priorities of the internal program, therefore research funds for some of the necessary theoretical advances are potentially available. Finally, the new NSF Earthscope initiative which has started this year will provide the temporary deployment of dense arrays, and will be passing through Indiana in 2008. There is an opportunity there to complement monitoring improvements with new sites that would be sufficient to answer fundamental questions on the active faults in Indiana, if operations could be coordinated, or matching funds sought.

4.6 Beyond the state of the Art

With the high technology resources available within the School of Engineering at Purdue, one could imagine that the monitoring network could go significantly beyond the state of the art. Exciting opportunities exist for real-time high performance computing solutions to the problem of seismic monitoring. Some possibilities are the following:

1) real-time event reporting and SHAKE MAP,

2) real-time strong motion recording (i.e. as in Kentucky), particularly on critical infrastructure,

3)dense array monitoring that allows detection down to magnitudes 1.2 and below using 20 station telemetered arrays serving the role of 120 conventional stations,

4) real-time multi-sensor infrastructure monitoring capable of detecting other catastrophic events besides earthquakes,

5) focused exploitation of the temporary Earthscope network in the Wabash Valley with up to 80 sites that would provide the detection level of the New Madrid network, and

6) 5 additional broadband sites in southwestern Indiana for detailed source studies in near-real time.

The probabilistic seismic hazard estimates to date are entirely based on theoretical and empirical relations for earthquake occurrence and seismic wave propagation. Proper use of the results of these studies by an agency would logically require extension of this analysis by incorporating a component of direct seismological observation, taking advantage of existing seismological infrastructure. Any prediction of strong ground motion amplification is more believable and useful when it has been validated with an actual recording. We are fortunate to have access to a recently established, state-of-the-art broadband digital seismograph network in Indiana, which can provide useful information related to earthquake hazards in the state. The seismic data will provide valuable constraints on earthquake source distribution, seismic velocity models, and wave propagation characteristics that can significantly impact site effects of future large earthquakes in the region.

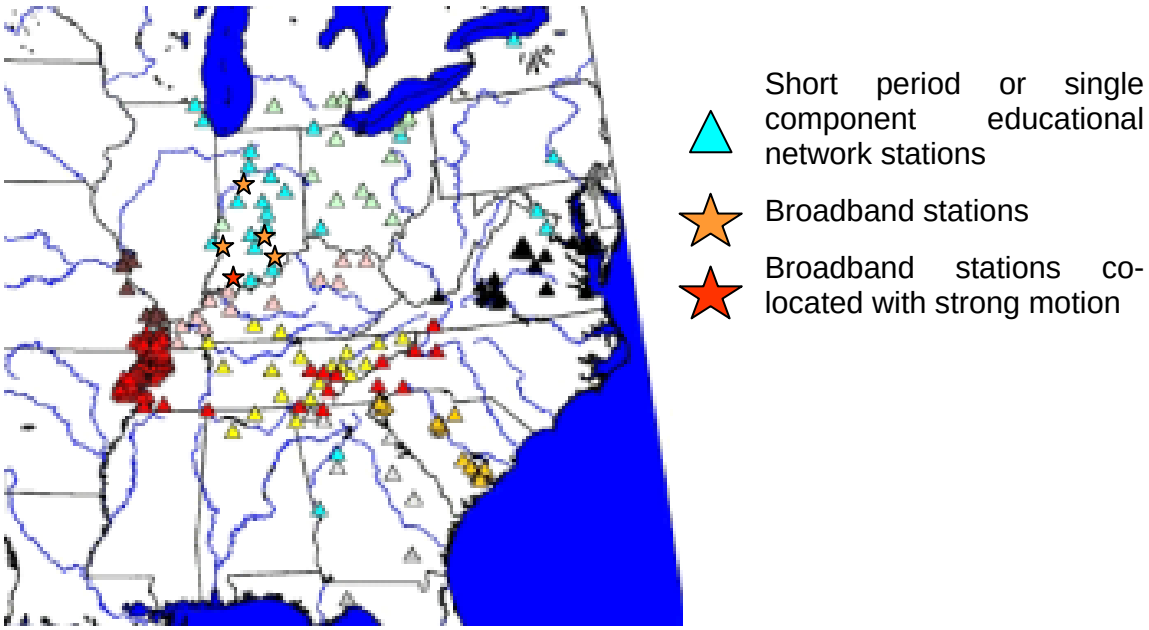

Figure 4-1 Current monitoring resources in the central and eastern US. Note that the data from the entire group of stations is not routinely analyzed together, making detection levels and response time highly variable.

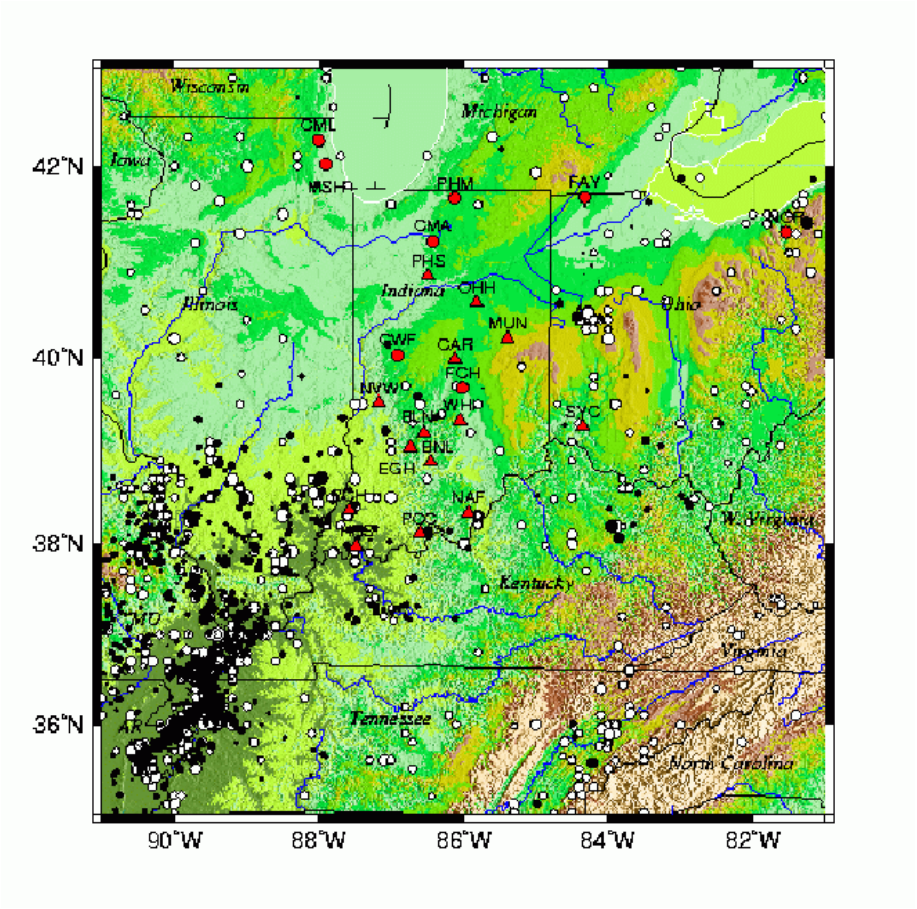

Figure 4-2 Recent seismicity and monitoring stations of the PEPP seismic network.

5 References

ATC/MCEER, Recommended LRFD Guidelines for the Seismic Design of Highway Bridges, Part I: Specifications and Part II: Commentary and Appendices, MCEER, Buffalo, NY, 2003.

Atkinson, G.A., and D.M. Boore, Some comparisons between recent ground-motion relations, *Seis. Res. Lett.*, *68* (1), 24-40, 1997.

Bauer, R.A., Compilation of databases and map perparation for regional and local seismic zonation studies in the CUSEC region: Collaborative research - organization of CUSEC state geologists with assistance from USGS and administrative suport from CUSEC, pp. 20, Illinois State Geological Survey, Champaign, IL, 1997.

Bauer, R.A., J. Kiefer, and N. Hester, Soil amplification maps for estimating earthquake ground motions in the Central US, *Engineering Geology*, *62* (1-3), 7-17, 2001.

Bear, G.W., J.A. Rupp, and A.J. Rudman, Seismic interpretation of the deep structure of the Wabash Valley fault system, *Seis. Research Letters*, *68* (4), 1997.

Bechtel-Jacobs, Paducah gaseous diffusion plant: Re-evaluation of site-specific soil column effects on ground motion, Report BJC/PAD-356, Department of Energy, 2002.

Bobet, A., R. Salgado, and D. Loukidis, Seismic design of deep foundations, pp. p. 20, Joint Transportation Research Program, Purdue University, West Lafayette, IN, 2001.

Braile, L.W., W.J. Hinze, J.L. Sexton, G.R. Keller, and E.G. Lidiak, The northeastern extension of the New Madrid seismic zone, *U.S. Geol. Surv. Prof. Paper 1236*, 175-184, 1982.

Braile, L.W., W.J. Hinze, J.L. Sexton, G.R. Keller, and E.G. Lidiak, Tectonic development of the New Madrid Rift Complex, Mississippi embayment, North America, *Tectonophysics*, *131* (1-21), 1986.

Campbell, K.W., Prediction of strong ground motion using the hybrid empirical method: Example application to eastern North America, *Bull. Seism. Soc. Am.*, 2002.

Campbell, K.W., Prediction of strong ground motion using the hybrid empirical method and its use in the development of ground-motion (attenuation) relations in eastern north America, *Bulletin of the Seismological Society of America*, *93* (3), 1012-1033, 2003.

Campbell, K.W., and Y. Bozorgnia, Updated near-source ground-motion (attenuation) relations for the horizontal and vertical components of peak ground acceleration and acceleration response spectra, *Bulletin of the Seismological Society of America*, *93* (1), 314-331, 2003.

Cramer, C.H., Site Specific Seismic Hazard Analysis that is Completely Probabilistic, *Bulletin of the Seismological Society of America*, *93* (4), 1841-1846, 2003.

Cramer, C.H., E. Schweig, J. Gomberg, and B. Waldron, The 2003 Memphis, Shelby County, Tennessee,Seismic Hazard Maps, *In preparation*, 2003.

Eggert, D.L., A.C. Samuelson, J.D. Bray, C.W. Chang, W.R. Eckhoff, K. Kayabali, E.J. McClees, T.R. West, M.C. Woodfield, and B. Zheng, Final Report to the City of

Evansville: Shear-wave and Earthquake Hazard Mapping of Evansville, Indiana, pp. 17, Indiana Geological Survey, Bloomington, IN, 1994.

Eggert, D.L., M.C. Woodfield, N.K. Bleuer, and E.J. Hartke, Geologic Terrain Map of the Evansville Region, Indiana, pp. 2 pl., Indiana Geological Survey, Bloomington, IN, 1997.

EPRI, Seismic hazard methodology for the central and eastern United Statest, 10 volumes, EPRI report NP-4726, Electric Power Research Institute, Palo Alto, CA, 1986.

FEMA-222A, NEHRP recommended provisions for the development of seismic regulations for new buildings, 1994 edition, Part 1 - provisions, pp. 290, Federal Emergency Management Agency, 1994.

Frankel, A., C. Mueller, T. Barnhard, D. Perkins, E.V. Leyendecker, N. Dickman, S. Hanson, and M. Hopper, National seismic hazard maps: documentation June 1996, U.S. Geological Survey Open-file Report 96-532, pp. 110 pp., USGS, 1996.

Frankel, A., M. Petersen, C. Mueller, K. Haller, R. Wheeler, E.V. Leyendecker, R. Wesson, S. Harmsen, C. Cramer, D. Perkins, and K. Rukstales, Documentation for the 2002 update of the National Seismic Hazard Maps, pp. 33, USGS, 2002.

Gomberg, J., B. Waldron, E. Schweig, H. Hwang, A. Webbers, R. VanArsdale, K. Tucker, R. Williams, R. Street, P. Mayne, W. Stephenson, J. Odum, C. Cramer, R. Updike, S. Hutson, and M. Bradle, Lithology and Shear-wave Velocity in Memphis, Tennessee, *Bulletin of the Seismological Society of America*, *in press*, 2003.

Gray, H.H., Map of Indiana showing thickness of unconsolidated deposits. Miscellaneous Map 37, Indiana Geological Survey., Indiana Geological Survey, Bloomington, IN, 1983.

Gray, H.H., Quaternary Geologic Map of Indiana, Indiana Geological Survey Miscellaneous Map 49, Indiana Geological Survey, Bloomington, IN, 1989.

Gray, H.H., C.H. Ault, and S.J. Keller, Bedrock Geologic Map of Indiana, Indiana Geological Survey Miscellaneous Map 48., Indiana Geological Survey, Bloomington, IN, 1987.

Hamburger, M., G. Pavlis, W.-Y. Kim, J. Haase, and M. Withers, Seismotectonic setting of the June 18, 2002 Darmstadt, Indiana Earthquake: or What's a nice earthquake like you doing in a place like this? EOS. Trans. Am. Geophys. Union 83(47), Fall Meet. Suppl., Abstract S22D-03, in *American Geophysical Union 2002 Fall Meeting*, San Francisco, CA, 2002.

Hamburger, M.W., and J. Rupp, The June 1987 southeastern Illinois earthquake: Possible tectonism associated with the La Salle Anticlinal Belt, *Seism. Res. Lett.*, *59*, 151-158, 1988.

Hamilton, E.L., Vp/Vs and Poisson's ratios in marine sediments and rocks, *J. Acoust. Soc. Am.*, *66* (4), 1093-1101, 1979.

Hardin, B.O., The Nature of Stress-Strain Behavior of Soils," Proc. Earthquake Engineering and Soil Dynamics Conference, ASCE, Pasadena, CA, Vol. 1, p. 3-90., *Proc. Earhthquake Engineering and Siol Dynamics Conference, ASCE*, *1*, 3-90, 1978.

Hardin, B.O., and V.P. Drnevich, Shear Modulus and Damping in Soils, *Journal of the Soil Mechanics and Foundations Division*, *98* (7), 667-692, 1972.

Idriss, I.M., and J.I. Sun, User's manual for SHAKE91, Center for Geotechnical Modeling, Dept. of Civil and Environmental Engineering, University of California, Davis, CA, 1992.

Imai, T., and K. Tonouchi, Correlation of N-value with S-Wave Velocity and Shear Modulus, in *Proceedings of the 2nd European Symposium on Penetration Testing*, pp. 57-72, Amsterdam, 1982.

Kim, W.Y., The 18 June 2002 Caborn, Indiana, earthquake: Reactivation of ancient rift in the Wabash Valley seismic zone?, *Bulletin of the Seismological Society of America*, *93* (5), 2201-2211, 2003.

Lee, R.C., A methodology to integrate site response into probabilistic seismic hazard analysis, Site Geotechnical Services, Savannah River Site, 2000.

Mueller, C., M. Hopper, and A. Frankel, Preparation of earthquake catalogs for the 1996 national seismic hazard maps, U.S. Geological Survey Open-File Report, 1996.

Munson, P.J., C.A. Munson, and E.C. Pond, Paleoliquefaction Evidence for a Strong Holocene Earthquake in South-Central Indiana, *Geology*, *23* (4), 325-328, 1995.

Nuttli, O.W., Seismicity of the central United States, in *Reviews in Engineering Geology*, pp. 67-93, Geo. Soc. Am, 1979.

Nuttli, O.W., Catalog of Central United States Earthquakes Since 1800 of mb = 3.0, St. Louis University, St. Louis. Mo, 1983.

Obermeier, S.F., Use of liquefaction-induced features for paleoseismic analysis - An overview of how seismic liquefaction features can be distinguished from other features and how their regional distribution and properties of source sediment can be used to infer the location and strength of Holocene paleo-earthquakes, *Engineering Geology*, *44* (1-4), 1-76, 1996.

Pavlis, G.L., A. Rudman, B. Pope, M. Hamburger, G. Bear, and H. Al-Shukri, Seismicity of the Wabash Valley Seismic Zone based on a temporary seismic array experiment, *Seis. Research Letters*, *73* (5), 751-760, 2002.

Reiter, L., *Earthquake Hazard Analysis: issues and insights*, Columbia University Press, New York, 1990.

Rockaway, T.D., Spatial Assessment of Earthquake Induced Geotechnical Hazards, Ph.D. thesis, Georgia Institute of Technology, Atlanta, GA, 1997.

Rudman, A.J., M.E. Biggs, R.F. Blakely, and J.F. Whaley, Statistical studies of Indiana Bedrock Velocities: Mapping applications, *Indiana Academy of Science*, *83* (1973), 284-290, 1973.

Seeber, L., and J.G. Armbruster, The NCEER-91 earthquake catalog: improved intensity-based magnitudes and recurrence relations for U.S. earthquakes east of New Madrid, NCEER-91-0021, National Center for Earthquake Engineering Research, 1991.

Sexton, J.L., L.W. Braile, W.J. Hinze, and M.J. Campbell, Seismic reflection profiling studies of a buried Precambrian rift beneath the Wabash Valley fault zone, *Geophysics*, *51*, 640-660, 1986.

Stauder, W., and O.W. Nuttli, Seismic studies: South central Illinois earthquake of November 9, 1968, *Bull. Seismo. Soc. Am.*, *60*, 973-981, 1970.

Street, R., E.W. Woolery, Z.M. Wang, and J.B. Harris, NEHRP soil classifications for estimating site-dependent seismic coefficients in the Upper Mississippi Embayment, *Engineering Geology*, *62* (1-3), 123-135, 2001.

Toro, G.R., N.A. Abrahamson, and J.F. Schneider, Model of strong ground motions from earthquakes in central and eastern North America: best estimates and uncertainties, *Seis. Research Letters*, *68* (1), 41-57, 1997.

Toro, G.R., and W.J. Silva, Scenario earthquakes for St.Louis, MO, and Memphis, TN, and seismic hazard maps for the central United States region including the effect of site conditions. (Final Technical Report), 2001.

USGS, Earthquake Hazards Program Web Page http://neic.usgs.gov/neis/bulletin/, USGS, 2003.

Wang, Z., E. Woolery, and J.A. Schaefer, A short note on ground-motion recordings from the June 18, 2002, Darmstadt, Ind., Earthquake, *Seis. Research Letters*, *74* (2), 148-152, 2002.

Whaley, J.F., R.F. Blakely, K.K. Like, and C.L. James, Seismic Refraction Data for Indiana (Indiana Geological Survey, Point Shapefile), Indiana Geological Survey, 2002.

Wheeler, R.L., and C.H. Cramer, Updated seismic hazard in the southern Illinois Basin: geological and geophysical foundations for use in the 2002 USGS National Seismic-hazard maps, *Seis. Research Letters*, *73* (5), 2002.

Final Report

Hardin Equation for Estimation of Shear Wave Velocity

Special Research Project by

Alison Hunyar

Directed by

Dr. Vincent P. Drnevich, P.E.

School of Civil Engineering

Purdue University

Dr. Jennifer Haase and Dr. Robert Nowack

School of Science, EAS Department

August 25, 2003

Table of Contents

List of Tables

List of Equations

Introduction

The value of shear wave velocity of near surface soils is one measurement of soil behavior when dynamically loaded. Currently, the shear wave velocity profile of a location may be obtained through field tests such as the standard penetration test (SPT), ASTM D1586, seismic refraction, ASTM D5777, or crosshole seismic testing, ASTM D4428/D4428M. Because each of these tests requires additional equipment and time in the field, an alternative method of approximating the shear wave velocity profile may be desirable for some applications. The following spreadsheet uses bore log data to generate a shear wave velocity profile for the location at which the bore log was recorded.

Spreadsheet Calculations

Hardin Equation

Equation 1, the Hardin Equation is used to calculate the shear modulus of a soil at minimum strain.

$$G_{max}=SF(e)OCR^{K}(\sigma_o')^{n}Pa^{(1-n)}$$

Equation 1: Hardin Equation for Shear Modulus (Hardin 1978)

In the above equation S refers to the "Stiffness Number" and is approximately equal to 625 (Hardin 1978), F(e) is the function of void ratio discussed later in the spreadsheet explanation, OCR^K is the overconsolidation ratio raised to a coefficient, K, related to the plasticity index of the soil. σ_o' is the mean effective stress of the soil at the point of measurement, n is a coefficient equal to 0.5, and Pa is atmospheric pressure.
G_{max} is related to shear wave velocity by the following equation,

$$V_s = \sqrt{\frac{G_{max}}{\rho}}$$

Equation 2: Shear Wave Velocity (Hardin 1978)

The spreadsheet uses information collected on a bore log to calculate each variable in the Hardin equation as well as density to generate the shear wave profile of a specific location.

Input Data

On the first page of the spreadsheet, the user is asked to input information about the site in question. The user first records the project name, location of the bore hole, the date of data collection, as well as the spreadsheet user's name in the table shown in Table 1 below.

Table 1: Location Information

Hardin Equation Estimation of Shear Wave Velocity Spreadsheet Calculation by Dr. Vincent P. Drnevich and Alison A. Hunyar Purdue University, July 2003			
Project:	Example	**User:**	A. Hunyar
Location:	West Lafayette, IN		
Date of Data Collection:	7/3/2003		

The user is then asked to enter project specific information in Table 2.

System of Units

The spreadsheet calculations may be performed in either English or SI units. Once the system of units is chosen, the units used in the spreadsheet automatically change to remain consistent throughout the calculations.

Soil Classification System

The user has a choice of three soil classification systems, the Unified Soil Classification (USC) system, the American Association of State Highway and Transportation Officials (AASHTO) system, or the United States Department of Agriculture (USDA) system. Detailed information about each of these three classification systems may be found in the "Soil Classification Information" worksheet included in Appendix B.

Ground Water Table (GWT)

Because the location of the ground water table (GWT) is necessary for further stress calculations, the depth from the ground surface to the ground water table in feet or meters must be recorded. Likewise, the height of capillary rise above the GWT must be recorded. If the height of capillary rise is unknown, the user may estimate this height based on the soil type at the GWT using Table 6 in the "Calculation Information" worksheet, included in Appendix A.

Ground Surface Elevation (GS_Elev)

The ground surface elevation in feet or meters in reference to a chosen datum is entered. For example, at this location the ground surface is 377.4 ft above mean sea level.

Specific Gravity of Soil Solids (SPGr)

An estimation of the average specific gravity of solids (SPGr) is entered. If a specific value is unknown, the user may use the estimated value of 2.7.

Table 2: Location Geometry

Units	English		"English" or "SI"
Classification System	USC		"USC," "AASHTO," or "USDA"
GWT	32.81	**(ft)**	Depth to Ground Water Table
Capillary Rise	16.4	**(ft)**	Height of Capillary Rise from Ground Water Table
GS_Elev	377.4	**(ft)**	Ground Surface Elevation
SPGr	2.7	(unitless)	Specific Gravity of Soil Solids

After the site specific information is recorded, the user enters the data collected on the bore log in table 3.

Depth (z)

Each measured depth in feet or meters recorded on the bore log is entered into the first column of the table 3 shown below. The data used as an example in this spreadsheet is from a bore log provided by the Indiana Geological Survey.

Bore Log Soil Classification

The soil type for each measured unit recorded on the bore log is entered into the spreadsheet in compliance with the soil classification system chosen. The user may refer to the "Soil Classification Information" worksheet included in Appendix B for detailed information about each classification system.

Relative Density and Relative Compaction

For granular soil layers, the relative density of the soil is estimated to be loose (L), medium (M), or dense (D). For cohesive soil layers, the relative compaction is estimated to be uncompacted (UC), to have some compaction (SC), or to be heavily compacted (HC).

Water Content (w)

The gravimetric water content, or the weight of water divided by the weight of soil solids, of each soil layer is recorded for further use in calculations. The water content may be obtained in the field using the Standard Test Method for Field Determination of Water (Moisture) Content of Soil by the Calcium Carbide Gas Pressure Tester Method, ASTM D4944, or in the laboratory using the Standard Test Method for Laboratory Determination of Water (Moisture) Content of Soil and Rock, ASTM D2216, or Standard Test Method for Determination of Water (Moisture) Content of Soil by the Microwave Oven Method, ASTMD4643.

Degree of Consolidation

Finally, the user must record the relative degree of consolidation of the soil as being normally consolidated (NC), lightly over consolidated (LOC), or highly over consolidated (HOC).

Table 3: Bore Log Data

Depth	Soil Classification	Granular Soils Relative Density	Cohesive Soils Relative Compaction	Water Content	Degree of Consolidation
(ft)	USC	L, M, D	UC, SC, HC	(%)	NC,LOC,HOC
0.00	ML		sc	10	LOC
8.20	ML		UC	10	LOC
16.40	CH		UC	10	LOC
24.60	CH		SC	10	LOC
32.80	CH		SC	30	LOC
41.00	CH		SC	30	LOC
49.20	S	M		10	LOC
57.40	S	M		10	LOC
65.60	Shale	D		N/A	HOC
73.80	Shale	D		N/A	HOC

Calculated Data

The "Calculated Data" worksheet first includes a repeat of table 2, "Location Geometry," recorded in the "Input Data" worksheet. The main calculated data table is shown in figures 4 and 5.

Table 4: Calculated Data

Depth	Elev.	Thickness	Granular or Cohesive	Dry Unit Weight	Total Unit Weight	Total Vertical Stress	Pore Pressure	Effective Vertical Stress	Coeff. of Earth Pressure	Coeff. Adjusted for Consolidation	Mean Effective Stress	Void R
(ft)	(ft)	(ft)	"G" or "C"	(lb/ft^3)	(lb/ft^3)	(lb/ft^2)	(lb/ft^2)	(lb/ft^2)	K_o	$K_{adjusted}$	(lb/ft^2)	
0.0	377.4	0.0	C	115	126.5	0.0	0.0	0.0	0.4	0.6	0.0	0.5
8.2	369.2	8.2	C	130	143.0	1172.6	0.0	1172.6	0.6	0.8	1016.6	0.3
16.4	361.0	8.2	C	130	143.0	2345.2	0.0	2345.2	0.6	0.8	2033.2	0.3
24.6	352.8	8.2	C	115	126.5	3382.5	-512.3	3894.8	0.6	0.8	3376.7	0.5
32.8	344.6	8.2	C	115	149.5	4608.4	-0.6	4609.0	0.6	0.8	3995.9	0.5
41.0	336.4	8.2	C	115	149.5	5834.3	511.1	5323.2	0.6	0.8	4615.1	0.5
49.2	328.2	8.2	G	100	110.0	6736.3	1022.7	5713.6	0.4	0.6	4164.6	0.7
57.4	320.0	8.2	G	100	110.0	7638.3	1534.4	6103.9	0.4	0.6	4449.1	0.7
65.6	311.8	8.2	ROCK	130	#####	######	2046.1	######	0.5	1.0	#####	ROCK
73.8	303.6	8.2	ROCK	130	#####	######	2557.8	######	0.5	#####	#####	ROCK

Table 5: Calculated Data (continued)

ctive Stress	Void Ratio	F(e)	Estimated OCR	Plasticity Index	(OCR)^K	Gmax	Vs	Measured Depths	Measured Values of Vs	Measured Depths	Measured Values of Vs	Measured Depths	Measured Values of Vs
			PI		(lb/ft^2))	(ft/s)	(ft)	(ft/s)	(ft)	(ft/s)	(ft)	(ft/s)
0.5	2.2	2	0	1.00	0.00E+00	0	2	257	7	850	7	363.0
0.3	2.8	2	30	1.13	2.87E+06	800	3	320	13	1056	13	726.0
0.3	2.8	2	30	1.13	4.07E+06	960	7	404	23	1333	20	379.5
0.5	2.2	2	30	1.13	4.19E+06	1030	10	452	30	1491	26	1320.0
0.5	2.2	2	30	1.13	4.56E+06	990	15	517	36	1706	33	1188.0
0.5	2.2	2	30	1.13	4.90E+06	1030	20	565	45	1864	40	957.0
0.7	1.6	2	0	1.00	2.95E+06	930	25	605	51	1997	46	1056.0
0.7	1.6	2	30	1.13	3.46E+06	1010	30	640	59	2113	53	792.0
ROCK	ROCK	4	10	1.00	#VALUE!	####	35	672	73	2217	59	957.0
ROCK	ROCK	4	15	1.00	#VALUE!	####	40	702	79	2317	66	825.0

Depth (z)

The first column contains the depth information copied from the "Input Data" worksheet.

Elevation (Elev.)

The elevation of each measured unit is calculated using the elevation of the ground surface entered in table 2 and the depths.

Thickness (h)

The thickness of each measured unit is calculated by the difference in the elevations.

Granular or Cohesive

Whether the soil is granular, "G", or cohesive, "C" is determined by a spreadsheet formula that uses the soil classification entered by the user in the soil classification information entered by the user on the "Input Data" worksheet table 8 in the "Soil Classification Information" worksheet, included in Appendix B, which identifies each soil type as being either granular or cohesive.

Dry Unit Weight (γ_d)

The dry unit weight of soil is the weight of soil solids per total volume and is determined using table 7 located in the "Calculation Information" worksheet shown in Appendix A. The formula entered into the spreadsheet uses the soil classification and relative density or relative compaction as indicated by the user and table 7 to assign a dry unit weight to each unit.

Total Unit Weight (γ)

The total unit weight, or total weight of soil and water divided by the total volume, of each measured unit is calculated using the relationship shown in equation 3. This

relationship uses the dry unit weight assigned in the previous column as well as the water content for that unit recorded by the user in the "Input Data" worksheet.

$$\gamma = \gamma_d (1 + w)$$

Equation 3: Total Unit Weight

Total Vertical Stress (σ_v)

The total unit weight is used to calculate the total vertical stress at each depth as shown in equation 4, where h is the thickness of the layer. At a given layer, the total vertical stress is the total unit weight of that layer multiplied by the thickness of that layer plus the total vertical stress of all above layers.

$$\sigma_v = \sum \gamma h$$

Equation 4: Total Vertical Stress

Pore Water Pressure (u)

The pore pressure of each layer is calculated based on the elevation of the ground water table as well as the height of capillary rise. Equation 5, where γ_w is the unit weight of water located in the "Calculation Information" worksheet, table 5 of Appendix A, is used to calculate the pore water pressure below the ground water table and equation 6 is used to calculate the pore water pressure in the zone of capillary rise. Like total vertical stress, pore water pressure of a given layer is the unit weight of water times the thickness of that layer plus the pore water pressure of all above layers.

$$u = \sum \gamma_w h_{belowGWT}$$

Equation 5: Pore Water Pressure

$$u = \sum -\gamma_w h_{aboveGWT}$$

Equation 6: Pore Water Pressure in the Zone of Capillary Rise

Effective Vertical Stress (σ_v')

The effective vertical stress of each unit is calculated by the difference of total stress and pore water pressure as shown in equation 7.

$$\sigma_v' = \sigma_v - u$$

Equation 7: Vertical Effective Stress

Coefficient of Lateral Earth Pressure (K_o)

The coefficient of lateral earth pressure, K_o, is used to determine the horizontal effective stress of each layer. K_o is calculated by equation 8 for granular soils and equation 9 for cohesive soils. For granular soils, the spreadsheet assigns a value of friction angle, ϕ', based on relative density using table 11 of the "Calculation Information" worksheet included in Appendix A, to be used in equation 8.

$$K_o = 1 - \sin\phi'$$

Equation 8: Coefficient of Earth Pressure, Granular Soils (Holtz & Kovacs, 1981)

$$K_o = 0.44 + 0.42(PI/100)$$

Equation 9: Coefficient of Earth Pressure, Cohesive Soils (Holtz & Kovacs, 1981)

Because the coefficient of earth pressure is dependent on the degree of consolidation of the soil, K_o must be adjusted if the soil is not normally consolidated. Equation 10 shows the relationship between K_o for normally consolidated soil and K_o for over consolidated soil where h is approximately equal to 0.5.

$$(K_o)_{OC} = (K_o)_{NC}(OCR)^h$$

Equation 10: Coefficient of Earth Pressure of Over Consolidated Soil (Holtz & Kovacs, 1981)

Mean Effective Stress (σ_o')

The mean effective stress is calculated using equation 11. Where σ_v' is the vertical effective stress.

$$\sigma_o' = \frac{(\sigma_v' + 2K_o\sigma_v')}{3}$$

Equation 11: Mean Effective Stress (Holts & Kovacs 1981)

Void Ratio (e)

The void ratio of each layer is calculated using equation 12 where SPGr is the specific gravity of soil solids recorded by the user in the "Input Data" worksheet, γ_w is the unit weight of water located in table 5 of the "Soil Classification" worksheet included in Appendix A, and γ_d is the dry unit weight of each soil layer as previously calculated.

$$e = \frac{SPGr * \gamma_w}{\gamma_d} - 1$$

Equation 12: Void Ratio Calculation

The function of void ratio shown in equation 13 is calculated for each soil.

$$F(e) = \frac{1}{0.3 + 0.7e^2}$$

Equation 13: Function of Void Ratio (Hardin 1978)

Overconsolidation Ratio (OCR)

The estimated value of overconsolidation ratio (OCR) is determined from the degree of consolidation entered by the user in the "Input Data" worksheet. The degree of

consolidation is assigned a value of 1 for normally consolidated, 2 for lightly over consolidated or 4 for heavily over consolidated.

Plasticity Index (PI)

The plasticity index (PI) of each soil layer is determined from the soil classification entered by the user in the "Input Data" worksheet. Each soil type is assigned a value of PI in table 15 the "Soil Classification Information" worksheet included in Appendix B.

Coefficient Related to Plasticity (K)

The value of PI is used to determine the value of the K coefficient as shown in Table 6. K is simply a coefficient related to PI and is not to be confused with K_o, the coefficient of lateral earth pressure used in the calculation of mean effective stress.

Table 6: Relationship of PI and K (Hardin, Drnevich 1972)

PI	K
0	0.00
20	0.18
40	0.30
60	0.41
80	0.48
100	0.50

Shear Modulus (G_{max})

The value of shear modulus is calculated using the Hardin Equation as shown by equation 14. Again, S is the stiffness number and Pa is the atmospheric pressure. Both of these constants are included in table 5 of the "Calculation Information" worksheet included in Appendix A. The remaining variables have been calculated by the spreadsheet as previously discussed.

$$G_{max} = SF(e)OCR^{K}(\sigma_o'\text{^}0.5)(Pa)\text{^}0.5$$

Equation 14: Hardin Equation

Shear Wave Velocity (V_s)

Finally, the shear wave velocity is calculated by equation 15, where ρ is the density of the soil layer calculated using the total unit weight previously calculated and the gravitational constant included in table 5 of the "Calculation Information" worksheet located in Appendix A.

$$V_s = \sqrt{\frac{G_{mas}}{\rho}}$$

Equation 15: Shear Wave Velocity Calculation

Comparison Data

The columns following the V_s column are left open for the user to enter any additional V_s data that may be available for the same location. In this example, three previously calculated V_s profiles were used for comparison with the spreadsheet calculation. The first set of data was calculated by Chi Park, graduate student at Purdue University, using SPT data. The second data set is downhole measurements provided by the Indiana Geological Survey. The third dataset is published downhole measurements (Eggert et al. 1994). The plot comparing the shear wave velocity profiles may be found in the "Output Data" worksheet included in Appendix C.

Works Cited

Das, Braja M. Principles of Geotechnical Engineering, 5th ed. PWS Boston, 2002, pp165-167. 53, 67, 82-88 .

Das, Braja M. Principles of Soil Dynamics. PWS-Kent, Boston. 1993.

Eggert, D.L., Samuelson, A.C., Bray, J.D., Chang, S.W., Eckhoff, W.R., Kayabali, K., McClees, E.J., West, T.R. Woodfield, M.D., Zheng, B. "Final Report to the City of Evansville: Shear-Wave and Earthquake Hazard Mapping of Evansville, Indiana. Indiana University-Indiana Geological Survey Open File report 94-19. 1994.

Hardin, B.O. "The Nature of Stress-Strain Behavior of Soils," Proc. Earthquake Engineering and Soil Dynamics Conference, ASCE, Pasadena, CA, Vol. 1, p. 3-90.

Hardin, B.O. and Drnevich, V.P. "Shear Modulus and Damping in Soils." Journal of the Soil Mechanics and Foundations Division, Vol. 98, No. 7, July 1972, pp.667-692.

Holtz, Robert D. and Kovacs, William D. An Introduction to Geotechnical Engineering. Prentice-Hall, Englewood Cliffs, NJ. 1981. p. 519-520, 607.

Jumikis, Alfreds R. Soil MechanicsRobert E. Krieger Publishing Company, Inc. Malabar, FL 1984 p.133

Appendix A

Calculation Information Worksheet, English Units

Table 5: Constants

S_Hardin	625		Stiffness Number
γ_w	62.4	(lb/ft^3)	Unit Weight of Water
g	32.2	(ft/s^2)	Gravitational Constant
Pa	2116.8	(lb/ft^2)	Atmospheric Pressure

Table 6: Typical Range of Capillary Rise

	Range of Capillary Rise		
Soil Type	**m**	**ft**	
Fine Gravel	0.02-0.1	0.07-0.33	
Coarse Sand	0.1-0.15	0.33-0.5	
Medium Sand	0.15-0.3	0.5-1	
Fine Sand	0.3-1	1-3	
Silt	1-10	3-30	
Clay	10-30	30-100	
Colloids	30+	100+	(Jumikis 1984)

Table 7: Typical Values for Dry Unit Weight of Soil

Granular Soils			
L	90	(lb/ft^3)	
M	100	(lb/ft^3)	
D	110	(lb/ft^3)	
Cohesive Soils			
UC	100	(lb/ft^3)	
SC	115	(lb/ft^3)	
HC	130	(lb/ft^3)	
ROCK	130	(lb/ft^3)	(Das 2002)

Table 8:Typical Values of Plasticity Index

Soil	**PI**	
Nonplastic	0	
Slightly Plastic	1-5	
Low Plasticity	5-10	
Medium Plasticity	10-20	
High Plasticity	20-40	
Very High Plasticity	>40	(Das 2002)

Table 9: Over Consolidation Ratio

Degree of Consolidation		OCR
Normally Consolidated	NC	1
Lightly Over Consolidated	LOC	2
Highly Over Consolidated	HOC	4

Table 10: K Coefficient

PI	K
0	0.00
20	0.18
40	0.30
60	0.41
80	0.48
100	0.50

(Hardin, Drnevich 1972)

Table 11: Friction Angle

Granular Soils

Relative Density		ϕ' (radians)	ϕ' (degrees)
Loose	L	0.54	31
Medium	M	0.62	35.5
Dense	D	0.70	40

Calculation Information Worksheet, SI Units

Table 5: Constants

S_Hardin	625		Stiffness Number
γ_w	9.81	(kN/m^3)	Unit Weight of Water
g	9.81	(m/s^2)	Gravitational Constant
Pa	101.325	(kN/m^2)	Atmospheric Pressure

Table 6: Typical Range of Capillary Rise

	Range of Capillary Rise		
Soil Type	**m**	**ft**	
Fine Gravel	0.02-0.1	0.07-0.33	
Coarse Sand	0.1-0.15	0.33-0.5	
Medium Sand	0.15-0.3	0.5-1	
Fine Sand	0.3-1	1-3	
Silt	1-10	3-30	
Clay	10-30	30-100	
Colloids	30+	100+	(Jumikis 1984)

Table 7: Typical Values for Dry Unit Weight of Soil

Granular Soils			
L	14	(kN/m^3)	
M	15	(kN/m^3)	
D	16	(kN/m^3)	
Cohesive Soils			
UC	15	(kN/m^3)	
SC	18	(kN/m^3)	
HC	20	(kN/m^3)	
ROCK	20	(kN/m^3)	(Das 2002)

Table 8:Typical Values of Plasticity Index

Soil	**PI**	
Nonplastic	0	
Slightly Plastic	1-5	
Low Plasticity	5-10	
Medium Plasticity	10-20	
High Plasticity	20-40	
Very High Plasticity	>40	(Das 2002)

Table 9: Over Consolidation Ratio

Degree of Consolidation		OCR
Normally Consolidated	NC	1
Lightly Over Consolidated	LOC	2
Highly Over Consolidated	HOC	4

Table 10: K Coefficient

PI	K
0	0.00
20	0.18
40	0.30
60	0.41
80	0.48
100	0.50

(Hardin, Drnevich 1972)

Table 11: Friction Angle

Granular Soils

Relative Density		ϕ' (radians)	ϕ' (degrees)
Loose	L	0.54	31
Medium	M	0.62	35.5
Dense	D	0.70	40

Appendix B

Table 12

Unified Soil Classification System (USC)	
Soil Name	**Soil Symbol**
Gravel	G
Well Graded Gravel	GW
Poorly Graded Gravel	GP
Sandy Gravel	GS
Silty Gravel	GM
Clayey Gravel	GC
Sand	S
Gravely Sand	SG
Silty Sand	SM
Clayey Sand	SC
Low Plasticity Silt	ML
High Plasticity Silt	MH
Low Plasticity Clay	CL
High Plasticity Caly	CH
Low Plasticity Organic	OL
High Plasticity Organic	OH
Peat	Pt

(Das 2002)

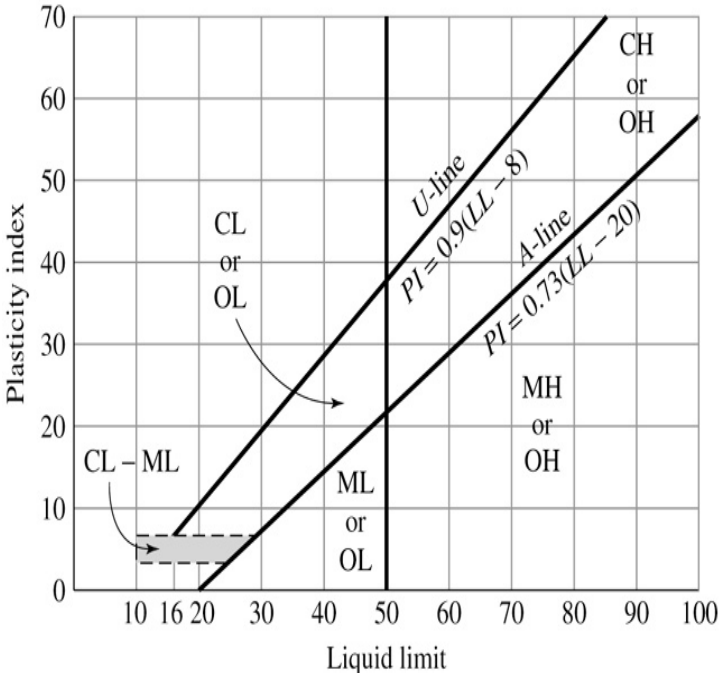

Table 13

American Association of State Highway and Transportation Officials (AASHTO)

Granular Materials (35% or less of total sample passing No. 200)

Sieve Analysis (% Passing)			Characteristics of Fraction Passing No. 40				
No. 10	No. 40	No. 200	Liquid Limit	Plasticity Index	Typical Material Compostition	Group Classification	Granular or Cohesive
50 (max.)	30 (max.)	15 (max.)		6 (max.)	Stone fragments, gravel, and sand	A-1-a	G
	50 (max.)	25 (max.)		6 (max.)	Stone fragments, gravel, and sand	A-1-b	G
		35 (max.)	40 (max.)	10 (max.)	Silty or clayey gravel and sand	A-2-4	G
		36 (max.)	41 (min.)	10 (max.)	Silty or clayey gravel and sand	A-2-5	G
		37 (max.)	40 (max.)	11 (min.)	Silty or clayey gravel and sand	A-2-6	G
		38 (max.)	41 (min.)	11 (min.)	Silty or clayey gravel and sand	A-2-7	G
	51 (min.)	10 (max.)	Not Plastic	Not Plastic	Fine Sand	A-3	G

Silt-Clay Materials (More that 35% of total sample passing No. 200)

Sieve Analysis (% Passing)		Characteristics of Fraction Passing No. 40					
No. 10	No. 40	No. 200	Liquid Limit	Plasticity Index	Typical Material Compostition	Group Classification	Granular or Cohesive
		36 (min.)	40 (max.)	10 (max.)	Silty soil	A-4	C
		37 (min.)	41 (min.)	10 (max.)	Silty soil	A-5	C
		38 (min.)	40 (max.)	11 (min.)	Clayey soil	A-6	C
		39 (min.)	41 (min.)	11 (min.)	Clayey soil	A-7	C
		40 (min.)	41 (min.)	11 (min.)	Clayey soil	A-7-5	C
		41 (min.)	41 (min.)	11 (min.)	Clayey soil	A-7-6	C

(Das 2002)

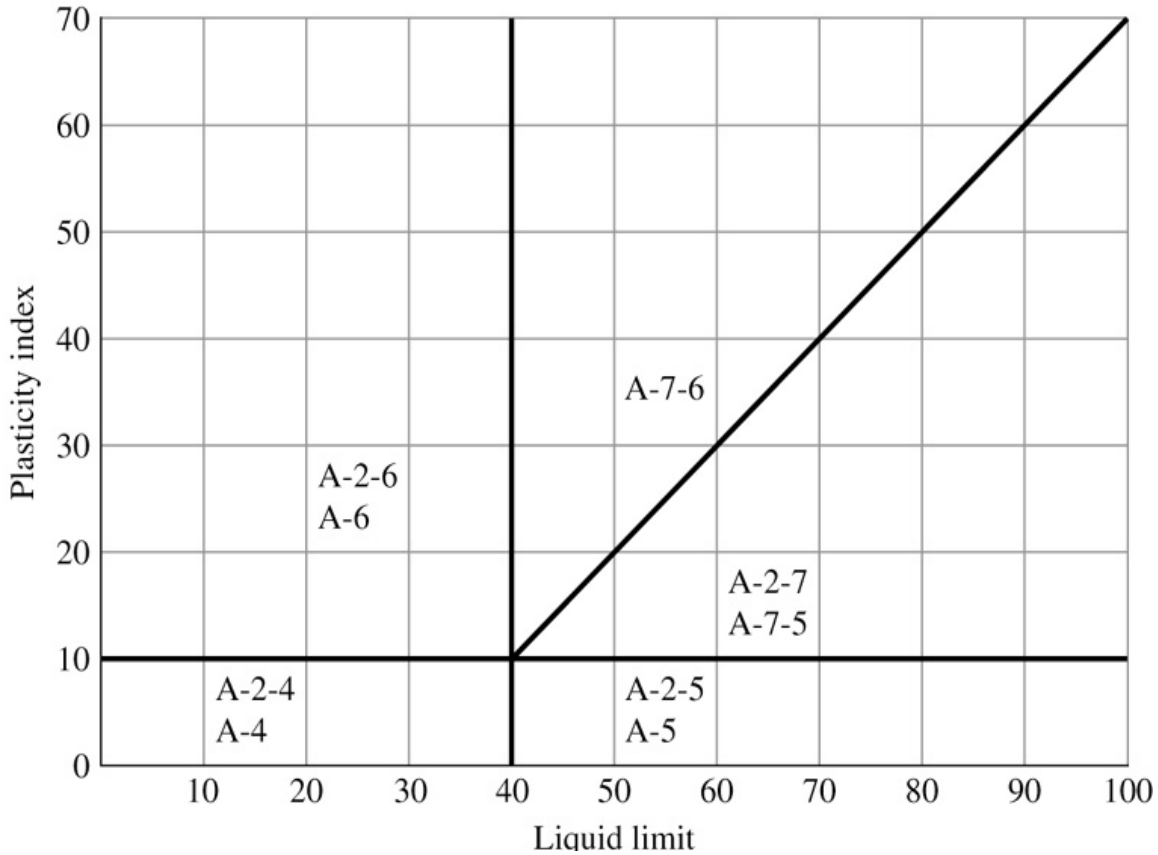

Table 14

United States Department of Agriculture (USDA)

% Sand	% Silt	% Clay	Soil Name	Granular or Cohesive
85-100	0-15	0-10	Sand	G
70-85	15-30	10-15	Loamy Sand	G
50-85	0-50	0-20	Sandy Loam	G
0-20	80-100	0-12	Silt	C
0-50	50-88	0-28	Silty Loam	C
0-45	0-40	40-100	Clay	C
45-65	0-18	36-55	Sandy Clay	C
0-20	40-60	40-60	Silty Clay	C
45-80	0-28	20-36	Sandy Clay Loam	C
0-20	40-72	28-40	Silty Clay Loam	C
20-45	15-52	28-40	Clay Loam	C
22-52	28-50	8-28	Loam	C

(Das 2002)

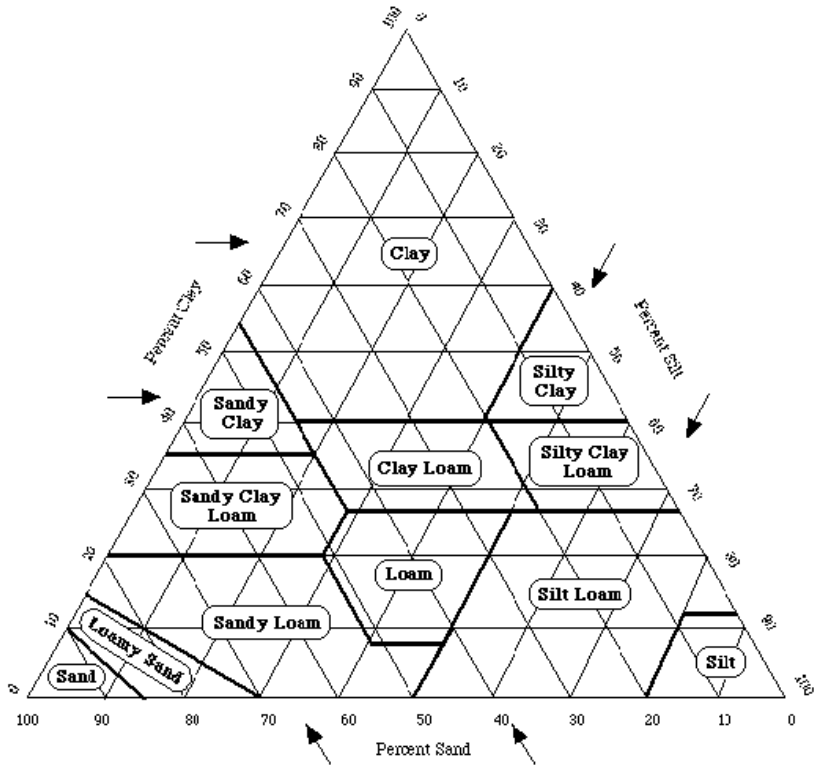

http://www.agronomy.psu.edu/Courses/SOILS101/Labs/texture.html

Table 15

Soil Symbol	Typical Plasticity Index Value
G	0
GW	0
GP	0
GS	0
GM	0
GC	0
S	0
SG	0
SM	0
SC	0
ML	10
MH	15
CL	15
CH	30
OL	10
OH	30
Pt	20
A-1-a	0
A-1-b	0
A-2-4	5
A-2-5	5
A-2-6	25
A-2-7	20
A-3	0
A-4	5
A-5	5
A-6	25
A-7	25
A-7-5	20
A-7-6	30
Sand	0
Loamy Sand	0
Sandy Loam	10
Silt	20
Silty Loam	12
Clay	35
Sandy Clay	15
Silty Clay	18
Sandy Clay Loam	15
Silty Clay Loam	15
Clay Loam	15
Loam	15

Table 16

Soil Symbol	Granular or Cohesive
G	G
GW	G
GP	G
GS	G
GM	G
GC	G
S	G
SG	G
SM	G
SC	G
ML	C
MH	C
CL	C
CH	C
OL	C
OH	C
Pt	C
A-1-a	G
A-1-b	G
A-2-4	G
A-2-5	G
A-2-6	G
A-2-7	G
A-3	G
A-4	C
A-5	C
A-6	C
A-7	C
A-7-5	C
A-7-6	C
Sand	G
Loamy Sand	G
Sandy Loam	G
Silt	C
Silty Loam	C
Clay	C
Sandy Clay	C
Silty Clay	C
Sandy Clay Loam	C
Silty Clay Loam	C
Clay Loam	C
Loam	C
Shale	ROCK
Sandstone	ROCK
Granite	ROCK
Limestone	ROCK
Siltstone	ROCK
Dolomite	ROCK

Appendix C

Output Data Plots

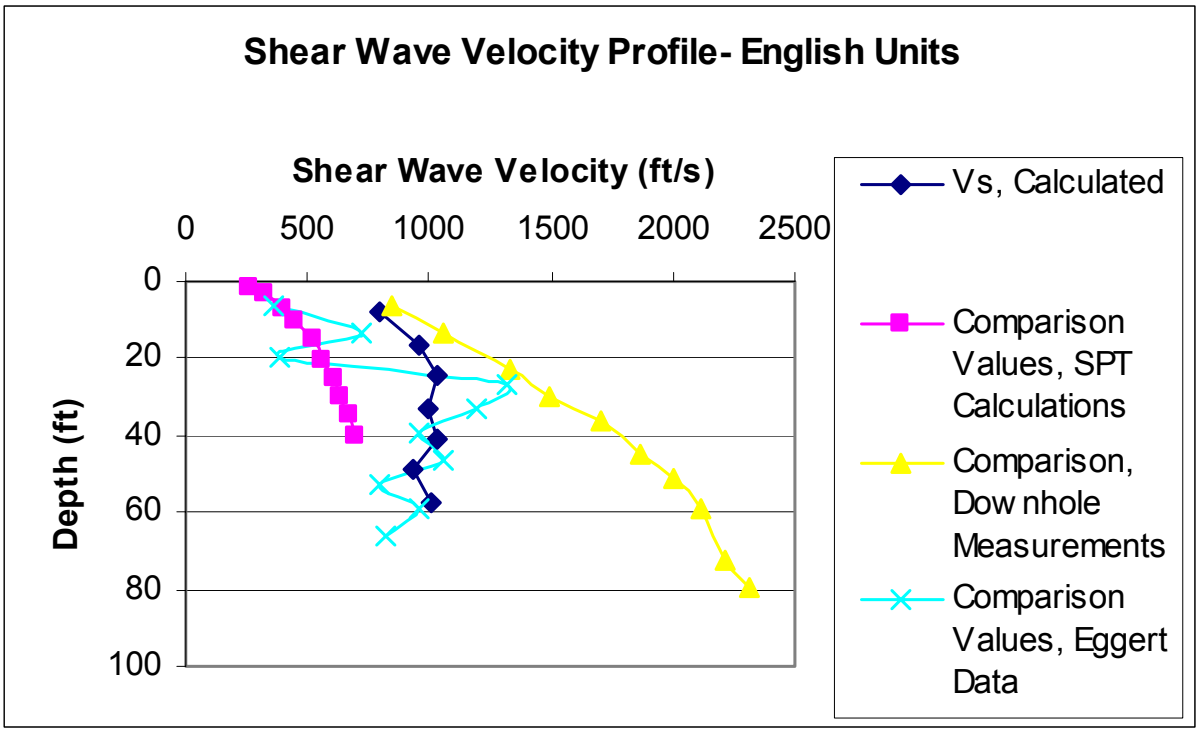

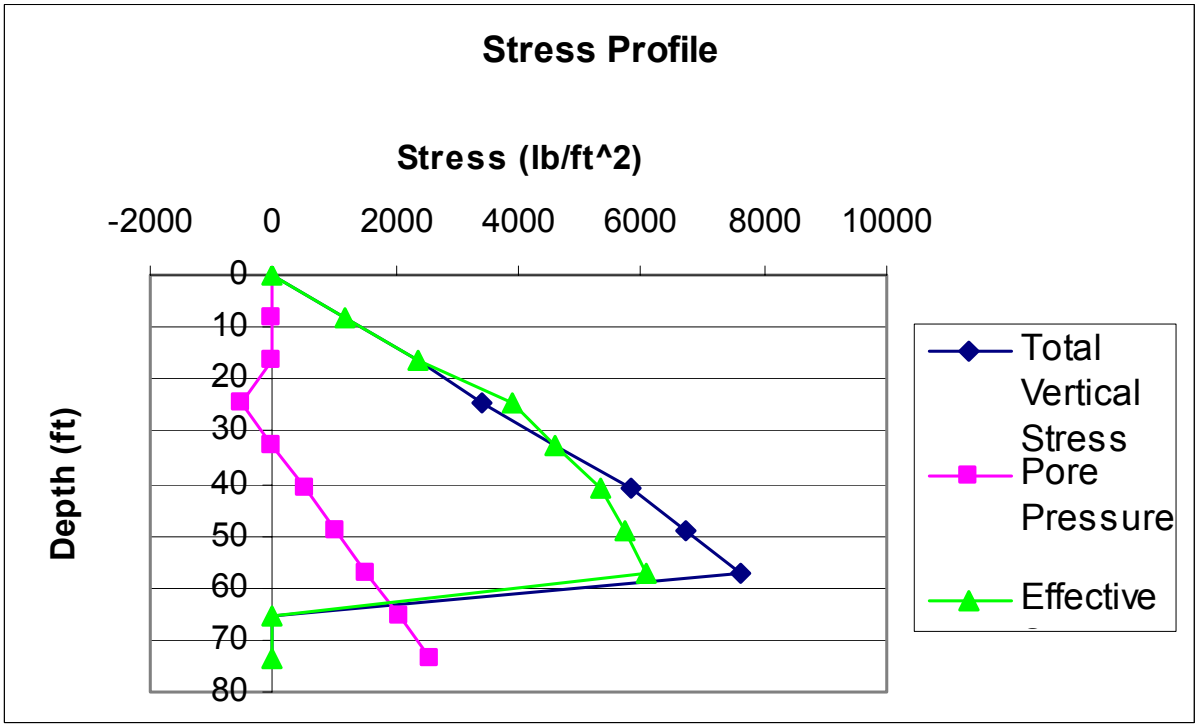

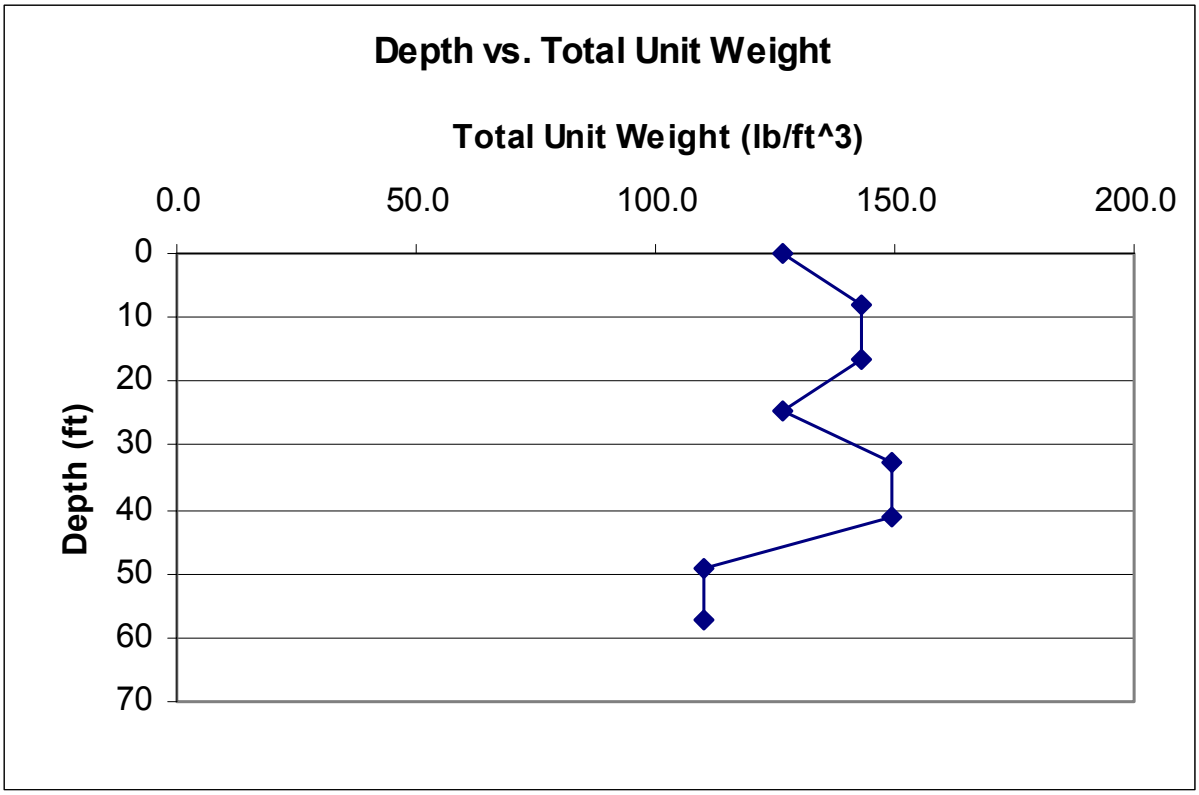
Depth vs. Total Unit Weight
Total Unit Weight (lb/ft^3)
0.0
50.0
100.0
150.0
200.0
Depth (ft)
0
10
20
30
40
50
60
70

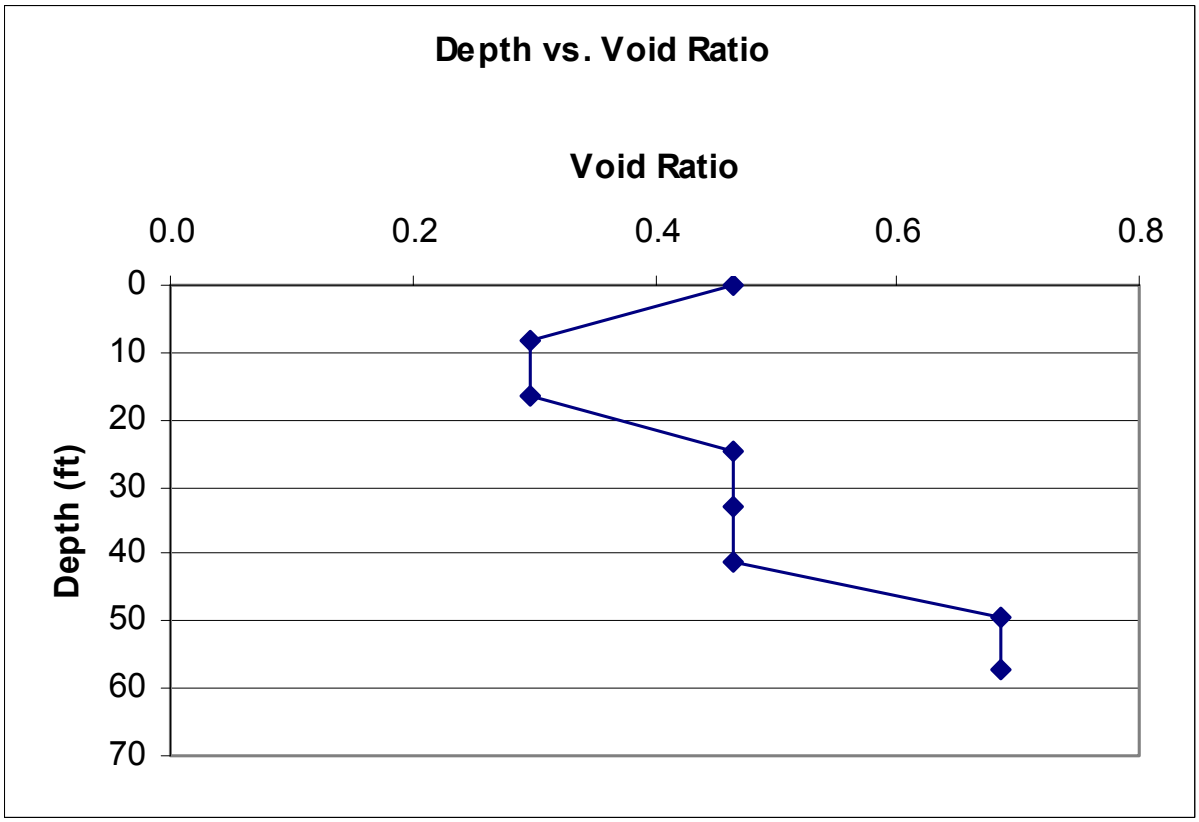
Depth vs. Void Ratio
Void Ratio
0.0
0.2
0.4
0.6
0.8
Depth (ft)
0
10
20
30
40
50
60
70